Heriot-Watt University

Analysis and approximation of a nonlocal equation

Ali Alshomrani

September 21, 2014

Submitted for the degree of

Doctor of Philosophy in Mathematics

on completion of research in the

Department of Mathematics,

School of Mathematical and Computer Sciences.

Abstract

In this thesis we study a nonlocal problem for $u(x,t), \quad 0 \leq x \leq 1$

$$\frac{\partial u}{\partial t}(x,t) = f\left(\hat{u}(x,t)\right) - u(x,t). \tag{*}$$

Here f is a nonlinear function and $\hat{u}$ is an average of u given by

$$K(x)\hat{u}(x,t) = \int_0^1 J(x-y)u(y,t)dy$$

where

$$K(x) = \int_0^1 J(x-y)dy.$$

We consider three different versions of the averaging function $J(x)$.

Chapter 2 and 3 contain an analytical study of equilibrium solutions to (*). Chapter 4 concentrates on a numerical approximation of the full problem given by (*). Finally, Chapter 5 studies and approximates slowly varying solutions to (*).

Acknowledgements

All praise be to Allah, the almighty, and peace be upon his slave and last messenger, Mohammad, (PBUH). It gives me a great pleasure to dedicate this acheivement to my parent, wife, kids and friends.

Special thanks to my supervisor Prof Dugald Duncan who helped in this study through his continuous supervision. I should also express my thanks to my second supervisor Prof Jack Carr for always being there when I needed him.

Contents

List of Figures

Chapter 1

Introduction

1.1 Inroduction

This thesis contains an analytical and numerical study of a nonlocal problem which was motivated by an example in mathematical biology. There are many examples of nonlocal problems in applications, older examples include the Boltzmann equation in statistical physics [69] and van der Waals in phase transitions [63]. In recent years many more nonlocal equations have been derived, especially in material science and biology. In the next section we briefly discuss some of the biological examples.

1.2 Examples of nonlocal problems

1.2.1 Nonlocal advection equations

In applications, advection is a transport mechanism of a substance carried along by a flow. We show how a nonlocal advection problem can arise. This example is based on the work

in [48].

Let $u(x,t)$ be the density of substance in the one dimensional region $0 < x < 1$. If $q = q(x,t)$ is the flux, the basic conservation law is

$$u_t + q_x = 0$$

and the usual assumption is that $q = q(u)$ so that

$$u_t + q'(u)u_x = 0. \tag{1.2.1}$$

If $q(u)$ is linear with $q(u) = cu$ then the general solution of (1.2.1) is

$$u(x,t) = f(x - ct)$$

so that (1.2.1) has travelling wave solutions. If q is nonlinear then in general (1.2.1) will not have smooth solutions and shocks will occur.

We could assume that the flux depends on the total mass of the system. As an example of this, suppose we want to model the digestion proceses in an organism. In this case we might assume that the speed in which food moves through the gut will depend on the quality of the food in the gut. In particular, in order to get maximum absorbtion of nutrients, the lower quality food would move quicker than the high quality food. Let $u(x,t)$ be the nutrient concentraion. The flux would have the form

$$q = v(t)u(x,t) \tag{1.2.2}$$

where the flow rate

$$v(t) = \int_0^1 F(u(x,t))dx$$

for some nonlinear function F. The resulting equation (1.2.1) will be nonlocal.

1.2.2 Aggregation models

There are many examples of biological aggregation in nature such as insect swarms, fish schools and colonies of bacteria. The traditional method used to model spatially distributed populations is to use a partial differential equation with diffusion terms. The idea used to model a group of individuals migrating together (a flock or swarm) is to think of it as a travelling wave solution which is zero (or very small) outside a finite region. However, it turned out to be difficult to design models which supported this idea and which were biologically meaningful. [51] showed that it was not possible to use the usual partial differential equation models which could describe locust swarm migration.

The models which described the required behaviour [51] were nonlocal and of the form

$$\frac{\partial f(x,t)}{\partial t} = \frac{\partial}{\partial x}\left(D\frac{\partial f(x,t)}{\partial t} - (V * f)(x,t))\right). \tag{1.2.3}$$

Here, x is one dimensional, $f(x,t)$ is the swarm density and D is the diffusion coefficient. The second term in the above equation represents the drift of individuals with a nonlocal, density dependent velocity V. One possible form for V is

$$(V * f)(x,t) = \int K(x-y)f(y,t)dy$$

where K is an even function with compact support.

1.2.3 Neural networks

Another rich source of examples of nonlocal equations come from neural field models [26]. We describe the standard model for a scalar neural field. Let $u(x,t)$ denote the local activity of a population of neurons at $x \in \mathbb{R}$. The equation for u is

$$\frac{\partial u(x,t)}{\partial t} = -u + \int_{-\infty}^{\infty} f(u(x-y,t))w(y)dy. \tag{1.2.4}$$

The even function $w(y)$ describes the strength of connections between neurons separated by a distance y. The output of a neuron is a spike train with firing rate $f(u)$. Equation (1.2.4) supports many types of solution such as travelling waves and pattern formation [15,30,67,70]. A review of methods for studying such equations is given in [17].

1.2.4 Modelling cell-cell adhesion

How cells organise into structured tissue is a very important area of study in many biological processes. One important factor in the formation of these aggregates are cell-cell interactions [2]. Let $n(x,t)$ be the cell density in a one dimensional domain. The dynamics are described by an equation similar to that given in (1.2.3),

$$\frac{\partial n(x,t)}{\partial t} = g(n(x,t)) + \frac{\partial}{\partial x}\left(Dn(x,t) - V(n(x,t))\right) \tag{1.2.5}$$

where g describes the cell kinetics. The V term describes the adhesive force between cells and is given by

$$(V * n)(x,t) = \int_{-R}^{R} A(n(x+y,t))w(y)dy.$$

The function w represents the adhesive force over the sensing region of the cell. The function A will increase when the cell density n is small but will decrease at larger cell densities because of cell packing.

1.2.5 Model for cell renewal

Mosaic tissues are composed of two or more cell types and are useful in understanding tissue growth. We describe a recent model for this [6] which is motivated by the work in the previous example. In this model the birth of cells replaces those cells lost to death, so that we only require a single equation. Let $a(\underline{x},t)$ be the proportion of cells of a particular type in two dimension. The equation for $a(\underline{x},t)$ is

$$\frac{\partial a}{\partial t} = \alpha(f(I_a) - a) \tag{1.2.6}$$

where α is the cell replacement rate and

$$I_a = (1/\text{area}) \int_0^R \int_0^{2\pi} a\left(\underline{x} + r\underline{\eta}\right) r d\theta dr.$$

Two forms of cellular interactions nonbiased and biased (linear and nonlinear f).The nonlinear function f has the property that $0 < f(u) < u$ for $0 < u < 1/2$ and $u < f(u) < 1$ for $1/2 < u < 1$ reflecting the bias that a cell will be replaced by the type of the majority

around it.

They also observed that the changes in the local environment interactions has an implication on the dynmics. Also, the model has the advantage of reproducing some of the pattern seen in a realistic tissues.

1.3 A one dimensional nonlocal problem

In this thesis we study a one dimensional equation motivated by the previous example. The equation for $u(x,t)$ is

$$u_t(x,t) = f\left(\frac{J*u}{K(x)}\right) - u(x,t) \tag{1.3.1}$$

for $0 \leq x \leq 1$ and $t \geq 0$ with given initial data $u(x,0)$. The kernel function is symmetric $J(x) = J(-x) \geq 0$ is involved in the convolution

$$(J*u)(x,t) = \int_0^1 J(x-y)u(y,t)dy.$$

From now on we use the notation

$$\bar{u}(x,t) = (J*u)(x,t), \quad \hat{u}(x,t) = \frac{J*u}{K(x)}. \tag{1.3.2}$$

The function $\hat{u}$ is the local kernel of u so that $K(x)$ is given by

$$K(x) = \int_0^1 J(x-y)dy.$$

The detailed assumptions on f are given in the next chapter. Typical examples of f are

given in Figure 1.1 where c and d are chosen so that $f(1) = 1$.

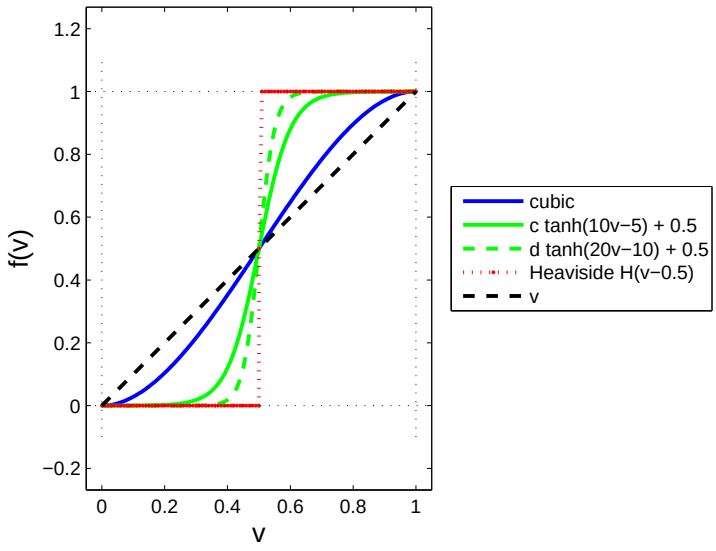

Figure 1.1: Examples of the function $f(v)$ in (1.3.1). The shape of the function has an impact on the behaviour of the solution. For oterwise identical problems, the time scale for evolution with the step function (cut off tail) is larger than the one with small tail. In general the process for a similar shape of f is similar but the time scales will vary.

In most of this thesis we will use the exponential decay kernel given by

$$J(x) = \frac{1}{2\varepsilon} e^{-|x|/\varepsilon}, \quad K(x) = 1 - \left(\frac{1}{2}\right)\left(e^{-x/\varepsilon} + e^{-(1-x)/\varepsilon}\right). \tag{1.3.3}$$

In the next section we show how we can transform (1.3.1) into a local equation for $\bar{u}(x,t)$ for this kernel. Figure 1.2 shows the graphs of $J(x-y)$ for three different values of ε. It shows how the kernels become concentrated near $x = y$ as ε decreases. Figure 1.2 shows $K(x)$ for

large and small value of ε. For large $\varepsilon, K(x)$ is almost constant while for small ε, $K(x)$ is very close to 1 except near 0 or 1.

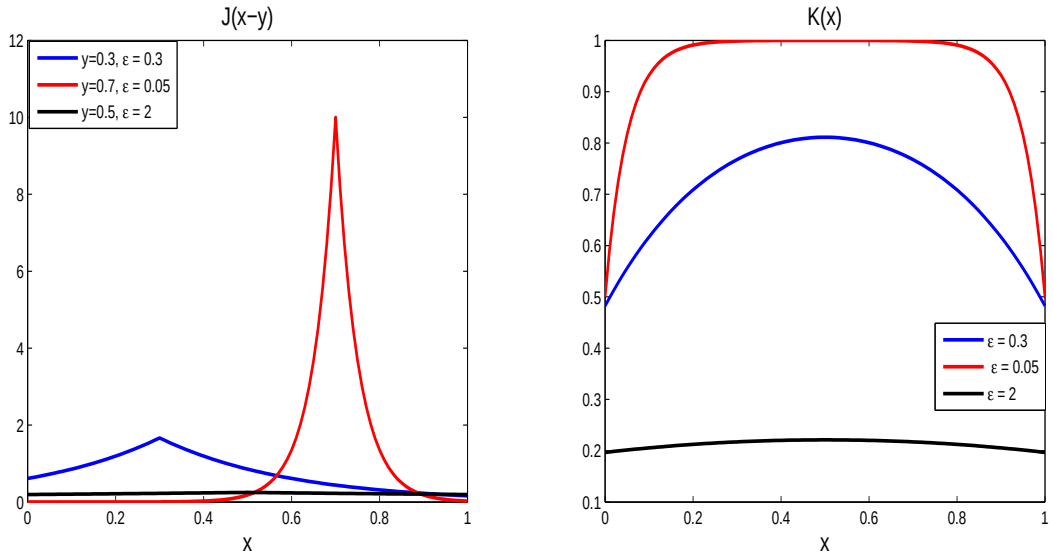

Figure 1.2: Graphs of $J(x-y)$ and $K(x)$ for the exponential kernel with three different values of ε.

We also consider the Gaussian kernel given by

$$J(x) = \sqrt{\frac{1}{\pi\varepsilon^2}} \exp\left(-\frac{x^2}{\varepsilon^2}\right), \quad K(x) = \frac{1}{2}\left(\text{erf}\,\left(\frac{x}{\varepsilon}\right) + \text{erf}\,\left(\frac{1-x}{\varepsilon}\right)\right)$$

where

$$\text{erf}\,(x) = \frac{2}{\sqrt{\pi}} \int_0^x \exp\left(-t^2\right) dt.$$

For small ε the Gausssian kernel decays even faster than the exponential kernel. This has implications for the slow behaviour of solutions for small ε described in Chapter 5.

Finally, motivated by the example in 1.2.4 (d) we consider the piecewise kernel

$$K(x)\int_0^1 J(x-y)u(y)dy = \begin{cases} \displaystyle\int_{-x}^{\varepsilon} u(x+y,t)\,dy \\ \displaystyle\int_{-\varepsilon}^{\varepsilon} u(x+y,t)\,dy \\ \displaystyle\int_{-\varepsilon}^{1-x} u(x+y,t)\,dy \end{cases}$$

where

$$K(x) = \begin{cases} x+\varepsilon & \text{when } 0 < x < \varepsilon \\ 2\varepsilon & \text{when } \varepsilon < x < 1-\varepsilon, \\ 1-x+\varepsilon & \text{when } 1-\varepsilon < x < 1. \end{cases} \tag{1.3.4}$$

The piecewise constant kernel is not differentiable in general at $x = \varepsilon$ and at $x = 1-\varepsilon$. The simplest way to show that is by differentiating $\hat{u}(x)$ when $\varepsilon < x < 1-\varepsilon$ and put $x = \varepsilon$ and do the same when $0 < x < \varepsilon$ and compare the both results. We obtain

$$\lim_{x\to\varepsilon^+} \hat{u}'(x) = \left(\frac{1}{2\varepsilon}\right)(u(2\varepsilon) - u(0)) \neq \left(\frac{1}{2\varepsilon}\right)(u(2\varepsilon) - \hat{u}(\varepsilon)) = \lim_{x\to\varepsilon^-} \hat{u}'(x).$$

1.4 Derivation of a local equation for the exponential decay kernel

In this section we show that for the exponential kernel given by (1.3.3), we can transform the nonlocal equation (1.3.1) into a local equation. This works because the kernel in (1.3.3) is the Green's function for the differential operator $w \to w''$. Similar ideas have been used

for other nonlocal equations [7, 8, 18, 40, 47, 65].

Theorem 1.4.1. *For the exponential decay kernel given by (1.3.3), equation, $\bar{u}(x,t)$ satisfies*

$$\left(\bar{u} - \varepsilon^2 \bar{u}_{xx}\right)_t = -\left(\bar{u} - \varepsilon^2 \bar{u}_{xx}\right) + f\left(\frac{\bar{u}}{K(x)}\right) \tag{1.4.1}$$

with the boundary conditions

$$\bar{u}(0,t) = \varepsilon \bar{u}'(0,t), \quad \bar{u}(1,t) = -\varepsilon \bar{u}'(1,t). \tag{1.4.2}$$

In addition, equilibrium solutions satisfy

$$\varepsilon^2 \bar{u}''(x) = \bar{u}(x) - f\left(\frac{\bar{u}(x)}{K(x)}\right) \tag{1.4.3}$$

with the boundary condition

$$\bar{u}(0) = \varepsilon \bar{u}'(0), \quad \bar{u}(1) = -\varepsilon \bar{u}'(1). \tag{1.4.4}$$

The equilibrium $u(x)$ can be found from (1.3.1) by

$$u(x) = f\left(\frac{\bar{u}(x)}{K(x)}\right). \tag{1.4.5}$$

Proof. From the definition of $\bar{u}$ and writing $\int_0^1 = \int_0^x + \int_x^1$

$$2\varepsilon \bar{u}(x,t) = \int_0^x \exp\left(-\left(\frac{x-y}{\varepsilon}\right)\right) u(y,t)\, dy + \int_x^1 \exp\left(-\left(\frac{y-x}{\varepsilon}\right)\right) u(y,t)\, dy \tag{1.4.6}$$

Differentiating w.r.t. x

$$2\varepsilon \bar{u}_x(x,t) = -\varepsilon^{-1} \int_0^x \exp\left(-\left(\frac{x-y}{\varepsilon}\right)\right) u(y,t)\, dy + \varepsilon^{-1} \int_x^1 \exp\left(-\left(\frac{y-x}{\varepsilon}\right)\right) u(y,t)\, dy, \tag{1.4.7}$$

and

$$\varepsilon^2 \bar{u}_{xx}(x,t) = \bar{u}(x,t) - u(x,t). \tag{1.4.8}$$

Using (1.4.8) in (1.3.1) gives the partial differential equation (1.4.1).

The boundary conditions (1.4.2) follow from putting $x = 0$ and $x = 1$ in (1.4.7). The results for equilibria follow from these results by putting $\bar{u}_t = 0$ in (1.4.1). □

1.5 Outline of thesis

In Chapters 2 and 3 we study equilibrium solutions of (1.3.1) for the exponential kernel. From Theorem 1.4.1 this reduces to a boundary value problem for the ordinary differential equation (1.4.3). In Chapter 2 we study properties of equilibria for a general sigmoidal function f in (1.4.3). We first show that we cannot replace the function $K(x)$ by 1 to approximate solutions. Further results explore the structure of solutions together with a numerical study. In Chapter 3 we study the special case when f is step function. We can give a complete analysis for this case. In particular, we show that nontrivial solutions exist for all ε in contrast to the results of numerical experiments in Chapter 2. We also give asymptotic results for large and small ε as well as the behaviour of solutions at the equilibrium which have a large number of oscillations (where solutions cross $(1/2)K(x)$ exactly $m + 1$ times).

In Chapter 4 we start by describing a semidiscrete spatial collocation method using a piecewise constant approximation in space for the general time dependent problem (1.3.1). We then analyse convergence of the approximation. We examine a special 1-periodic, linear version of the problem which has an exact solution that is reasonably easy to compute in terms of a Fourier series, and hence serves as a benchmark to measure the accuracy of the approximation. We use a simple error estimate based on mesh halving to measure the errors in the other cases. We also present numerical results for the nonlinear problem and give

a brief investigation of the computational time required using different ODE solvers and different ways to evaluate the spatial averaging operator, including the FFT. We finish with a numerical approximation for the full local equation given by (1.4.1).

In Chapter 5 we study the dynamics of solutions which change very slowly. This occurs when ε is small for both the exponential kernel and the Gaussian kernel although we focus on the first case. We derive formal asymptotics for the motion of the transition layers and compare the predictions with those of numerical solutions. There are some issues involved with the design of numerical methods here and we also include a discussion of these.

Chapter 2

Equilibrium solutions with a continuous nonlinearity

2.1 Introduction

Equilibrium solutions to the nonlocal problem (1.3.1) satisfy

$$u = f(\hat{u}), \quad 0 \leq x \leq 1. \tag{2.1.1}$$

In this chapter we study (2.1.1) when $\hat{u}(x)$ is given by the exponential decay kernel

$$\hat{u}(x) = \frac{1}{2\varepsilon K(x)} \int_0^1 \exp\left(-|\frac{x-y}{\varepsilon}|\right) u(y)dy, \tag{2.1.2}$$

$$1 - h(x) = K(x) = 1 - \frac{e^{-x/\varepsilon} + e^{-(1-x)/\varepsilon}}{2} \tag{2.1.3}$$

and the function f is Lipschitz continuous. Writing $\bar{u}(x) = \hat{u}(x)K(x)$, from (1.4.3), $\bar{u}(x)$ satisfies the nonautonomous boundary value problem

$$\varepsilon^2 \bar{u}''(x) = \bar{u}(x) - f\left(\frac{\bar{u}(x)}{K(x)}\right), \quad 0 \le x \le 1, \tag{2.1.4}$$

$$\bar{u}(0) = \varepsilon \bar{u}'(0), \quad \bar{u}(1) = -\varepsilon \bar{u}'(1), \tag{2.1.5}$$

with $0 \le \bar{u}(x) \le K(x)$ for $0 \le x \le 1$.

In the rest of this chapter we make the following assumptions about the function f:

$$f(0) = 0, \quad f\left(\frac{1}{2}\right) = \frac{1}{2}, \quad f(1) = 1 \tag{2.1.6}$$

and

$$f'(z) \ge 0 \quad \text{for} \quad 0 \le z \le 1, f(z) < z \quad \text{for} \quad 0 < z < \frac{1}{2}, f(z) > z \quad \text{for} \quad \frac{1}{2} < z < 1. \tag{2.1.7}$$

In addition we will assume that f satisfies the symmetry condition

$$f(z) + f(1-z) = 1, \quad 0 \le z \le 1 \tag{2.1.8}$$

although this is not needed for all our results. Graphs of three examples of an f satisfying these condition are shown in Figure 2.1.

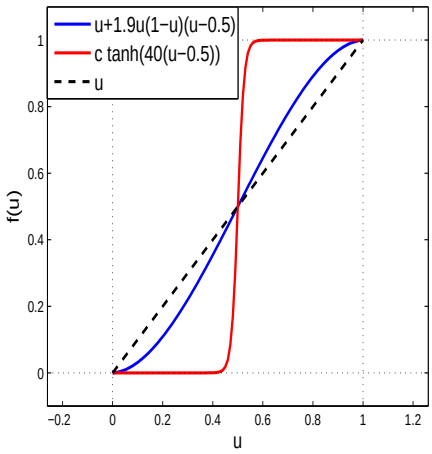

Figure 2.1: Typical examples of $f(u)$ that satisfy (2.1.6)-(2.1.7) and (2.1.8).

The equivalent equilibrium equation for $\hat{u}(x)$ is

$$\varepsilon^2 K(x)\hat{u}''(x) + 2\varepsilon^2 K'(x)\hat{u}'(x) = \hat{u}(x) - f\left(\hat{u}(x)\right). \tag{2.1.9}$$

This equation is clearly more complicated than (2.1.4) since the coefficient of the second derivative is a function of x and there is an additional term involving $\hat{u}'(x)$. For this reason it is easier to work with $\bar{u}(x)$.

2.2 Autonomous ODE

If ε is small, then

$$K(x) = 1 - \frac{1}{2}\left(e^{-x/\varepsilon} + e^{-(1-x)/\varepsilon}\right) \approx 1$$

except for x very close to 0 or 1. This suggests that we could replace the $K(x)$ in (2.1.4) by 1 in order to obtain an approximation to the solution. We show that this procedure does not work, since for any ε there is no solution to the boundary value problem if $K(x) \equiv 1$ in (2.1.4).

We scale the boundary value problem by the change of variable $\varepsilon x = w$ and set $K \equiv 1$. The resulting problem is

$$z'' = z - f(z) \tag{2.2.1}$$

with $0 \leq z \leq 1$ and with the boundary conditions

$$z(0) = z'(0), \quad z(\varepsilon^{-1}) = -z'(\varepsilon^{-1}), \tag{2.2.2}$$

where we use prime for differentiation with respect to w. The boundary value problem has the solution $z \equiv 0$, we show that this is the only solution.

Theorem 2.2.1. *There is no solution to the boundary value problem (2.2.1)-(2.2.2) with* $0 < z(w) \leq 1$ *for* $0 \leq w \leq \varepsilon^{-1}$.

Proof. We assume that $f(0) = 0, f\left(\frac{1}{2}\right) = \frac{1}{2}$ and $f(1) = 1$ and that $z > f(z) > 0$ for $0 < z < 1/2$ while $f(z) > z$ for $1/2 < z < 1$. We also assume the symmetry condition

$$f(z) + f(1 - z) = 1, \quad 0 \leq z \leq 1. \tag{2.2.3}$$

We want a solution of (2.2.1)-(2.2.2) with $0 < z(w) \leq 1$ for $0 \leq w \leq \varepsilon^{-1}$. From (2.2.1), any solution $z(w)$ of (2.2.1) satisfies

$$[z'(w)]^2 = H\left(z(w)\right) + C, \tag{2.2.4}$$

where C is a constant and

$$H(z) = z^2 - 2\int_0^z f(y)dy = 2\int_0^z (y - f(y))\, dy. \tag{2.2.5}$$

In order to describe the phase plane for (2.2.1) we need to study the function $H(z)$. From (2.2.5)

$$H'(z) = 2(z - f(z)) \tag{2.2.6}$$

so $H'(z) > 0$ for $0 < z < 1/2$ and $H'(z) < 0$ for $1/2 < z < 1$. Integrating the symmetry condition (2.2.3) over the interval $[0, 1]$ we see that $H(1) = 0$. Since $H(0) = 0$ it follows that $H(z) > 0$ for $0 < z < 1$.

If $C = 0$ in (2.2.4), then the above analysis shows that the solution with $z' \geq 0$ is the heteroclinic orbit connecting 0 and 1. The solution with $z' \leq 0$ connects 1 and 0. Negative values of C correspond to periodic solution "inside" these connecting orbits. For solutions z with $0 < z \leq 1$ and $C > 0$ the orbits lie outside the connecting orbits. The phase portrait for the autonomous case is shown in Figure 2.2.

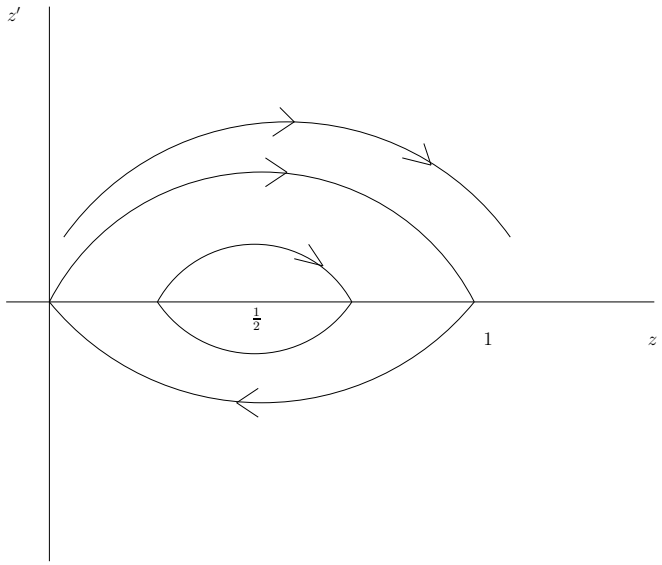

Figure 2.2: Phase portrait for (2.2.1). The heteroclinic orbit is the one connecting 0 and 1 forward and backward. To start with the left boundary condition then the orbit of z for $0 < z \leq 1$ lies outside the hetroclinic loop so $z'(w) > 0$. It follows that the boundary condition $z(\varepsilon^{-1}) = -z'(\varepsilon^{-1}) > 0$ can not be satisfied.

We compute the slope of the hetroclinic orbit with $z' > 0$ at $z = 0$. Taking $C = 0$ in (2.2.4) and using L'Hopital's rule

$$\lim_{w\to-\infty} \frac{(z'(w))^2}{z^2(w)} = \lim_{z\to 0} \left(1 - \frac{f(z)}{z}\right) = 1 - f'(0),$$

so that the slope is less than 1.

Suppose now that $z(w)$ is a solution of (2.2.1) with $z(0) = z'(0) > 0$. It follows that the orbit of z for $0 < z \leq 1$ lies outside the hetroclinic loop so $z'(w) > 0$. It follows that the boundary condition $z(\varepsilon^{-1}) = -z'(\varepsilon^{-1}) > 0$ can not be satisfied. This completes the proof. □

2.3 Properties of the equilibrium solutions

If f is the linear function $f(u) = u$ then the boundary value problem (2.1.4)-(2.1.5) has infinitely many solutions given by

$$\bar{u}(x) = \frac{\bar{u}(0)}{K(0)} K(x). \tag{2.3.1}$$

For a nonlinear function f satisfying the conditions in Section 2.1, the boundary value problem has the three solutions

$$0, K(x) \text{ and } \frac{1}{2} K(x). \tag{2.3.2}$$

In this section we study the properties of all equilibrium solutions. The first result uses the fact that $K(x) = K(1-x)$ (that inherits from J being symmetric) and (2.1.8) to show that we can generate additional solutions from a solution $\bar{u}(x)$.

Theorem 2.3.1. *Let $\bar{u}(x)$ be a solution of (2.1.4)-(2.1.5).*

(a) $\bar{u}(1-x), K(x) - \bar{u}(x)$ and $K(x) - \bar{u}(1-x)$ are solutions of (2.1.4)-(2.1.5).

(b) If $\bar{u}(0) = \bar{u}(1)$, then $\bar{u}(x) = \bar{u}(1-x)$ for all $x \in [0,1]$.

(c) If $\bar{u}(0) + \bar{u}(1) = K(0)$, then $\bar{u}(x) + \bar{u}(1-x) = K(x)$ for all $x \in [0,1]$.

Proof. (a) Let $w(x) = \bar{u}(1-x)$. Then $w''(x) = \bar{u}''(1-x)$, and since $K(x) = K(1-x), w(x)$ satisfies (2.1.4). Also

$$w(0) - \varepsilon w'(0) = \bar{u}(1) + \varepsilon \bar{u}'(1) = 0$$

and

$$w(1) + \varepsilon w'(1) = \bar{u}(0) + \varepsilon \bar{u}'(0) = 0$$

so $w(x)$ is also solution of the boundary value problem.

To prove that $K(x)-\bar{u}(x)$ is a solution let $w(x)=K(x)-\bar{u}(x)$. From the definition of $K(x)$ in (2.1.3), $\varepsilon^2 K''(x)=K(x)-1$. Hence

$$\begin{aligned}\varepsilon^2 w''(x) &= K(x)-1-\bar{u}(x)+f\left(\frac{K(x)-w(x)}{K(x)}\right)\\ &= w(x)-1+f\left(1-\frac{w(x)}{K(x)}\right).\end{aligned}$$

From (2.1.8),

$$f\left(1-\frac{w(x)}{K(x)}\right)=1-f\left(\frac{w(x)}{K(x)}\right)$$

so that $w(x)$ satisfies (2.1.4). Also

$$K(0)=\varepsilon K'(0)=\frac{1-e^{-1/\varepsilon}}{2}$$

so that

$$w(0)-\varepsilon w'(0)=-\bar{u}(0)+\varepsilon\bar{u}'(0)=0.$$

Similarly, $w(1)+\varepsilon w'(1)=0$ and this proves that $w(x)$ satisfies the boundary conditions. Finally, the above results show that $K(x)-\bar{u}(1-x)$ is also a solution.

(b) Define $p(x)=\bar{u}(x)-\bar{u}(1-x)$. From $\bar{u}(0)=\bar{u}(1)$ and the boundary conditions, $p(0)=p'(0)=0$. Also, a calculation shows that

$$\varepsilon^2 p''(x)=p(x)-f\left(\frac{\bar{u}(x)}{K(x)}\right)+f\left(\frac{\bar{u}(x)-p(x)}{K(x)}\right). \tag{2.3.3}$$

Since f is Lipschitz, the initial value problem for (2.3.3) has a unique solution so that $p(x)=0$ for all x as required.

(c) Define $p(x)=\bar{u}(x)+\bar{u}(1-x)-K(x)$. Similar calculations to part (b) show that $p(x)=0$ for all x. □

Let $\bar{u}(x)$ be a solution to the boundary value problem. The result above says that we have

three additional solutions, $\bar{u}(1-x), K(x)-\bar{u}(x)$ and $K(x)-\bar{u}(1-x)$. In the next section we present some numerical studies of the boundary value problem. These results indicate that all solutions have one of the following symmetry properties for $0 \leq x \leq 1$:

$$\bar{u}(x) + \bar{u}(1-x) = K(x) \tag{2.3.4}$$

or

$$\bar{u}(x) = \bar{u}(1-x). \tag{2.3.5}$$

We refer to solutions as non-symmetric if they satisfy (2.3.4) and symmetric for (2.3.5).

If we have a non-symmetric solution $\bar{u}(x)$ then $\bar{u}(1-x)$ is a distinct solution but $K(x)-\bar{u}(x)$ and $K(x)-\bar{u}(1-x)$ give the solutions $\bar{u}(x)$ and $\bar{u}(1-x)$ again. If $\bar{u}(x)$ is a symmetric solution then $K(x)-\bar{u}(x)$ is a distinct solution but $\bar{u}(1-x)$ and $K(x)-\bar{u}(1-x)$ give the solutions $\bar{u}(x)$ and $K(x)-\bar{u}(x)$.

In Figures 2.3**(a)-(b)** and 2.4**(a)-(b)**, solutions of the boundary value problem are shown with $f(u) = u+1.9u(1-u)(u-0.5)$ and $\varepsilon = 0.1$. Figures 2.3**(a)-(b)** show the non-symmetric solutions $\bar{u}(x)$ and $K(x)-\bar{u}(x)$. Note that these two solutions cross the curve $\frac{1}{2}K(x)$ at the same point $x = \frac{1}{2}$. Figures 2.4**(a)-(b)** show the symmetric solutions $\bar{u}(x)$ and $K(x)-\bar{u}(x)$. Again note that both of these solutions cross $\frac{1}{2}K(x)$ at the same points. Also, the solution which cross the curve $\frac{1}{2}K(x)$ once is a single layer solution and twice is the two layers solution and so on.

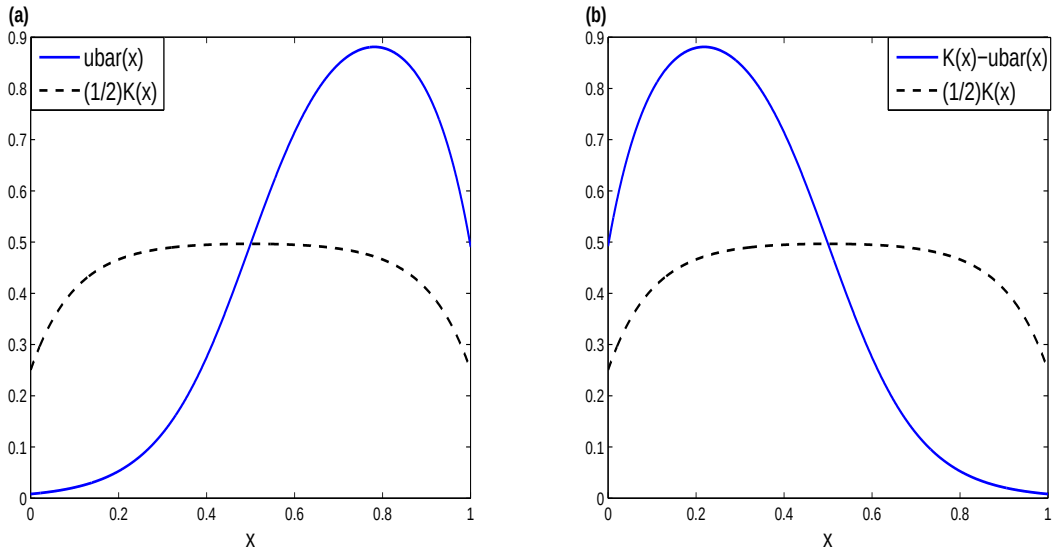

Figure 2.3: Single layer solutions which cross $\frac{1}{2}K(x)$ only once with $\varepsilon = 0.1$.

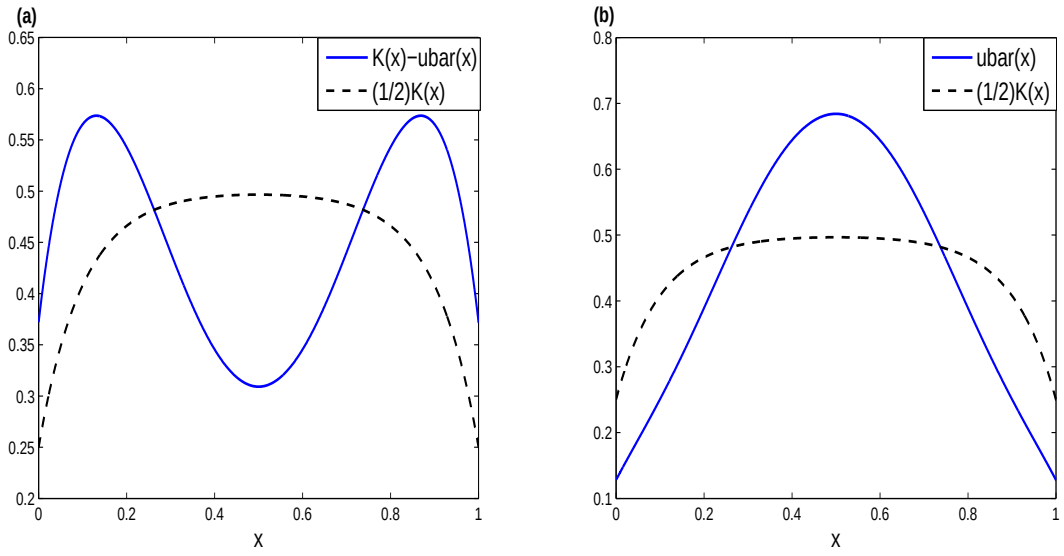

Figure 2.4: Two layers solutions which cross $\frac{1}{2}K(x)$ twice with $\varepsilon = 0.1$.

Let $\bar{u}(x)$ be a solution of the boundary value problem not equal to any of the three solutions in (2.3.2). We will prove later that we must have

$$\bar{u}(c) = \frac{1}{2}K(c) \tag{2.3.6}$$

for some c. Note that we cannot have $\bar{u}'(c) = \frac{1}{2}K'(c)$. Since if this were the case, $\bar{u}(x) = \frac{1}{2}K(x)$ for all x by uniqueness of the initial value problem for (2.1.4). It follows that we can call a point c which satisfies (2.3.6) a crossing point. Note that we cannot have c equal to 0 or 1 since this would imply $\bar{u}(x) = \frac{1}{2}K(x)$.

In Figures 2.3 and 2.4, the solution with an odd number of crossing points (one) is non-symmetric while the solution with an even number of crossing points (two) is symmetric. For a solution satisfying either (2.3.4) or (2.3.5) we prove that this is always this the case.

Theorem 2.3.2. *Let $\bar{u}(x)$ be a solution to the boundary value problem satisfying either (2.3.4) or (2.3.5) and not equal to any of the solutions in (2.3.2). Suppose $\bar{u}(x)$ has m crossing points. Then if m is even $\bar{u}(x)$ is symmetric while if m is odd $\bar{u}(x)$ is non-symmetric.*

Proof. If a is a crossing point then from (2.3.4) and (2.3.5), $1 - a$ is also a crossing point. Suppose first that m is odd so that $c = 1/2$ is a crossing point. If $\bar{u}(x)$ is symmetric then $\bar{u}(1/2) = (1/2)K(1/2)$ and $\bar{u}'(1/2) = 0 = (1/2)K'(1/2)$ so that $\bar{u}(x) = (1/2)K(x)$, a contradiction. Suppose now that m is even. So that $c = 1/2$ is not a crossing point. From (2.3.4), if $\bar{u}(x)$ is non-symmetric, $\bar{u}(1/2) = (1/2)K(1/2)$ a contradiction. □

Theorem 2.3.3. *Let $\bar{u}(x)$ be a solution of the boundary value problem not equal to any of the solutions in (2.3.2). Then $\bar{u}(x)$ has to cross $\frac{1}{2}K(x)$ at least once.*

Proof. Since $\bar{u}(x)$ and $K(x) - \bar{u}(x)$ are solutions, if we have a solution $\bar{u}(x)$ which does not

cross $\frac{1}{2}K(x)$ then we may assume that for all $x \in [0,1]$,

$$\bar{u}(x) < \frac{1}{2}K(x).$$

The function $K(x)$ satisfies $K(0) = \varepsilon K'(0)$ and $K(1) = -\varepsilon K'(1)$ and the equation

$$\varepsilon^2 K'' = K - 1. \tag{2.3.7}$$

The function $\bar{u}$ satisfies the same boundary conditions and

$$\varepsilon^2 \bar{u}'' = \bar{u} - f\left(\frac{\bar{u}}{K}\right). \tag{2.3.8}$$

Multiplying (2.3.7) by $\bar{u}$ and (2.3.8) by K, then substracting we obtain

$$\begin{aligned}\varepsilon^2 \left(K''\bar{u} - K\bar{u}''\right) &= Kf\left(\frac{\bar{u}}{K}\right) - \bar{u} \\ &= K\left[f\left(\frac{\bar{u}}{K}\right) - \frac{\bar{u}}{K}\right].\end{aligned}$$

Integrating the left hand side of the above we obtain

$$\varepsilon^2 \int_0^1 \left(K''\bar{u} - K\bar{u}''\right) dx = \varepsilon^2 \left[K'(1)\bar{u}(1) - \bar{u}'(1)K(1)\right] - \varepsilon^2 \left[K'(0)\bar{u}(0) - \bar{u}'(0)K(0)\right] \quad = 0$$

using the boundary conditions. It follows that

$$\int_0^1 K\left[f\left(\frac{\bar{u}}{K}\right) - \frac{\bar{u}}{K}\right] dx = 0. \tag{2.3.9}$$

Since $\bar{u}(x) < \frac{1}{2}K(x)$,

$$f\left(\frac{\bar{u}}{K}\right) < \frac{\bar{u}}{K}$$

which contradicts (2.3.9) and this completes the proof. □

Let $\bar{u}(x)$ be a solution not equal to any of those in (2.3.2). Using part (a) of Theorem (2.3.1),

we may assume that

$$0 < \bar{u}(0) < \frac{1}{2}K(0). \tag{2.3.10}$$

By Theorem (2.3.3), there exists a crossing point $c \in (0,1)$ so that

$$\bar{u}(c) = \frac{1}{2}K(c). \tag{2.3.11}$$

Using part (a) of Theorem 2.3.1 again, there is always a solution $\bar{u}(x)$ satisfying (2.3.10) such that one of the crossing points satisfies $c \leq 1/2$. Note that if $\bar{u}(x)$ satisfies either (2.3.4) or (2.3.5) then there is always a crossing point c satisfying $c \leq 1/2$. We obtain a lower bound on $\bar{u}(0)$ for such solutions in the next result.

Theorem 2.3.4. *Let $\bar{u}(x)$ be a solution not equal to any of those in (2.3.2). Suppose also that (2.3.10) and (2.3.11) hold for some $c \leq \frac{1}{2}$. Then*

$$\bar{u}(0) \geq \frac{1}{2}\left(e^{-1/(2\varepsilon)} - e^{-1/\varepsilon}\right). \tag{2.3.12}$$

Proof. From (1.4.6), $\bar{u}(x) = I_1(x) + I_2(x)$ where

$$I_1(x) = \frac{1}{2\varepsilon}\int_0^x \exp\left(-\frac{(x-y)}{\varepsilon}\right) u(y)dy, \quad I_2(x) = \frac{1}{2\varepsilon}\int_x^1 \exp\left(-\frac{(y-x)}{\varepsilon}\right) u(y)dy.$$

Then

$$\varepsilon\bar{u}'(x) = -I_1(x) + I_2(x) \leq \bar{u}(x).$$

Integrating this inequality gives

$$\bar{u}(x) \leq \bar{u}(0)e^{x/\varepsilon}. \tag{2.3.13}$$

If (2.3.12) is not true, we prove that $\bar{u}(x)$ cannot have a crossing point $c \leq 1/2$, that is, we prove that

$$\frac{1}{2}K(x) - \bar{u}(x) > 0 \quad \text{for} \quad 0 \leq x \leq \frac{1}{2} \tag{2.3.14}$$

From our assumption that (2.3.12) is not true and (2.3.13),

$$g(x) = 4e^{x/\varepsilon}\left(\frac{1}{2}K(x) - \bar{u}(x)\right) > -1 + 2e^{x/\varepsilon} - e^{2x/\varepsilon}\left(2e^{-1/(2\varepsilon)} - e^{-1/\varepsilon}\right) = G(x).$$

Factoring the quadratic polynomial $G(x)$

$$G(x) = \left(e^{1/2\varepsilon} - e^{x/\varepsilon}\right)\left(e^{x/\varepsilon}\left(2e^{-1/(2\varepsilon)} - e^{-1/\varepsilon}\right) - e^{-1/(2\varepsilon)}\right).$$

Then for $0 \le x \le 1/2$,

$$e^{1/2\varepsilon} - e^{x/\varepsilon} \ge 0$$

and

$$e^{x/\varepsilon}\left(2e^{-1/(2\varepsilon)} - e^{-1/\varepsilon}\right) - e^{-1/(2\varepsilon)} \ge e^{-1/(2\varepsilon)} - e^{-1/\varepsilon} > 0$$

so that $G(x) \ge 0$ and $g(x) > 0$ as required. □

The numerical studies in Section 2.4 look for equilibrium solutions with one or more layers for $0.01 \le \varepsilon \le 1000$. They indicate that for large ε, the only solutions of the boundary value problem are those listed in (2.3.2). We are not able to prove this, instead we show that any additional solution must be close to $\frac{1}{2}K(x)$.

Theorem 2.3.5. *For large ε, any solution $\bar{u}(x)$ other than those in (2.3.2) must satisfy*

$$\bar{u}(x) = \frac{1}{2}K(x) + O\left(\varepsilon^{-2}\right), \quad 0 \le x \le 1. \tag{2.3.15}$$

Also, for $0 \le x \le 1$,

$$\bar{u}(x) = \bar{u}(0) + \varepsilon^{-1}\bar{u}(0)x - \varepsilon^{-2}\frac{x^2}{4} + O\left(\varepsilon^{-3}\right) \tag{2.3.16}$$

where

$$\bar{u}(0) = \frac{1}{4\varepsilon} + O\left(\varepsilon^{-2}\right).$$

Proof. A calculation shows that for $0 \leq x \leq 1$, and large ε,

$$K(x) = \frac{1}{2\varepsilon} - \frac{x^2 + (1-x)^2}{4\varepsilon^2} + O\left(\varepsilon^{-3}\right),$$

$$\frac{1}{K(x)} = 2\varepsilon + x^2 + (1-x)^2 + O\left(\varepsilon^{-1}\right). \tag{2.3.17}$$

It follows that $\bar{u}(0) = O\left(\varepsilon^{-1}\right)$ and $\bar{u}'(0) = O\left(\varepsilon^{-2}\right)$. Since $\bar{u}''(x) = O\left(\varepsilon^{-2}\right)$ it follows that $\bar{u}'(x) = O\left(\varepsilon^{-2}\right)$ and

$$\bar{u}(x) = \bar{u}(0) + O\left(\varepsilon^{-2}\right)$$

By Theorem 2.3.3, $\bar{u}(x)$ must cross $\frac{1}{2}K(x)$ at least once so

$$\bar{u}(0) = \frac{1}{4\varepsilon} + O\left(\varepsilon^{-2}\right)$$

and

$$\bar{u}(x) = \frac{1}{4\varepsilon} + O\left(\varepsilon^{-2}\right) = \frac{1}{2}K(x) + O\left(\varepsilon^{-2}\right).$$

From (2.3.17),

$$\frac{\bar{u}(x)}{K(x)} = \frac{1}{2} + O\left(\varepsilon^{-1}\right)$$

so that

$$\varepsilon^2\bar{u}''(x) = \bar{u}(x) - \frac{1}{2} + O\left(\varepsilon^{-1}\right) = -\frac{1}{2} + O\left(\varepsilon^{-1}\right)$$

where we have used $f\left(\frac{1}{2}\right) = \frac{1}{2}$. Integrating the above equation leads to (2.3.16).

We can use the result in Theorem 2.3.5 to improve the bound on $\bar{u}(0)$. Suppose that $\bar{u}(0) < \frac{1}{2}K(0)$ and that $\bar{u}(x)$ has a crossing point $c \leq 1/2$. Then

$$\frac{1}{2}\left(e^{-1/(2\varepsilon)} - e^{-1/\varepsilon}\right) \leq \bar{u}(0) < \frac{1}{2}K(0).$$

A calculation shows that

$$\frac{1}{8\varepsilon^2} \leq \frac{1}{4\varepsilon} - \bar{u}(0) \leq \frac{3}{16\varepsilon^2}.$$

□

2.4 Numerical results

In this section we compute some solutions of (2.1.4)-(2.1.5) in order to demonstrate some of the results in the previous section. Matlab has a number of codes for solving boundary value problems. We use them and the package CHEBFUN [57] to compute approximate solutions. In both methods we set $'RelTol' = 10^{-12}$ and $'AbsTol' = 10^{-14}$. CHEBFUN is a open source software system written in MATLAB for numerical computation with functions of a real variable. It is based on the idea of overloading MATLAB's commands for vectors and matrices to analogous commands for functions and operators. The mathematical basis of Chebfun is numerical algorithms involving piecewise polynomial interpolants and Chebyshev polynomials, and this is where the name "CHEB" comes from [33,56,66,68]. Another approach based on the shooting method of solving boundary value problem is through the built in MATLAB bvp solvers. A list of bvp solvers developed by L. Shampine and J.Kierzenka [45,64].

For the nonlinear function we use two examples. The cubic

$$f(\bar{u}) = \bar{u} + \lambda\bar{u}(1-\bar{u})(\bar{u}-1/2) \tag{2.4.1}$$

satisfies all the conditions in Section 3.1 if $0 < \lambda < 2$. One important property of f that seems to influence solutions is the steepness of f which we measure as $f'\left(\frac{1}{2}\right)$. For (2.4.1) we have that $f'\left(\frac{1}{2}\right) = 1 + \frac{\lambda}{4}$. For the examples in this section we always have $\lambda = 1.9$.

We also use the example

$$f(\bar{u}) = \frac{1}{2} + \frac{\tanh(\gamma(\bar{u}-1/2))}{2\tanh(\gamma/2)} \tag{2.4.2}$$

which satisfies the conditions in Section 3.1 for all $\gamma > 0$. For this example

$$f'\left(\frac{1}{2}\right) = \frac{\gamma}{2\tanh(\gamma/2)} \tag{2.4.3}$$

which for large γ is approximately $\gamma/2$.

Example A. We begin by computing some single layer solutions (one crossing) which will be non-symmetric. The aim is to show how solutions depend on $f'\left(\frac{1}{2}\right)$ and ε. We compute solutions for three functions f : (i) the cubic with $\lambda = 1.9$, (ii) example (2.4.2) with $\gamma = 5$ (iii) example (2.4.2) with $\gamma = 40$. For (i), $f'\left(\frac{1}{2}\right) = 1.475$ (ii) $f'\left(\frac{1}{2}\right) \approx 2.5$ (iii)$f'\left(\frac{1}{2}\right) \approx 20$ so the slopes are increasing. We also compute solutions for three values: $\varepsilon = 0.05; \varepsilon = 0.1$; and $\varepsilon = 0.15$.

Figure 2.5**(a)** shows $\bar{u}(x)$ for the three functions f when $\varepsilon = 0.05$. As expected all solutions cross $\frac{1}{2}K(x)$ at $x = \frac{1}{2}$. The results show that the slope of the solution $\bar{u}(x)$ at $x = \frac{1}{2}$ increases as $f'\left(\frac{1}{2}\right)$ increases.

Figure 2.5**(b)** shows $\bar{u}(x)$ for $\varepsilon = 0.1$. Again the slope of $\bar{u}(x)$ increases at $x = \frac{1}{2}$ as $f'\left(\frac{1}{2}\right)$ increases. In addition, the slope of $\bar{u}(x)$ at $x = \frac{1}{2}$ for all three functions is less than the corresponding values for $\varepsilon = 0.05$.

Figure 2.5**(c)** shows $\bar{u}(x)$ for $\varepsilon = 0.15$. Identical trends to these demonstrated in **(a)** and **(b)** are repeated here.

For a non-symmetric solution $\bar{u}(x)$,

$$\bar{u}(0) + \bar{u}(1) = K(0). \tag{2.4.4}$$

For all cases above, (2.4.4) holds to seven decimal places.

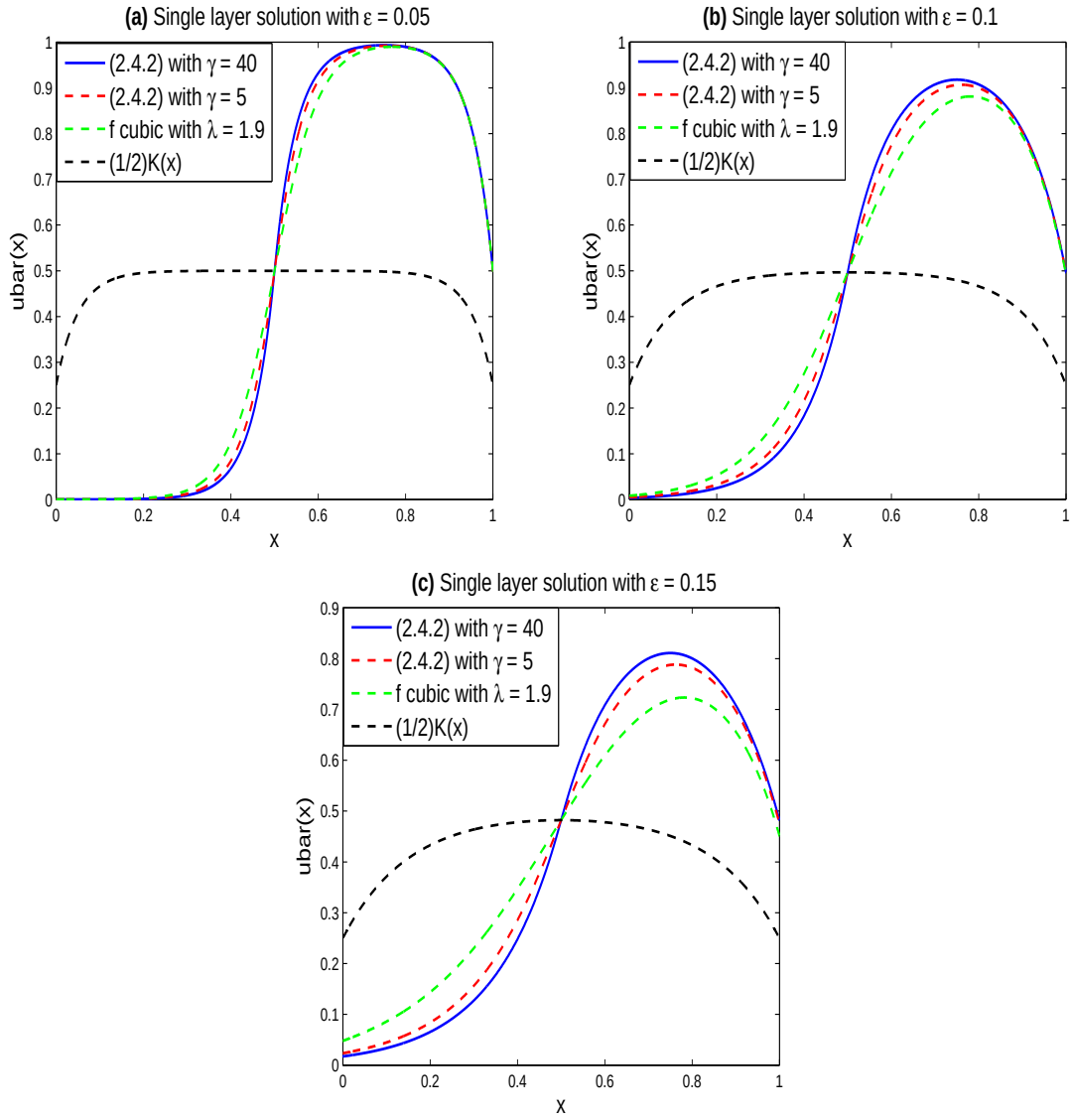

Figure 2.5: Single layer solutions. Parameter values given in **Example A.** $\frac{1}{2}K(x)$ also plotted to show the crossing place. The slope of $\bar{u}(x)$ increases at $x = \frac{1}{2}$ as $f'\left(\frac{1}{2}\right)$ increases or ε decreases.

Example B. We compute two layer solutions for the three functions in Example A with

$\varepsilon = 0.05$ and $\varepsilon = 0.1$. Figure 2.6**(a)** shows the results for $\varepsilon = 0.05$ while Figure 2.6**(b)** gives the results for $\varepsilon = 0.1$. All solutions appear to be symmetric with $\bar{u}'\left(\frac{1}{2}\right) = 0$ as expected. Increasing $f'\left(\frac{1}{2}\right)$ leads to an increase in $\bar{u}'(x)$ at the crossing points. Also, increasing ε, decreases $\bar{u}'(x)$ at the crossing points.

For a symmetric solution $\bar{u}(x)$,

$$\bar{u}(0) = \bar{u}(1). \tag{2.4.5}$$

For all cases above, (2.4.5) holds to seven decimal places.

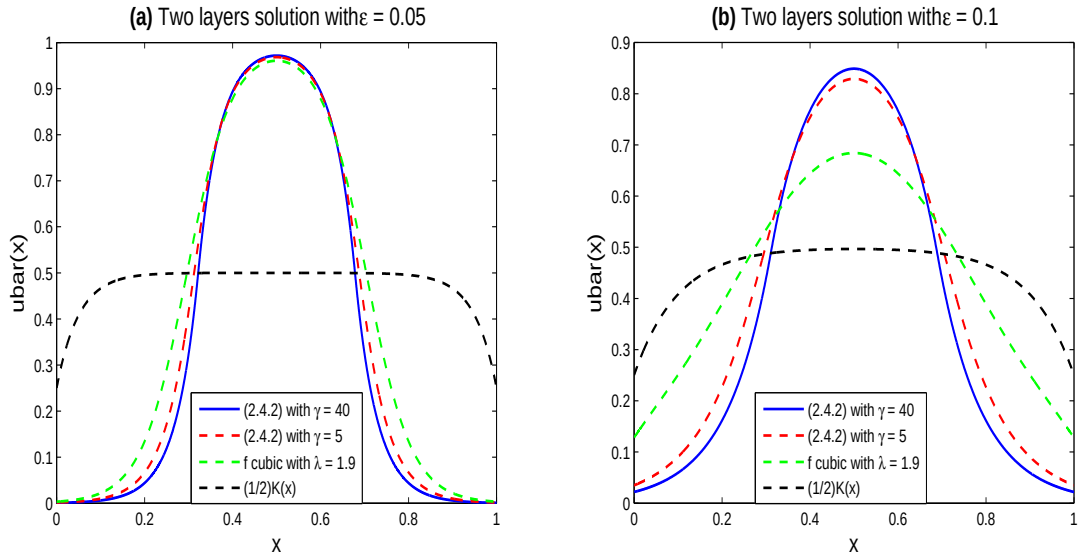

Figure 2.6: Two layer solutions with two crossing of $1/2K(x)$, also plotted. Parameter values given in **Example B.** The slope of $\bar{u}(x)$ increases at the crossing place as $f'\left(\frac{1}{2}\right)$ increases or ε decreases.

Before giving our next set of numerical results, we explore how solutions depend on the

initial value $\bar{u}(0)$. Let $\bar{u}(x)$ be a solution of the initial value problem for (2.1.4) with

$$\bar{u}(0) = \varepsilon \bar{u}'(0) = \alpha. \tag{2.4.6}$$

If

$$\bar{u}(1) + \varepsilon \bar{u}'(1) = 0 \tag{2.4.7}$$

then we have a solution to the boundary value problem corresponding to α. For such a solution, if in addition we have that $\bar{u}(0) = \bar{u}(1)$, then it must be a symmetric solution.

Any solution $\bar{u}(x)$ must satisfy $\bar{u}(x) \leq K(x)$ for all x. Since

$$K(0) = \frac{1 - e^{-1/\varepsilon}}{2} < \frac{1}{2}$$

we only consider values of $\bar{u}(0) < 1/2$. Also, since $K(x) - \bar{u}(x)$ is also a solution then if $\alpha < \frac{1}{2}K(0)$ corresponds to a solution so does $K(0) - \alpha$.

Example C. For this set of numerical studies, we explore the number of solutions to the boundary value problem depend on ε and the function f. To do this we solve the initial value problem for (2.1.4) with data given by (2.4.6), with $\alpha < K(0)$. The resulting solution $\bar{u}(x)$ will be a solution of the boundary value problem if (2.4.7) holds. We plot the quantity $\bar{u}(1) + \varepsilon \bar{u}'(1)$ as a function of α, and note that zeros of it correspond to solutions to the boundary value problem.

We also plot $\bar{u}(0) - \bar{u}(1)$ as a function of α. From the above,

- If $\bar{u}(1) + \varepsilon \bar{u}'(1) = 0$ and $\bar{u}(0) - \bar{u}(1) = 0$ then α is the initial value of a symmetric

solution.

- If $\bar{u}(1) + \varepsilon\bar{u}'(1) = 0$ and $\bar{u}(0) - \bar{u}(1) \neq 0$ then α is the initial value of a non-symmetric solution.

From the above analysis we have that the graphs of $\bar{u}(1) + \varepsilon\bar{u}'(1)$ and $\bar{u}(0) - \bar{u}(1)$ are antisymmetric about $\alpha = \frac{1}{2}K(0)$. We can also identify the three solutions in (2.3.2) from these graphs. The solutions 0 and $K(x)$ correspond to $\alpha = 0$ and $\alpha = K(0)$. The solution $\frac{1}{2}K(x)$ is the only solution which is both symmetric and non-symmetric (in the sense of (2.3.4) and (2.3.5)) and corresponds to $\alpha = \frac{1}{2}K(0)$.

In Figure 2.7 we have used the function given by (2.4.2) with $\gamma = 2.5$. Note that for this function

$$f'\left(\frac{1}{2}\right) \approx 1.25. \tag{2.4.8}$$

Figure 2.7**(a)** shows the graphs of $\bar{u}(1) + \varepsilon\bar{u}'(1)$ and $\bar{u}(0) - \bar{u}(1)$ as a function of α with $\varepsilon = 1.5$. The result shows that we only have the three solutions given in (2.3.2).

Figure 2.7**(b)** shows the graphs for $\varepsilon = 1$. For $\alpha < \frac{1}{2}K(0)$ we have two additional solutions, one symmetric and the other non-symmetric.

In Figure 2.7**(c)** we have $\varepsilon = 0.05$. We now have gained two symmetric and three non-symmetric solutions for $\alpha < \frac{1}{2}K(0)$. In general, these pictures show that for large enough ε there are no additional solutions and that the number of solutions increases as ε decreases.

Let α_k be the initial values for these solutions with

$$0 < \alpha_1 < \alpha_2 < \alpha_3 < \alpha_4 < \alpha_5 < \frac{1}{2}K(0).$$

The symmetric solutions correspond to the initial values α_2 and α_4 while the others correspond to non-symmetric solutions.

In Figure 2.8 the function f is given by (2.4.2) with $\gamma = 25$. In this case

$$f'\left(\frac{1}{2}\right) \approx 12.5 \tag{2.4.9}$$

which is much larger than the slope in (2.4.8). Compared with results in Figure 2.7 we will see that this leads to

- more solutions for the same ε .
- larger value of ε needed to only have solutions given by (2.3.2).

Figure 2.8**(a)** shows that the only solutions are those given by (2.3.2) for $\varepsilon = 5.5$. Figure 2.8**(b)** shows the results for $\varepsilon = 1.5$ where we have an additional non-symmetric solutions. Note that there were no additional solutions for the same value of ε in Figure 2.7.

Figures 2.8**(c)** and 2.8**(d)** show that as we decrease ε that we increase the number of solutions. We conjecture that as $\varepsilon \to 0$, the number of solutions increase without bound.

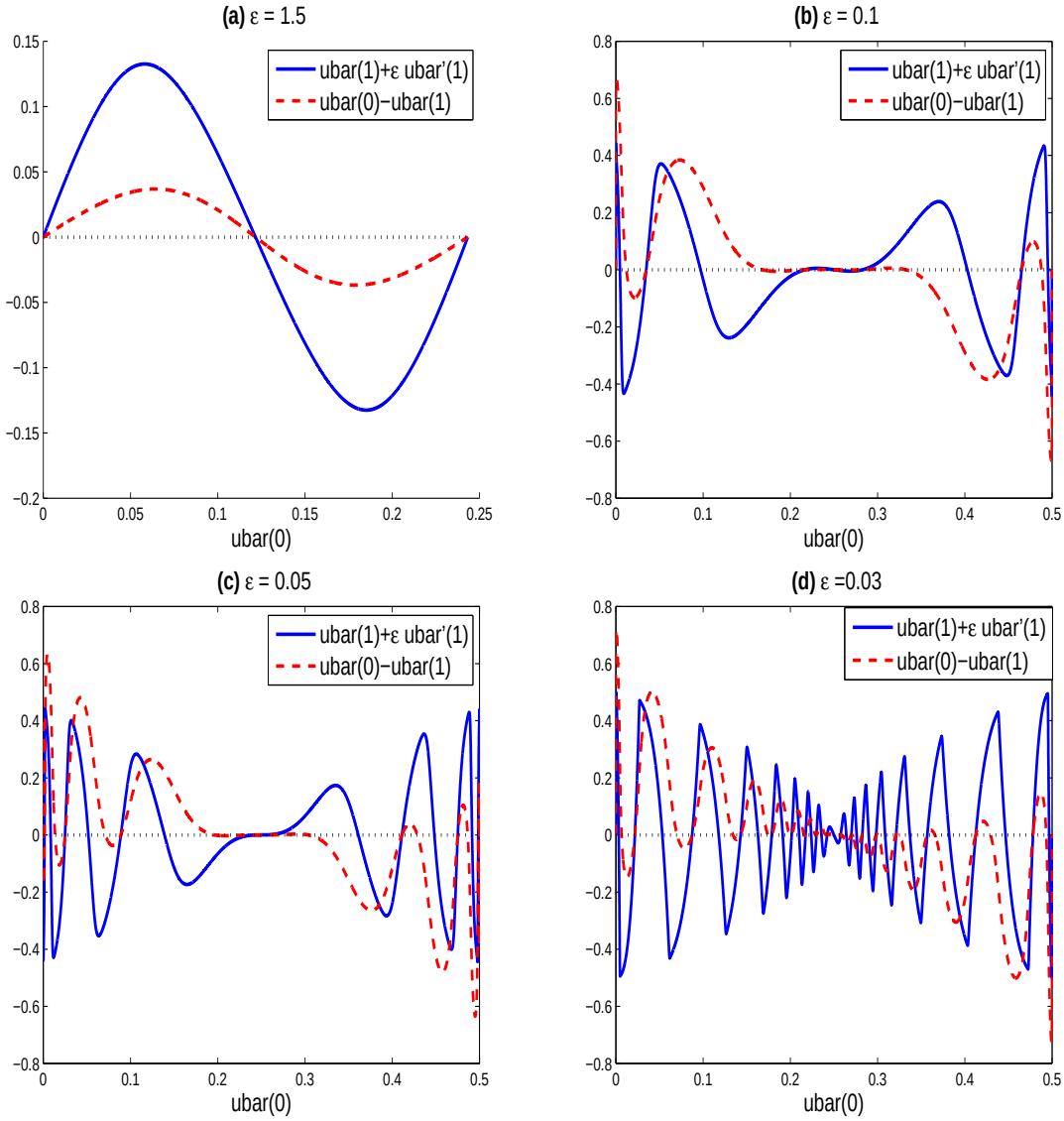

Figure 2.7: Solutions to the boundary value problem with f given by (2.4.2) and $\gamma = 2.5$ occur at the values of $\bar{u}(0)$ where $\bar{u}(1) + \bar{u}(0)$ and $\bar{u}(1) + \varepsilon\bar{u}(0)$ are zero.

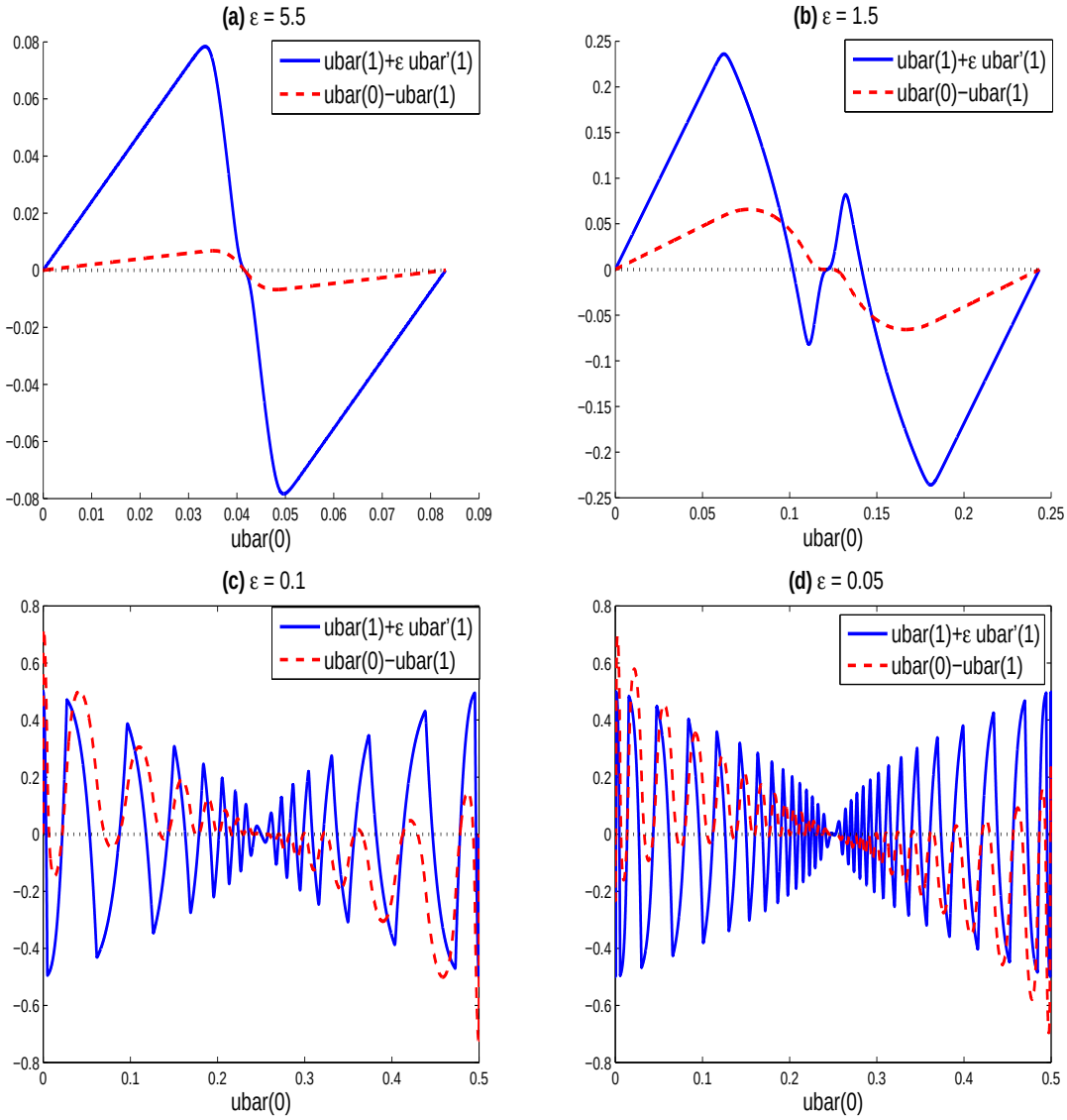

Figure 2.8: Solutions to the boundary value problem with f given by (2.4.2) and $\gamma = 25$ occur at the values of $\bar{u}(0)$ where where $\bar{u}(1) + \bar{u}(0)$ and $\bar{u}(1) + \varepsilon\bar{u}(0)$ are zero.

In this example we let f be given by (2.4.2) with $\gamma = 80.$ and $\varepsilon = 0.2$. In this case

$$f'\left(\frac{1}{2}\right) \approx 40$$

so by experience with the previous examples we expect the boundary value problem to have many solutions.

In Figure 2.9 we have plotted the graph of solutions $\bar{u}(x)$ with n layers for $1 \leq n \leq 4$. As expected, all the non-symmetric solutions cross $\frac{1}{2}K(x)$ at $x = 1/2$ while all the symmetric solutions satisfies $\bar{u}'\left(\frac{1}{2}\right) = 0$. We also note that the crossing points of solutions are interlaced.

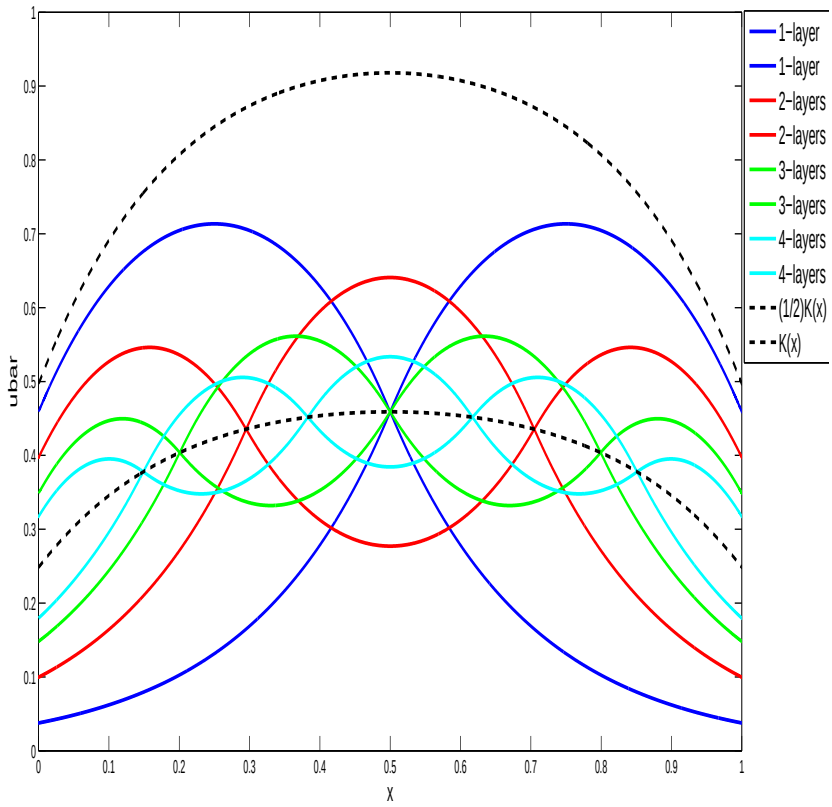

Figure 2.9: Solutions with $1 \leq n \leq 4$ layers (one to five crossing for $\frac{1}{2}K(x)$) with $\varepsilon = 0.2$. The graph of the solutions as expected, all the non-symmetric solutions cross $\frac{1}{2}K(x)$ at $x = 1/2$ while all the symmetric solutions satisfies $\bar{u}'\left(\frac{1}{2}\right) = 0$. Again $\frac{1}{2}K(x)$ and $K(x)$ also plotted to show the crossing place and the upper bound respectively.

Chapter 3

Equilibrium solutions with a discontinuous nonlinearity

3.1 Introduction

In this chapter we study solutions of the equilibrium equation (1.3.1-1.3.2) when the function f is given by

$$f(\bar{u}) = \begin{cases} 1 & \text{when } \bar{u} \geq \frac{1}{2} \\ \\ 0 & \text{when } \bar{u} < \frac{1}{2} \end{cases} \tag{3.1.1}$$

and the kernel is given by the kernel (1.3.3). This f could arise in the simplest on-off switch mechanism in the original cell renewal model, and also is the limit case as f get steeper. The resulting system is a non-smooth dynamical system [19, 31, 39, 58].

A solution is a C^1 function $\bar{u} : [0,1] \to \mathbb{R}$ that satisfies

$$\varepsilon^2 \bar{u}''(x) = \bar{u}(x) - f\left(\frac{\bar{u}(x)}{1-h(x)}\right) \tag{3.1.2}$$

where

$$h(x) = \frac{1}{2}\left(e^{-x/\varepsilon} + e^{-(1-x)/\varepsilon}\right)$$

and $\varepsilon > 0$, for all $x \in (0,1)$ except for a finite number of points x_k for which $2\bar{u}(x_k) = 1 - h(x_k)$, together with the boundary conditions

$$\bar{u}(0) = \varepsilon \bar{u}'(0), \quad \bar{u}(1) = -\varepsilon \bar{u}'(1). \tag{3.1.3}$$

The goal is to give a complete description of all solutions and to classify them according to the number of points for which $2\bar{u}(x_k) = 1 - h(x_k)$. We show in the next section that if a solution hits this switching boundary (where the solution crosses (1/2)K(x)) then it immediately leaves it; that is, if for some x_k we have $2\bar{u}(x_k) = 1 - h(x_k)$ then $2\bar{u}'(x_k) \neq (1 - h(x_k))'$. This will justify looking for solutions with only a finite number of points on the switching boundary. The solutions of (3.1.2) alternate between solutions of

$$\varepsilon^2 \bar{u}''(x) = \bar{u}(x) \quad \text{and} \quad \varepsilon^2 \bar{u}''(x) = \bar{u}(x) - 1$$

as $\bar{u}(x)$ crosses the switching boundary $(1 - h(x))/2$ and f jumps between 0 and 1.

We can solve each of these equations and construct solutions to the boundary value problem by gluing the various pieces of solution together. However, the procedure becomes quite complicated and it is difficult to see the structure of the solutions if we use this method. In

the next section we show how a change of variables can be used which exposes the structure of solutions to (3.1.2)-(3.1.3).

In Section 2.2 we considered the approximation $K(x) = 1$ in (3.1.2) so that

$$\varepsilon^2 \bar{u}''(x) = \bar{u} - f(\bar{u}). \tag{3.1.4}$$

We proved that if f was smooth (C^1 suffices) then the boundary value problem (3.1.4)-(3.1.3) does not have a solution. Below we prove that this result still holds for the discontinuous f given by (3.1.1).

Theorem 3.1.1. *With f given by (3.1.1), the boundary value problem (3.1.4)-(3.1.3) does not have a solution.*

Proof. Without loss of generality we may assume that $\bar{u}(0) < 1/2$. Solving $\varepsilon^2 \bar{u}''(x) = \bar{u}$,

$$\bar{u}(x) = \alpha e^{x/\varepsilon}, \quad 0 \le x \le x_1.$$

At the transition point x_1,

$$\bar{u}\,(x_1) = \alpha e^{x_1/\varepsilon} = \frac{1}{2}. \tag{3.1.5}$$

Solving $\varepsilon^2 \bar{u}''(x) = \bar{u} - 1$ for $x_1 \le x \le x_2$,

$$\bar{u}(x) = Ae^{-x/\varepsilon} + Be^{x/\varepsilon} + 1$$

Using continuity of $\bar{u}$ and $\bar{u}'$ at $x = x_1$,

$$\alpha e^{x_1/\varepsilon} = Ae^{-x_1/\varepsilon} + Be^{x_1/\varepsilon} + 1$$

$$\alpha e^{x_1/\varepsilon} = -Ae^{-x_1/\varepsilon} + Be^{x_1/\varepsilon}$$

so that $A = -\frac{1}{2}e^{x_1/\varepsilon}, B = \alpha - \frac{1}{2}e^{-x_1/\varepsilon}$, using (3.1.5), $B = 0$ and $A = -\frac{1}{4\alpha}$ and so

$$\bar{u}(x) = 1 - \frac{1}{4\alpha}e^{-x/\varepsilon}, \quad x_1 \leq x \leq x_2.$$

Hence for $x_1 \leq x \leq x_2, \bar{u}'(x) > 0$ so the boundary condition (3.1.3) at $x = 1$ cannot be satisfied and $\bar{u}(x) > \frac{1}{2}$. This completes the proof. □

As in the continuous case, $\bar{u}(x) = 0$ and $\bar{u}(x) = K(x) = 1 - h(x)$ are always equilibrium solutions. Also, Theorem 2.3.1 part (a) holds so that if $\bar{u}(x)$ is an equilibrium solution so too are $\bar{u}(1-x), K(x) - \bar{u}(x)$ and $K(x) - \bar{u}(1-x)$.

3.2 Existence of solutions

For a solution $\bar{u}(x)$ of (3.1.2)-(3.1.3) we define regions 1 and 2 of [0,1] by

$$R_1 = \{x : \bar{u}(x) < \frac{1}{2}(1 - h(x))\}, \quad R_2 = \{x : \bar{u}(x) > \frac{1}{2}(1 - h(x))\}.$$

Because of the special nature of the function $f(\bar{u})$, we have that

$$\varepsilon^2\bar{u}''(x) = \bar{u}(x) \quad \text{for} \quad x \in R_1, \quad \varepsilon^2\bar{u}''(x) = \bar{u}(x) - 1 \quad \text{for} \quad x \in R_2.$$

We change variables so that we have a single equation. For $x \in R_1$ define $v(x) = v_1(x)$ by

$$v_1(x) = \frac{1}{2}(1 - h(x)) - \bar{u}(x) \tag{3.2.1}$$

and for $x \in R_2$, $v(x) = v_2(x)$ is defined by

$$v_2(x) = \bar{u}(x) - \frac{1}{2}\left(1 - h\left(x\right)\right). \tag{3.2.2}$$

A calculation shows that in both cases $v(x)$ satisfies

$$\varepsilon^2 v''(x) = v(x) - \frac{1}{2} \tag{3.2.3}$$

and the boundary conditions

$$v(0) = \varepsilon v'(0), \quad v(1) = -\varepsilon v'(1). \tag{3.2.4}$$

The phase portrait for (3.2.3) is shown in Figure 3.1. Note that we are using $\varepsilon v'$ for the vertical axis. Equation (3.2.3) has the equilibrium point $v = \dfrac{1}{2}$ which is a saddle. The stable and unstable manifolds of this equilibrium are straight lines with slopes ± 1 in the v, $\varepsilon v'$ plane where the Jacobian is

$$A = \begin{bmatrix} 0 & \frac{1}{\varepsilon} \\ \frac{1}{\varepsilon} & 0 \end{bmatrix}.$$

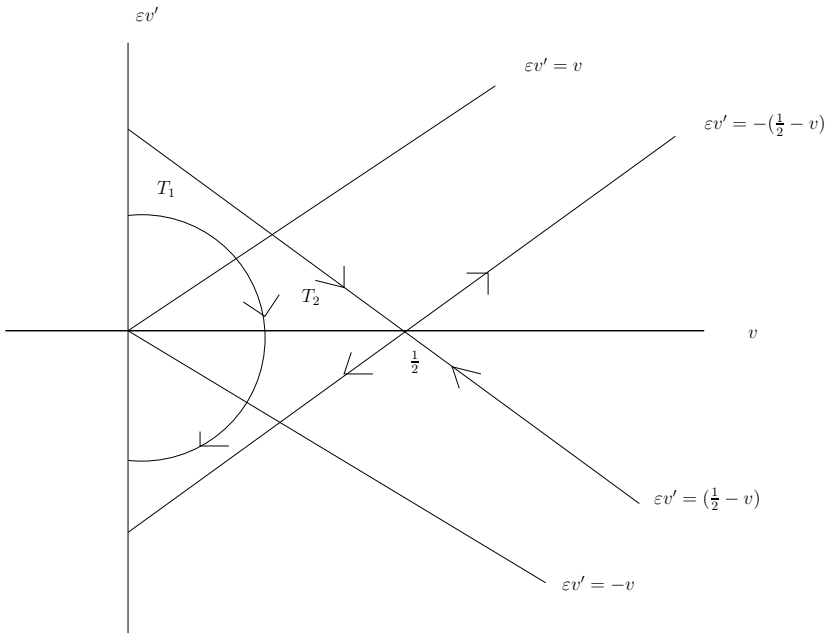

Figure 3.1: Phase plane of (3.2.3). A solution of the boundary value problem (3.2.3)-(3.2.4) starts on the line $\varepsilon v' = v$ at $x = 0$ and finishes at $x = 1$ on the line $\varepsilon v' = -v$. It follows the same orbit for equation (3.2.3) with each transition untill it hits $v(x_k) = 0, v'(x_k) < 0$ representing a solution in a particular region or phase.

If $\bar{u}$ is a solution of the boundary value problem (3.1.2)-(3.1.3) then $1 - h(x) - \bar{u}(x)$ is also a solution. Hence to study all solutions we can assume that

$$0 < \bar{u}(0) = \alpha < \frac{1}{2}\left(1 - h\left(0\right)\right) \tag{3.2.5}$$

for the rest of this chapter. This means that $x = 0$ is in the R_1 and that

$$v(0) = \frac{1 - \left(4\alpha + e^{-1/\varepsilon}\right)}{4} > 0. \tag{3.2.6}$$

For solutions to the boundary value problem, we show that the relevant part of the phase

portrait in Figure 3.1 is the triangle T formed by the the lines $\varepsilon v' = \pm\left(\frac{1}{2} - v\right)$ and $v = 0$. From (3.2.6) we have that $v(0) < \frac{1}{4}$ and that v starts on the line $\varepsilon v' = v$ inside the triangle T. The switching boundary which divides the R_1 and R_2 is now given by $v = 0$. The solution evolves until at some point $x_1 > 0$ we have $v(x_1) = 0$. At this point we have that $v'(x_1) < 0$ so that the solution will move to R_2. From (3.2.2) the new solution $v = v_2$ satisfies

$$v(x_1) = 0, \quad v'(x_1) = -v_1'(x_1) > 0. \tag{3.2.7}$$

The solution $v_2(x)$ would then be followed untill $v_2(x_2) = 0, v_2'(x_2) < 0$ and the solution would return to R_1. We would then follow the solution $v = v_1$ with

$$v(x_2) = 0, \quad v'(x_2) = -v_2'(x_2) > 0. \tag{3.2.8}$$

Suppose that at the point $x = 1$, the solution was on the line $\varepsilon v' = -v$. This would mean that we had a solution $\bar{u}(x)$ of the boundary value problem which starts and ends in R_1 and is in the R_2 for $x_1 < x < x_2$.

In general, a solution of the boundary value problem (3.2.3)-(3.2.4) starts on the line $\varepsilon v' = v$ at $x = 0$ and finishes at $x = 1$ on te line $\varepsilon v' = -v$. It follows the same orbit for equation (3.2.3) with each transition untill it hits $v(x_k) = 0, v'(x_k) < 0$ representing a solution in a particular region or phase. It is convenient to describe solution with $m + 2$ phases with $m = 0, 1, 2, ...$ so that there are $m + 1$ transition points x_k. The solution described above

with three phases has $m = 1$ and transition points x_1, x_2. Any solution v of (3.2.3) satisfies

$$(\varepsilon v')^2 = \left(v - \frac{1}{2}\right)^2 + k$$

where k is constant. The orbits we are interested in have $v(0) = \dfrac{1 - \left(4\alpha + e^{-1/\varepsilon}\right)}{4}$ and $\varepsilon v'(0) = v(0)$ so that

$$(\varepsilon v')^2 = \left(v - \frac{1}{2}\right)^2 - \frac{1}{4}\left(4\alpha + e^{-1/\varepsilon}\right) \tag{3.2.9}$$

To make progress we need to calculate the "time" taken for solutions to go from various places on the orbits (3.2.9). By summetry, we only need to calculate T_1 and T_2 where

- T_1 is the "time" taken to travel from $v = 0$ to $\varepsilon v' = v$ with $v > 0$.
- T_2 is the "time" to go from from $\varepsilon v' = v$ to $\varepsilon v' = 0$.

Lemma 3.2.1. *Assume α satisfies (3.2.5) and define $q = q(\alpha)$ by*

$$q = 1 - \left(4\alpha + e^{-1/\varepsilon}\right)$$

Then

$$T_1 = \varepsilon \ln\left(1 + \sqrt{q}\right), \quad T_2 = -\frac{\varepsilon}{2}\ln\left(1 - q\right). \tag{3.2.10}$$

Proof. Since $x = 0$ is in R_1 we have $\varepsilon^2 \bar{u}''(x) = \bar{u}(x)$ for small x and the boundary condition $\varepsilon \bar{u}' = \bar{u}$ at $x = 0$ implies that $\bar{u}(x) = \alpha e^{x/\varepsilon}$. Hence

$$v(x) = \frac{1}{2} - \frac{1}{4}e^{-x/\varepsilon} - \frac{1}{4}e^{x/\varepsilon}\left(4\alpha + e^{-1/\varepsilon}\right). \tag{3.2.11}$$

In order to calculate T_1, we need to find the point $x < 0$ for which $v(x) = 0$. We would then

have $T_1 = -x$. Solving $v(x) = 0$ gives

$$e^{2x/\varepsilon}\left(4\alpha + e^{-1/\varepsilon}\right) - 2e^{x/\varepsilon} + 1 = 0$$

and this leads to

$$T_1 = -x = -\varepsilon \ln\left(\frac{1 - \sqrt{1 - 4\alpha + e^{-1/\varepsilon}}}{4\alpha + e^{-1/\varepsilon}}\right) = \varepsilon \ln(1 + \sqrt{q}).$$

From (3.2.9), if $v'(\bar{x}) = 0$ and $v(\bar{x}) < \dfrac{1}{2}$ we have that

$$v(\bar{x}) = \frac{1 - \sqrt{4\alpha + e^{-1/\varepsilon}}}{2}.$$

Solving this equation with $v(x)$ given by (3.2.11) gives

$$T_2 = \bar{x} = -\frac{\varepsilon}{2} \ln(1 - q).$$

and this completes the proof.

□

We use Lemma 3.2.1 to prove the existence of a unique solution to the boundary value problem with $m + 2$ phases for any $m = 0, 1, 2, ...$ for α satisfying (3.2.5). Before doing this we study the solution with two phases ($m = 0$) since we can find an exact expression for α in this case.

Suppose that we have a solution to the boundary value problem that is in R_1 for $0 \leq x < \bar{x}$ and R_2 for $\bar{x} < x \leq 1$. For such a solution to exist, we need to find α with

$$0 < 4\alpha < 1 - e^{-1/\varepsilon} \tag{3.2.12}$$

and

$$2\left(T_1 + 2T_2\right) = 1. \tag{3.2.13}$$

From Lemma 3.2.1, we require

$$2\varepsilon \ln\left(\frac{1}{1-\sqrt{q}}\right) = 1.$$

Hence

$$\alpha = \frac{e^{-1/(2\varepsilon)} - e^{-1/\varepsilon}}{2}.$$

Clearly $\alpha > 0$ and since

$$1 - e^{-1/\varepsilon} - 4\alpha = \left(1 - e^{-1/(2\varepsilon)}\right)^2 > 0$$

we have that (3.2.12) holds for all $\varepsilon > 0$. This shows that there is a unique solution of this type. For this solution the transition point is $x = \frac{1}{2}$ since $v\left(\frac{1}{2}\right) = 0$.

We give the details of the representation of solutions to the boundary value problem with $m+2$ phases. The transition points $x_k, \quad k = 1, \cdots, m+1$ are given by

$$x_k = T_1 + 2T_2 + (k-1)\left(2T_1 + 2T_2\right), \quad k = 1, \cdots, m+1.$$

The solution of (3.2.3) with $v(0)$ given by (3.2.6) is given in equation (3.2.11). Note that

$$v\left(-T_1\right) = v\left(2T_2 + T_1\right) = 0$$

and

$$v(0) = \varepsilon v'(0) = v\left(2T_2\right) = -\varepsilon v'\left(2T_2\right).$$

For the initial portion of the solution

$$\bar{u}(x) = \frac{1}{2}\left(1 - h\left(x\right)\right) - v(x), \quad 0 \leq x \leq x_1$$

and in the next interval

$$\bar{u}(x) = \frac{1}{2}\left(1 - h\left(x\right)\right) + v\left(x - x_1 - T_1\right), \quad x_1 \leq x \leq x_2.$$

The solution continues in this way, alternating between regions 1 and 2. For a solution with $\bar{u}(1) = -\varepsilon\bar{u}'(1)$ we must have that

$$2\left(T_1 + 2T_2\right) + m\left(2T_1 + 2T_2\right) = x_{m+1} + T_1 + 2T_2 = x_{m+1} + x_1 = 1$$

and in the final interval the solution will be in R_1 if m is odd and in R_2 if m is even. Hence

$$\bar{u}(x) = \frac{1}{2}\left(1 - h\left(x\right)\right) + (-1)^{m+1} v\left(x - x_{m+1} - T_1\right), \quad x_{m+1} \leq x \leq 1.$$

Theorem 3.2.2. *For all $\varepsilon > 0$ and $m = 0, 1, 2, ...$ there is a unique solution with $m + 2$ phases with α satisfying (3.2.12).*

Proof. We have a solution with $m + 2$ phases if

$$2\left(T_1 + 2T_2\right) + m\left(2T_1 + 2T_2\right) = 1.$$

By Lemma 3.2.1, the equation is

$$\varepsilon \ln\left[\frac{\left(1 + \sqrt{q}\right)^m}{\left(1 - \sqrt{q}\right)^{m+2}}\right] = 1.$$

Write $\delta = e^{-1/\varepsilon}$ and $z = 1 - \sqrt{q}$. Then the equation is

$$H(z) = z^{m+2} - \delta(2-z)^m = 0. \tag{3.2.14}$$

We have $H(0) < 0, H(1) > 0$ and $H'(z) > 0$ for $0 < z < 1$. Hence H has a unique zero $\bar{z}$ in the interval $(0,1)$. To complete the proof we need to show that $0 < 4\alpha < 1 - \delta$. Since

$$q = (1-\bar{z})^2 = 1 - 2\bar{z} + \bar{z}^2 = 1 - 4\alpha - \delta$$

we have that

$$4\alpha = 2\bar{z} - \bar{z}^2 - \delta$$

and

$$1 - \delta - 4\alpha = (1-\bar{z})^2 > 0.$$

To prove that $\alpha > 0$ we need to show that

$$\bar{z} > 1 - \sqrt{1-\delta}.$$

We have $H(\bar{z}) = 0$ and $H'(\bar{z}) > 0$. Hence if we can show that $H\left(1 - \sqrt{1-\delta}\right) < 0$ then this will show that $\alpha > 0$. Now

$$H\left(1-\sqrt{1-\delta}\right) = \left(1-\sqrt{1-\delta}\right)^{m+2} - \delta\left(2 - \left(1-\sqrt{1-\delta}\right)\right)^m$$

and

$$-\left(1-\sqrt{1-\delta}\right)^m H\left(1-\sqrt{1-\delta}\right) = \left(\sqrt{\delta}\right)^{2(m+1)} - \left(1-\sqrt{1-\delta}\right)^{2(m+1)} > 0$$

since $\sqrt{\delta} + \sqrt{1-\delta} > 1$ for $0 < \delta < 1$. □

3.3 Structure and asymptotic behaviour of solutions

The change of variables involved in the construction of solutions to the boundary value problem makes clear the structure of solutions. We recall that we assume (3.2.5) so that solutions $\bar{u}(x)$ start in R_1. For $m = 0, 1, \cdots$ we have a solution with $m+2$ phases with $m+1$ transition points $0 < x_1 < \cdots < x_k < x_{m+1} < 1$. The transition points satisfy $x_1 = 1 - x_{m+1}$ and the spacing between the crossing points is constant, that is $x_{k+1} - x_k$ is a constant for $k = 1, \cdots, m$. The symmetries enjoyed by $\bar{u}(x)$ depend on the parity of m.

Theorem 3.3.1. *For m odd we have that*

$$\bar{u}(x) = \bar{u}(1 - x) \tag{3.3.1}$$

while for m even we have

$$\bar{u}(x) + \bar{u}(1 - x) = 1 - h(x) \tag{3.3.2}$$

Proof. Theorem 2.3.1 about symmetries of solutions of the general boundary value problem assumed that the nonlinearity was continuous. A simple modification to the proof shows that Theorem 2.3.1 also holds when f is given by (3.1.1) and we made use of these results. If m is odd then the final phase is in R_1. Hence $\bar{u}(0) = \bar{u}(1)$ so that $\bar{u}(x) = \bar{u}(1 - x)$. If m is even then the final phase is in R_2 and

$$\frac{1}{2}\left(1 - h\left(0\right)\right) - \bar{u}(0) = \bar{u}(1) - \frac{1}{2}\left(1 - h\left(1\right)\right).$$

Since $h(0) = h(1)$ we have that

$$\bar{u}(0) + \bar{u}(1) = 1 - h(0)$$

and so by Theorem 2.3.1, (3.3.2) holds. □

Before studying the general case of the asymptotic behaviour of solutions, it is instructive to look at the two phase solution ($m = 0$) for large and small ε. For this solution (3.3.2) holds and for $0 \leq x \leq \frac{1}{2}$ it is given by

$$\bar{u}(x) = \alpha e^{x/\varepsilon} = \left(\frac{e^{-1/(2\varepsilon)} - e^{-1/\varepsilon}}{2} \right) e^{x/\varepsilon} \tag{3.3.3}$$

and for $\frac{1}{2} \leq x \leq 1$ by

$$\bar{u}(x) = 1 - \frac{\delta}{2} e^{x/\varepsilon} - \frac{(\delta)^{-1/2}}{2} e^{-x/\varepsilon}. \tag{3.3.4}$$

The solution increases on the interval $\left[0, \frac{3}{4}\right]$ and decreases on $\left[\frac{3}{4}, 1\right]$. Also,

$$\bar{u}\left(\frac{1}{2}\right) = \frac{1 - h\left(\frac{1}{2}\right)}{2} = \frac{1 - \delta^{1/2}}{2} = \bar{u}\,(1)$$

and the maximum value of $\bar{u}$ is

$$\bar{u}\left(\frac{3}{4}\right) = 1 - \delta^{1/4}.$$

Consider first the case of ε small. For $0 \leq x < \frac{1}{2}$ with x bounded away from $1/2$, the solution is exponentially close to 0. For $x > 1/2$ with x bounded away from $1/2$ and 1 the solution is exponentially close to 1. At the transition point $x = 1/2$ and at $x = 1$ there are sharp transition layers. In Figure 3.2**(a)** we show the exact solution $\bar{u}(x)$ for $\varepsilon = 0.02$. We also show the solution $K(x) - \bar{u}(x)$. For the general case of fixed $m > 0$ and small ε we will have a similar picture. Away from transition points $x_1, x_2, \cdots, x_{m+1}$ the solution is exponentially close to either 0 or 1 and near the transition points the solution changes rapidly.

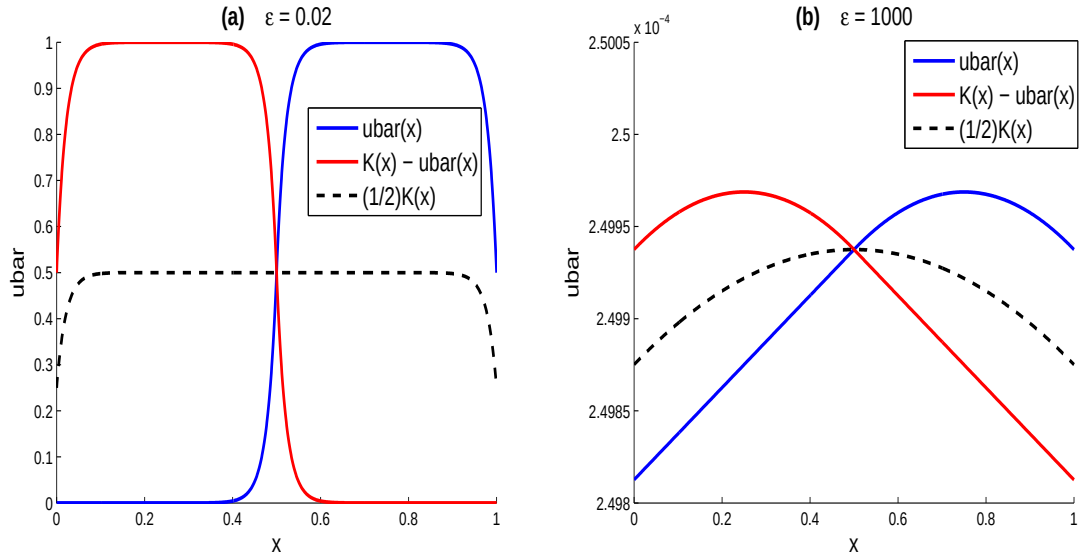

Figure 3.2: Exact solutions with a single layer (one crossing of $\frac{1}{2}K(x)$) with $\varepsilon = 0.02$ and 1000. For small ε the solution is exponentially close to either 0 or 1 and near the crossing point the solution changes rapidly. For large ε the solution is exponentially small.

We return to the $m = 0$ case with ε large. Using (3.3.3) and (3.3.4) we calculate that $\bar{u}(x)$ is small for all x with maximum value given by

$$\bar{u}\left(\frac{3}{4}\right) = \frac{1}{4\varepsilon} - \frac{1}{32\varepsilon^2} + O\left(\varepsilon^{-3}\right)$$

and

$$\bar{u}\left(\frac{3}{4}\right) - \bar{u}(0) = \frac{5}{32\varepsilon^2} + O\left(\varepsilon^{-3}\right).$$

For $0 \leq x \leq 1/2$ the solution is approximately linear with

$$\bar{u}\left(x\right) = \frac{1}{4\varepsilon} - \frac{3}{16\varepsilon^2} + \frac{x}{4\varepsilon^2} + O\left(\varepsilon^{-3}\right).$$

Figure 3.2**(b)** shows an exact solution $\bar{u}(x)$ with $\varepsilon = 1000$. As predicted, the solution is very small and is approximately linear for $0 < x < 1/2$. We also show the solution $K(x) - \bar{u}(x)$. For the general case of fixed $m > 0$ the solutions are all small when ε is large.

In the section that follows, we examine solutions for large and small ε with a fixed number of transition layers. Figure 3.3 shows the exact solutions for k transition layers $(2 \leq k \leq 5)$ for $\varepsilon = 0.02$ and for $\varepsilon = 1000$. It is clear that for large ε the solution is exponentially small. For small ε the solution is either 0 or 1 apart from the transition layers.

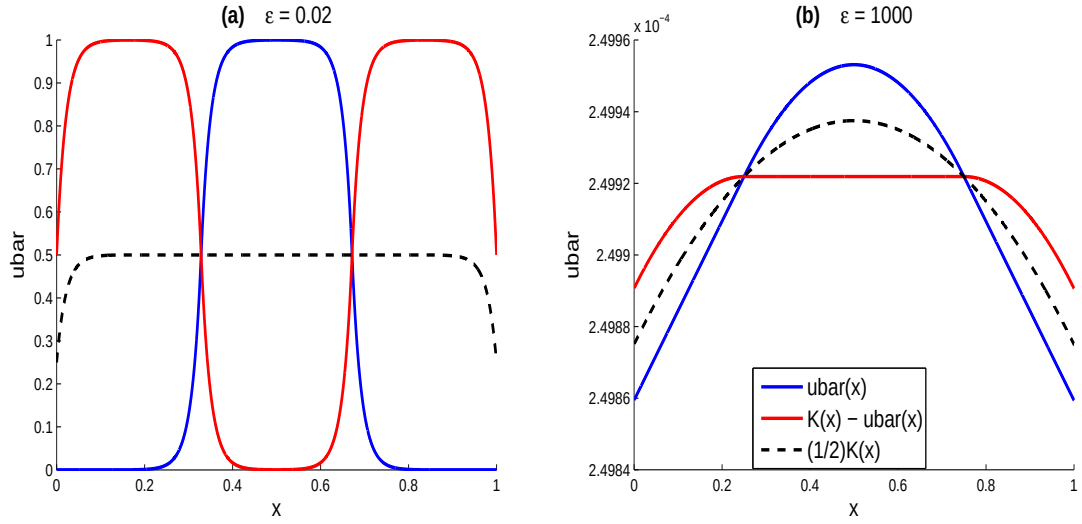

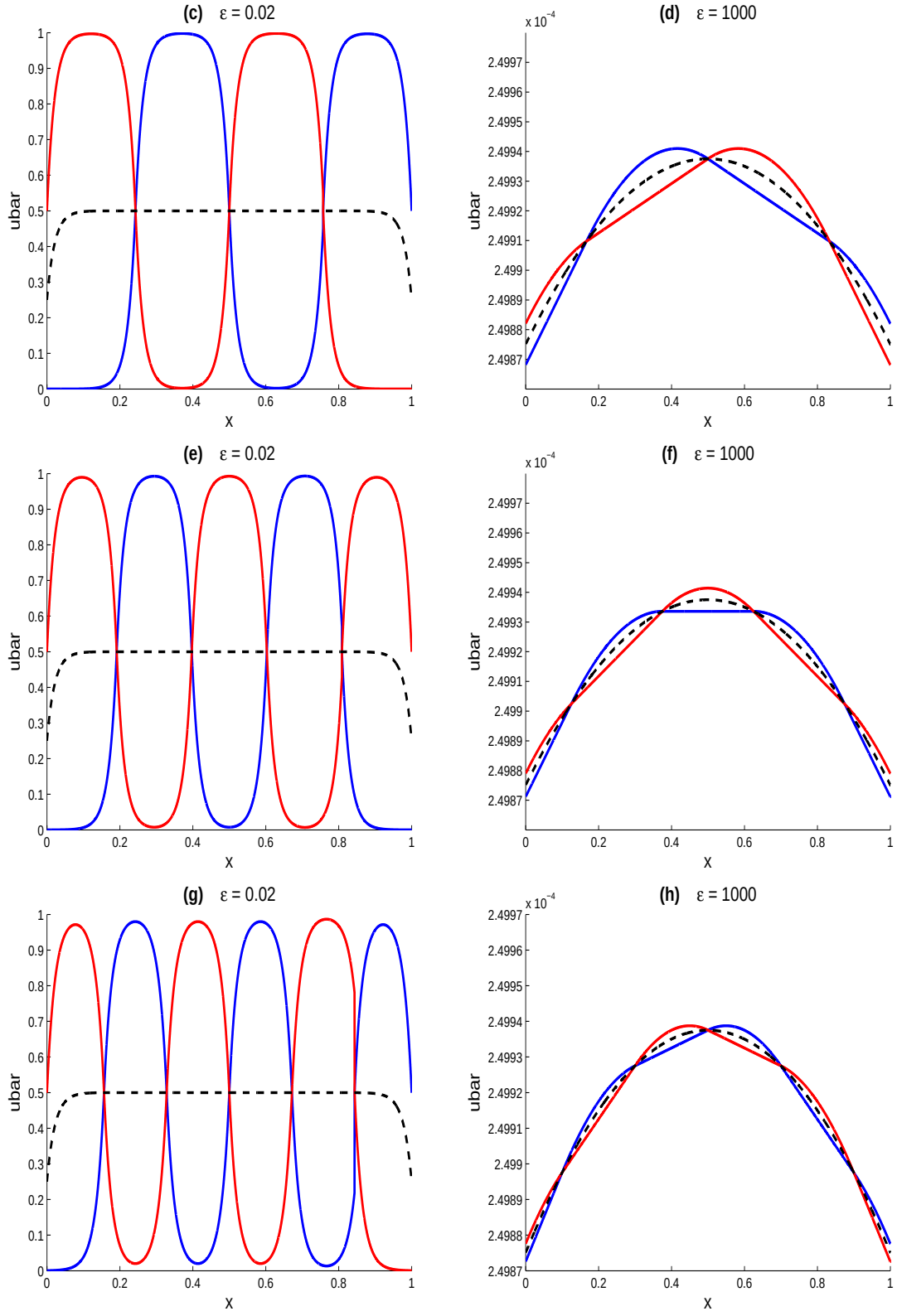

Figure 3.3: Exact solutions with two to five layers for small and large ε.

3.3.1 Asymptotic behaviour for large ε and fixed m

We assume throughout this subsection that $\bar{u}$ is a solution with $m+2$ phases and that ε is large. Since $\bar{u}$ is bounded, $\bar{u}''$ will be small and the solution will be almost constant for $0 \leq x \leq 1$. Since $\bar{u}$ crosses the curve

$$\frac{1}{2}\left(1 - h\left(x\right)\right) \tag{3.3.5}$$

$m+1$ times we see that $\bar{u}(x)$ will be close to (3.3.5). The minimum and maximum values of (3.3.5) occur at $x = 0$ and $x = 1/2$ with

$$\frac{1}{2}\left(1 - h\left(0\right)\right) = \frac{1-\delta}{4} = \frac{1}{4\varepsilon} - \frac{1}{8\varepsilon^2}$$

and

$$\frac{1}{2}\left(1 - h\left(\frac{1}{2}\right)\right) = \frac{1-\delta^{1/2}}{2} = \frac{1}{4\varepsilon} - \frac{1}{16\varepsilon^2}.$$

Hence (3.3.5) is very small for $0 \leq x \leq 1$ and changes by a quantity which is $O\left(\varepsilon^{-2}\right)$.

Theorem 3.3.2. *For fixed m and large ε,*

$$\bar{u}(x) = \frac{1}{2}\left(1 - h\left(x\right)\right) + O\left(\varepsilon^{-2}\right), \quad 0 \leq x \leq 1.$$

Proof. We begin by estimating the solution of (3.2.14). Write $\theta = \varepsilon^{-1}$ and

$$H\left(z, \theta\right) = z^{m+2} - e^{-\theta}\left(2 - z\right)^m = 0. \tag{3.3.6}$$

Since $H(1,0) = 0$ and $H_z\left(1,0\right) = 2m + 2 \neq 0$, by the Implicit Function Theorem, (3.3.6) has a unique zero $z = z(\theta)$ with $z(0) = 1$ for small θ so that

$$z = 1 + O\left(\theta\right).$$

Since $q = 1 - (4\alpha + \delta) = (1 - z)^2$, we have that

$$1 - (4\alpha + \delta) = O\left(\varepsilon^{-2}\right) \tag{3.3.7}$$

and

$$\alpha = \frac{1}{4\varepsilon} + O\left(\varepsilon^{-2}\right).$$

It is interesting to note that the leading order term for α does not depend on m. We use this information to show that $v(x) = O\left(\varepsilon^{-2}\right)$. The maximum value of v is at $v' = 0$. From (3.2.9), the maximum value of v is

$$v = \frac{1}{2} - \frac{1}{2}\left(4\alpha + \delta\right)^{1/2} = O\left(\varepsilon^{-2}\right)$$

by (3.3.7). The result follows. □

3.3.2 Asymptotic behaviour for fixed ε and large m

Let $\varepsilon > 0$ be fixed and m be large. Let $\bar{u}$ be a solution with $m + 2$ phases. Since $\bar{u}$ has to cross the curve (3.3.5) we will have that $\bar{u}(x)$ is close to (3.3.5) for $0 \leq x \leq 1$. The proof of this will follow the same ideas as the proof of Theorem 3.3.2.

Theorem 3.3.3. *For fixed ε and large m,*

$$\bar{u}(x) = \frac{1}{2}\left(1 - h\left(x\right)\right) + O\left(m^{-2}\right), \quad 0 \leq x \leq 1.$$

Proof. Let $z = 1 + am^{-1} + bm^{-2} + O(m^{-3})$ where a and b do not depend on m. Then a calculation shows that

$$H\left(z\right) = z^{m+2} - \delta\left(2 - z\right)^m = e^a\left[1 + \frac{2b - a^2 + 4a}{2m}\right] - e^{-1/\varepsilon}e^{-a}\left[1 - \frac{2b + a^2}{2m}\right] + O\left(m^{-2}\right).$$

Let $a = \frac{-1}{2\varepsilon}$, then

$$H(z) = e^a \left(\frac{2b + 2a}{m} + O\left(m^{-2}\right) \right).$$

So by considering $4b + 2a$ positive and negative we obtain

$$z = 1 - \frac{1}{2\varepsilon m} + O\left(m^{-2}\right).$$

Hence

$$1 - (4\alpha + \delta) = O\left(m^{-2}\right)$$

and as in the proof of Theorem 3.3.2 we obtain $v(x) = O\left(m^{-2}\right)$ which completes the proof.

□

3.3.3 Asymptotic behaviour for fixed m and small ε

For the $m = 0$ case in which we have two phases, there is the exact expression for $\bar{u}(0) = \alpha = \frac{\delta^{1/2} - \delta}{2}$ so that α is exponentially small for ε small. For the case of a general m we obtain a similar estimate for α. In equation (3.2.14) we change variables via

$$z = c_m \delta^{\frac{1}{m+2}} y, \quad c_m = 2^{\frac{m}{m+2}}, \quad \theta = \delta^{\frac{1}{m+2}}$$

which leads to the equation

$$\bar{H}(y, \theta) = y^{m+2} - \left(1 - \frac{\theta c_m}{2}\right)^m = 0. \tag{3.3.8}$$

We have $\bar{H}(1, 0) = 0, \bar{H}_z(1, 0) \neq 0$ so by the Implicit Function Theorem, (3.3.8) has a solution $y = 1 + O(\theta)$ for small θ. It follows that for small ε, the solution of (3.2.14) is exponentially

small with

$$z = c_m \delta^{\frac{1}{m+2}} + O\left(\delta^{\frac{2}{m+2}}\right). \tag{3.3.9}$$

For x in the first interval $[0, x_1]$ we have that $\bar{u}(x) = \alpha e^{x/\varepsilon}$. A similar analysis to the one for the $m = 0$ case shows that $\bar{u}(x)$ is exponentially small in this first interval except near $x = x_1$ where there is a sharp transition layer. Next, we study the asymptotic behaviour when x is in a region $[x_k, x_{k+1}]$ which does not contain the points $x = 0$ or $x = 1$. The solution in this interval is given by

$$\bar{u}(x) = \frac{1 - h(x)}{2} + (-1)^{k+1} v(x - x_k - T_1), \quad x_k \le x \le x_{k+1}. \tag{3.3.10}$$

We will show that $\bar{u}(x)$ is exponentially close to either 0 or 1 except near the points x_k and x_{k+1}.

We write I_k for the interval $[x_k, x_{k+1}]$. Since I_k does not contain the points 0 and 1 we have that $\dfrac{1 - h(x)}{2}$ is exponentially close to $1/2$ in this interval. Hence

$$\frac{1 - h(x)}{2} = \frac{1}{2} + O\left(e^{-a/\varepsilon}\right), \quad x \in I_k \tag{3.3.11}$$

where a is a constant depending only on m.

From earlier calculations, we have that

$$v(x) = \frac{1}{2} - \frac{1}{4} e^{-x/\varepsilon} - \frac{e^{x/\varepsilon}}{4}(4\alpha + \delta), \quad -T_1 \le x \le T_1 + 2T_2. \tag{3.3.12}$$

We will show that except for an interval of length order ε at x_k and x_{k+1}, the $v(x - x_k - T_1)$ term in (3.3.10) is exponentially close to $1/2$. This will show that $\bar{u}(x)$ is close to 1 or 0

depending on the parity of k.

The initial value for $v(0)$ given by (3.2.6) is exponentially close to $1/4$. It follows that the orbit of (3.2.3) is very close to the stable and unstable manifolds for the equilibrium $v = 1/2$. The solution will spend most of the time near $1/2$ corresponding to $0 \leq x \leq 2T_2$ in (3.3.12).

We will show that $T_1 = O(\varepsilon)$ and this will correspond to the layers of width $O(\varepsilon)$ near x_k and x_{k+1} in which the solution $\bar{u}(x)$ changes rapidly.

By Lemma 3.2.1,

$$T_1 = \varepsilon \ln\left(1 + \sqrt{q}\right), \quad T_2 = -\frac{\varepsilon}{2} \ln(1 - q)$$

where $q = 1 - (4\alpha + \delta)$. Using $z = 1 - \sqrt{q}$ we have that

$$T_1 = \varepsilon \ln(2 - z), \quad T_2 = -\frac{\varepsilon}{2} \ln(4\alpha + \delta) = -\frac{\varepsilon}{2} \ln\left(2z - z^2\right). \tag{3.3.13}$$

Using the estimate for z given by (3.3.9) we have that

$$T_1 = \varepsilon \ln(2) + O\left(\delta^{\frac{1}{m+2}}\right), \quad T_2 = \frac{1}{2(m+2)} + O(\varepsilon). \tag{3.3.14}$$

Let $g(y) = \frac{1}{2} - v(x - x_k - T_1)$ where $y = x - x_k - T_1$. Then

$$g(y) = \frac{1}{4} e^{-y/\varepsilon} + \frac{1}{4} e^{y/\varepsilon} (4\alpha + \delta) \tag{3.3.15}$$

for y in the interval $[-T_1, T_1 + 2T_2]$. We show that $g(y)$ is exponentially small in a subinterval which omits the endpoints. From the symmetry of the phase plane for the v equation we have that

$$g(y + T_2) = g(T_2 - y), \quad 0 \leq y \leq T_1 + T_2.$$

It follows that we only need to study $g(y)$ for y in half the interval

$$J = [T_2, T_1 + 2T_2]\,.$$

From the estimate for T_2 in (3.3.14) we have that the first term in (3.3.15) is $O\left(e^{-a/\varepsilon}\right)$ for $y \in J$. For the second term in (3.3.15) we first note that by (3.3.13),

$$4\alpha + \delta = e^{-2T_2/\varepsilon}$$

and hence

$$(4\alpha + \delta)\, e^{y/\varepsilon} = e^{-(2T_2 - y)/\varepsilon}. \tag{3.3.16}$$

For y bounded away from $2T_2$ the term in (3.3.16) is exponentially small. The remaining part of the interval J given by $[2T_2, 2T_2 + T_1]$ has length $\varepsilon \ln 2$ by (3.3.14) during which the solution changes rapidly.

Finally, when m is even we need to consider $\bar{u}(x)$ near $x = 1$. In this case we only need to study $g(y)$ in the interval $[-T_1, 2T_2]$ and the function $g(y)$ is small except near $2T_2$. The change in the solution $\bar{u}(x)$ in this case comes from the $e^{-(1-x)/\varepsilon}$ term in $h(x)$.

3.4 Summary

In this chapter we have given a complete analysis of the equilibrium equation (3.1.2)-(3.1.3) when f is the step function. This consists of two linear equations. Each of these equations can be solved analytically and the solution of the boundary value problem can be found by combining solutions to the two problems. However, this is very complicated to carry out and

it would be difficult to obtain general results by following this procedure.

In Section 3.2 we show that a change of variables leads to the single equation (3.2.3). This allows us to clearly understand the structure of solutions to the boundary value problem. We prove that nontrivial solutions exist for any value of ε. We also derive detailed information about solutions for large and small ε as well as the behaviour of solutions which intersect the switching boundary a large number of times. This detailed information about a special case is useful as framework for understanding the general case. The stability of the equilibrium will be discussed in details as a future work.

Chapter 4

Numerical approximation of the time dependent problem

4.1 Introduction

We start in Section 4.2 by describing a semidiscrete spatial collocation method using a piecewise constant approximation in space for the general problem (1.3.1). This approximation is similar to the methods described in [4, 25] for a related nonlocal problem, and it is analysed for convergence in Section 4.3 in a similar way. In Section 4.4 we examine a special 1-periodic, linear version of the problem which has an exact solution that is reasonably easy to compute in terms of a Fourier series, and hence serves as a benchmark to measure the accuracy of the approximation. We use a simple error estimate based on mesh halving to measure the errors in the other cases. In Section 4.5 we present numerical results for the nonlinear problem with each kernel. We continue in Section 4.6 with a brief investigation of the computational time required using different ODE solvers and different ways to evaluate

the spatial averaging operator, including the FFT. We finish in Section 4.7 with a numerical approximation for the full local equation given by (1.4.1).

4.2 Piecewise constant spatial collocation approximation

In this section we describe a spatial collocation approximation of the full problem

$$u_t = f(\hat{u}) - u \tag{4.2.1}$$

where

$$\hat{u}(x,t) = \frac{1}{K(x)} \int_0^1 J(x-y)u(y,t)dy$$

defined in Section 1.3. We use a piecewise constant approximation in space defined by

$$u(x,t) \approx u_h(x,t) = \sum_{k=1}^{N} u_k(t)\phi_{k-1/2}(x) \tag{4.2.2}$$

where the basis functions are

$$\phi_{k-1/2}(x) = \begin{cases} 1, & x \in (x_{k-1}, x_k) \\ 0, & \text{otherwise,} \end{cases}$$

and the x_k are the node points. We use a uniform grid of width $h = 1/N$ so that $x_k = kh$. The midpoint values are $x_{k-1/2} = (x_{k-1} + x_k)/2$.

The collocation method consists of substituting the approximate solution (4.2.2) into the full problem equation (4.2.1) above and requiring it to be satisfied at the element midpoints

$x = x_{j-1/2}$. This gives a set of equations for the element values $u_j(t)$ in the form

$$\frac{du_j}{dt} = f(\hat{u}_h(x_{j-1/2}, t) - u_j, \quad \text{for } j = 1, \ldots, N$$

where

$$\hat{u}_h(x_{j-1/2}, t) = \left(\frac{1}{K(x_{j-1/2})}\right) \int_0^1 J(x_{j-1/2} - y) \sum_{k=1}^{N} u_k(t)\phi_{k-1/2}(y)\, dy.$$

We can write

$$\hat{u}_h(x_{j-1/2}, t) = \sum_{k=1}^{N} A_{j,k} u_k$$

where

$$A_{j,k} = \left(\frac{1}{\int_0^1 J(x_{j-1/2} - y)dy}\right) \int_{x_{k-1}}^{x_k} J(x_{j-1/2} - y)dy \quad \forall j, k = 1, \cdots, N.$$

We finally obtain a system of N first order nonlinear ODEs

$$\frac{du_j}{dt} = \left(f\left(\sum_{k=1}^{N} A_{j,k} u_k\right) - u_j\right), \quad j = 1, ..., N \tag{4.2.3}$$

which can be solved by different ODE solvers in Matlab e.g. ode45 and ode15s. The resulting nonlinear system of ODEs can be linked to similar system that comes from Hopfield model in neural networks. In the continuous model,

$$\frac{du_j}{dt} = \gamma\left(\sum_{j=1}^{N} w_{i,j} s(u_j) - u_j\right), \quad j = 1, ..., N$$

By scaling gamma and reorganizing the second term in the equation we can see how the system can be applied to a Hopfield model [1, 50, 62, 71].

4.3 Convergence analysis

Here we carry out a theortical convergence analysis for the scheme in Section 4.2 and describe how to verify this prediction by numerical experiment.

In this section we use the definitions

$$(\mathbb{L}u)(x) = \frac{1}{K(x)} \int_0^1 J(x-y)u(y)dy, \quad x \in [0,1]$$

$$(\mathbb{L}_h u)(x) = \frac{1}{K(x_{j-1/2})} \int_0^1 J(x_{j-1/2}-y)u(y)dy, \quad x \in (x_{j-1}, x_j)$$

for $j = 1, \cdots, N$. Also, we use the fact that $0 \leq u \leq 1$ for all $t \geq 0$.

Theorem 4.3.1. *If f is Lipshitz, $K(x)$ and $J(x)$ are sufficently smooth, and u_h is bounded, the piecewise constant collocation approximation u_h defined in Section 4.2 satisfies*

$$\|u - u_h\| = O(h) \quad \forall t \in [0,T]\,,$$

where u is the exact solution of (1.3.1).

Proof. Define $e = u - u_h$ and differentiate with respect to t to get

$$e_t = f(\mathbb{L}u) - u + u_h - f(\mathbb{L}_h u_h)$$

$$= -e + f(\mathbb{L}u) - f(\mathbb{L}_h u_h).$$

Multiplying by ε and integrating over the domain (notice that f is Lipshitz with constant

L) gives

$$\begin{aligned}(e_t, e) &= -(e, e) + (e, f(\mathbb{L}u) - f(\mathbb{L}_h u_h)) \\ &\leq -\|e\|^2 + \|e\|\|f(\mathbb{L}u) - f(\mathbb{L}_h u_h)\| \\ &\leq -\|e\|^2 + L\|e\|\|\mathbb{L}u - \mathbb{L}_h u_h\| \\ &\leq -\|e\|^2 + L\|e\|(\|\mathbb{L}(u - u_h)\| + \|(\mathbb{L} - \mathbb{L}_h)u_h\|) \\ &\leq -\|e\|^2 + LC_1\|e\|^2 + L\|e\|\|(\mathbb{L} - \mathbb{L}_h)u_h\|\end{aligned}$$

where $C_1 = \|\mathbb{L}\|$. The left hand side $(e_t, e) = \frac{1}{2}\frac{d}{dt}\|e\|^2$ and so after cancelling the common factor $\|e\|$ we have

$$\frac{d}{dt}\|e\| \leq -\|e\| + LC_1\|e\| + L\|(\mathbb{L} - \mathbb{L}_h)u_h\|.$$

Now we consider the last term

$$\|(\mathbb{L} - \mathbb{L}_h)u_h\|^2 = \sum_{j=1}^{N} \int_{x_{j-1}}^{x_j} \left(\mathbb{L}u_h - \mathbb{L}_h u_h\right)^2 dx$$

$$= \sum_{j=1}^{N} \int_{x_{j-1}}^{x_j} \left[\frac{1}{K(x)} \int_0^1 J(x-y)u_h(y)dy - \frac{1}{K(x_{j-1/2})} \int_0^1 J(x_{j-1/2} - y)u_h(y)dy\right]^2 dx.$$

We obtain

$$\|(\mathbb{L} - \mathbb{L}_h)u_h\|^2 = \sum_{j=1}^{N} \int_{x_{j-1}}^{x_j} I_j^2 dx \tag{4.3.1}$$

where

$$I_j = \frac{1}{K(x)K(x_{j-1/2})} \int_0^1 (J(x-y)K(x_{j-1/2}) - K(x)J(x_{j-1/2} - y))u_h(y)dy.$$

We do a Taylor expansion for $J(x-y) = J(x_{j-1/2} - y) + \left(x - x_{j-1/2}\right) J'(x_{j-1/2} - y) + \cdots$ (avoiding $y = x_{j-1/2}$ at this stage) and $K(x) = K(x_{j-1/2}) + \left(x - x_{j-1/2}\right) K'(x_{j-1/2}) + \cdots$

and substitute it in I_j

$$I_j = \frac{x - x_{j-1/2}}{K(x)} \int_0^1 J'(x_{j-1/2} - y) u_h(y) dy - \frac{(x - x_{j-1/2}) K'(x_{j-1/2})}{K(x) K(x_{j-1/2})} \int_0^1 J(x_{j-1/2} - y) u_h(y) dy + \cdots$$

The apparent difficulty with $J'(0^+) \neq J'(0^-)$ for the exponential decay kernel is removed on the process of integration since we have

$$\int_0^1 J'(x_{j-1/2} - y) u_h(y) dy = \int_0^{x_{j-1/2}} J'(x_{j-1/2} - y) u_h(y) dy + \int_{x_{j-1/2}}^1 J'(x_{j-1/2} - y) u_h(y) dy$$

and the integrals on the right hand side are well defined.

Now we can Taylor expand $\frac{1}{K(x)} = \frac{1}{K(x_{j-1/2})} + (x - x_{j-1/2}) \left(\frac{-K'}{K^2}\right) + \cdots$ to get

$$|I_j| \leq C_2 |x - x_{j-1/2}| \tag{4.3.2}$$

where

$$C_2 = \int_0^1 \frac{J'(x_{j-1/2} - y)}{K(x_{j-1/2})} u_h(y) dy - \int_0^1 \frac{K'(x_{j-1/2}) J(x_{j-1/2} - y)}{K(x_{j-1/2})^2} u_h(y) dy,$$

and substitute in (4.3.1) to get

$$\|(\mathbb{L} - \mathbb{L}_h) u_h\|^2 \leq C_2^2 \sum_{j=1}^N \int_{x_{j-1}}^{x_j} (x - x_{j-1/2})^2 dx = C_2^2 \frac{h^2}{12} \tag{4.3.3}$$

which implies that

$$\frac{d}{dt}\|e\| \leq -\|e\| + LC_1\|e\| + LC_2 \frac{h}{\sqrt{12}}$$

and that can be solved exactly giving

$$\|e(t)\| \leq \frac{\sqrt{3}}{6} \quad \frac{C_2 L h}{LC_1 - 1} \left(e^{(LC_1 - 1)t} - 1\right) + \|e(0)\| e^{(LC_1 - 1)t}. \tag{4.3.4}$$

Provided the initial approximation is chosen so that $u_h(x, 0) = u(x, 0) + O(h)$ the result follows. □

4.4 A linear test case with an exact solution

Here we introduce a linear problem which has an exact solution defined in terms of Fourier series and use this as a test for the numerical scheme defined in Section 4.2.

We consider our model problem (1.3.1) in the linear case $f(u) = u$ on a 1-periodic space domain with the piecewise constant kernel. The periodic linear model problem is then

$$u_t(x,t) = \hat{u}(x,t) - u(x,t), \quad x \in [0,1], t > 0 \tag{4.4.1}$$

where

$$\hat{u}(x,t) = \frac{1}{2\varepsilon}\int_{-\varepsilon}^{\varepsilon} u(x+y,t)dy$$

and $u(x,t)$ is 1-periodic in x.

Assuming that u is smooth enough, we write it as the Fourier expansion

$$u = \sum_{n=-\infty}^{\infty} a_n(t)\exp(2\pi i n x),$$

and from definition of $\hat{u}$ we have

$$\hat{u} = \sum_{n=-\infty}^{\infty} a_n(t)\exp(2\pi i n x)\ \mathrm{sinc}(2\pi n\varepsilon), \quad \text{for} \quad n = 0, \pm 1, \pm 2, \ldots.$$

To obtain this we apply the definition of $\hat{u}$ term by term and get

$$\left(\frac{1}{2\varepsilon}\right)\int_{-\varepsilon}^{\varepsilon}\exp(2\pi i n(x+s))\,ds = \left(\frac{\exp(2\pi i n x)}{2\varepsilon}\right)\int_{-\varepsilon}^{\varepsilon}\exp(2\pi i n s))\,ds$$

$$= \exp(2\pi i n x)\,\mathrm{sinc}(2\pi n\varepsilon)$$

for $n = 0, \pm 1, \pm 2, \ldots$.

Using the shorthand $\gamma_n = \operatorname{sinc}(2\pi n\varepsilon)$, our model (4.4.1) gives

$$\sum_{n=-\infty}^{\infty} \dot{a}_n(t) \exp(2\pi i n x) = \sum_{n=-\infty}^{\infty} a_n(t)(\gamma_n - 1) \exp(2\pi i n x)$$

and the orthonormality of the Fourier basis gives the equation for the Fourier amplitudes,

$$\dot{a}_n = a_n (\gamma_n - 1) \quad \forall n \in \mathbb{Z}. \tag{4.4.2}$$

Solving these equations we get

$$a_n(t) = \exp((\gamma_n - 1)t) a_n(0) \quad \forall n \in \mathbb{Z}$$

and since $\gamma_0 = 1$ and $\gamma_n < 1$ for $n \neq 0$ we have $u \to a_0(0)$ as $t \to \infty$.

Parameter ε plays an important role in determining the time the solution takes to approach equilibrium. For all $\varepsilon > 0$ we have

$$u(x,t) - a_0(0) = \mathcal{O}\left(\mathrm{e}^{-\mu t}\right)$$

and the rate is determined by the size of $\mu > 0$. When $0 \leq \varepsilon \leq 1/2$ we have

$$\mu = 1 - \gamma_1$$

and for small ε

$$\mu = 1 - \gamma_1 = \frac{2}{3}\pi^2 \varepsilon^2 + \mathcal{O}(\varepsilon^4).$$

As ε increases towards $1/2$, μ increases steadily towards 1. For all values $\varepsilon > 1/2$ we have $0.85 < \mu \leq 1$. So in summary μ is small and convergence to equilibrium is very slow when ε is small. It speeds up when ε is bigger, but never converges in less than $\mathcal{O}(1)$ time since $\mu \leq 1$.

For the numerical experiments we use the method described in Section 4.2 applied with two different types of initial data: discontinuous layers

$$u(x,0) = \frac{1}{2}\left(H\left(x-0.1\right) - H\left(x-0.2\right) + H\left(x-0.6\right) - H\left(x-0.9\right)\right), \tag{4.4.3}$$

and the smooth function

$$u(x,0) = \frac{1}{\pi \coth\left(\pi\right)} \sum_{n=1}^{10000} \frac{2}{1+n^2} \cos\left(2\pi n x\right). \tag{4.4.4}$$

These are illustrated in Figure 4.1.

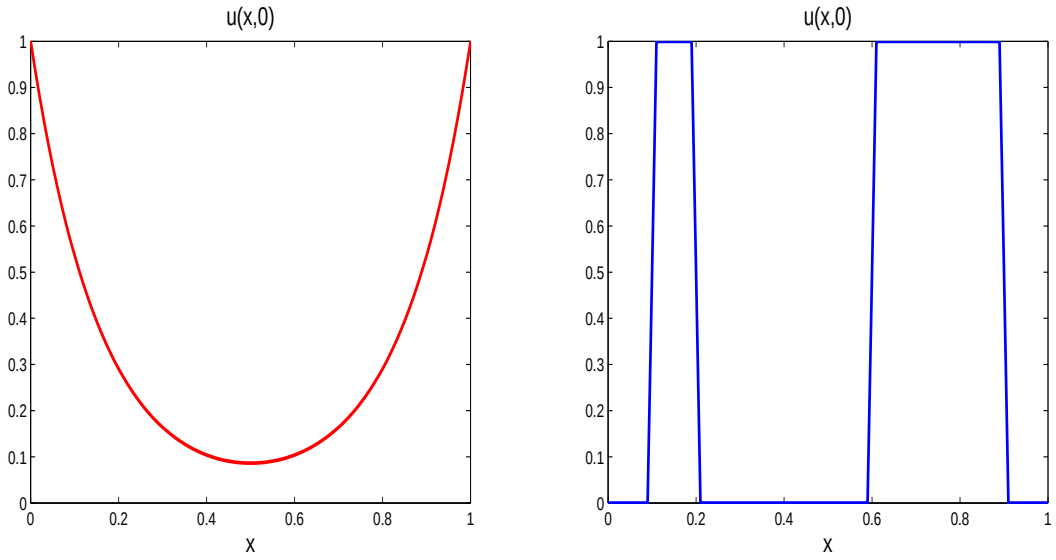

Figure 4.1: The initial conditions (4.4.3) on the left and (4.4.4) on the right.

We test the scheme for each of the kernels defined in Section 1.3. Because we have the exact solution for the piecewise kernel, we use that to measure the error directly. In other cases we measure the error by comparing approximate solutions on mesh size h and $h/2$. So the "exact error" in the following Figure is $\|u_h - u\|_{L_2}$ while the "L_2 error estimate" in the Figures is $\|u_h - u_{h/2}\|_{L_2}$, both at fixed times.

In Figure 4.2 we show results for the smooth initial data and piecewise kernel. We see that there is very good agreement between the exact and estimated errors in this case. Also, the error appears to behave like $O(h^2)$ as $h \to 0$, although the convergence analysis of the previous section predicts $O(h)$.

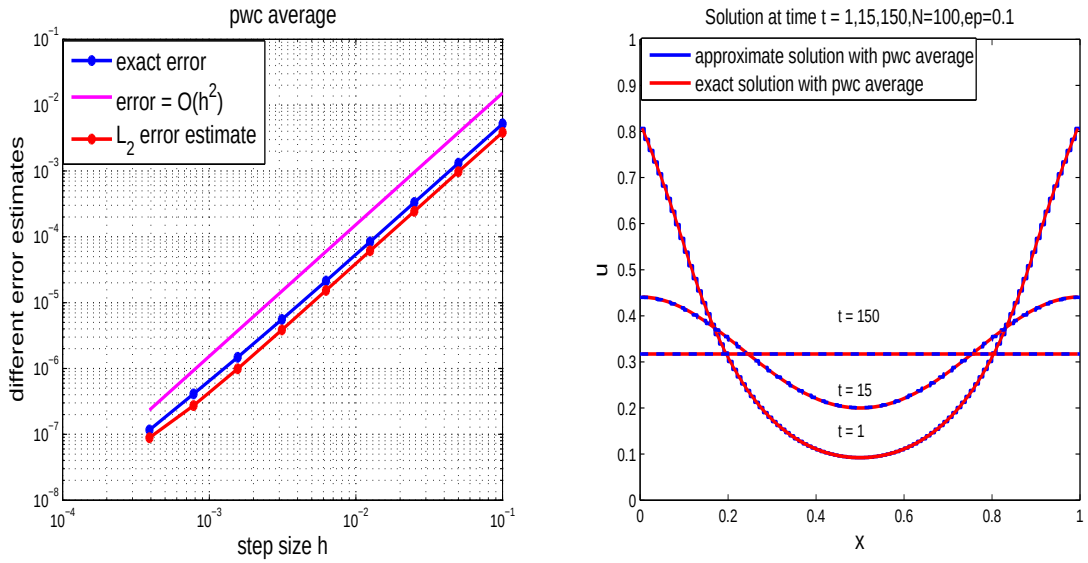

Figure 4.2: A comparison between the exact error and L_2 estimated error at $t = 10$ (left). The other picture shows the solution for the linear case with the piecewise kernel at $t = [1, 15, 150]$ and the exact solution for the same kernel at the same time. In both picures we use $\varepsilon = 0.1$.

In Figure 4.3 we show results for the larger value $\varepsilon = 0.35$ and compare the three different kernels for both smooth and discontinuous initial data. The discontinuous case (on the right) appears to converge as expected like $O(h)$. The smooth case converges like $O(h^2)$ for larger values of h, but shows clear evidence of a reduction in order towards $O(h)$ for small values of h.

The error estimate (4.3.4) contains a term involving the initial error, which in the smooth case satisfies $\|e(0)\| = O(h^2)$. It appears that the constants of proportionality involved are significantly smaller on the first term in (4.3.4) multiplying h and so the $O(h^2)$ behaviour dominates until h gets very small. The constants depend on ε, and this explains the slight

difference in where the convergence shifts from $O(h^2)$ to $O(h)$ between Figure 4.2 and Figure 4.3. In the discontinuous case, the initial error $\|e(0)\| = 0$ and so there is only an $O(h)$ convergence observed.

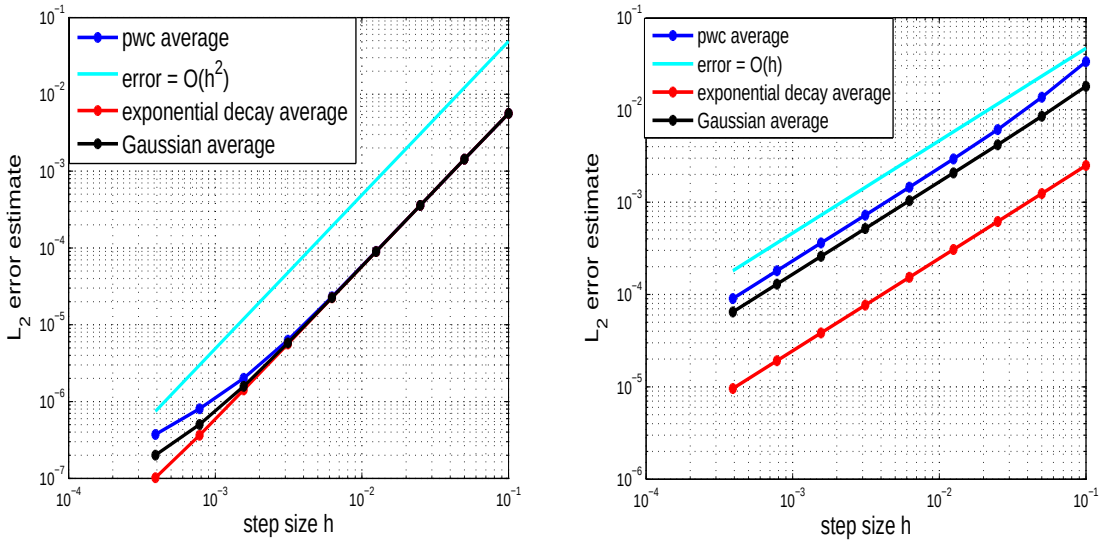

Figure 4.3: We compute the error at $t = 10$ with $\varepsilon = 0.35$, and the smooth initial data (left) and the discontinuous one (right).

In Figure 4.4 we show that $u_h \to a_0(0)$ as $t \to \infty$ as expected. We use discontinuous layer initial data for all three kernels with $\varepsilon = 0.1$. We notice that all the kernels converge to approximately the same equilibrium although the speed of convergence is different for each case. From the pictures we see that the exponential decay kernel converged in about 26 time units but the other kernels need about 150 time units.

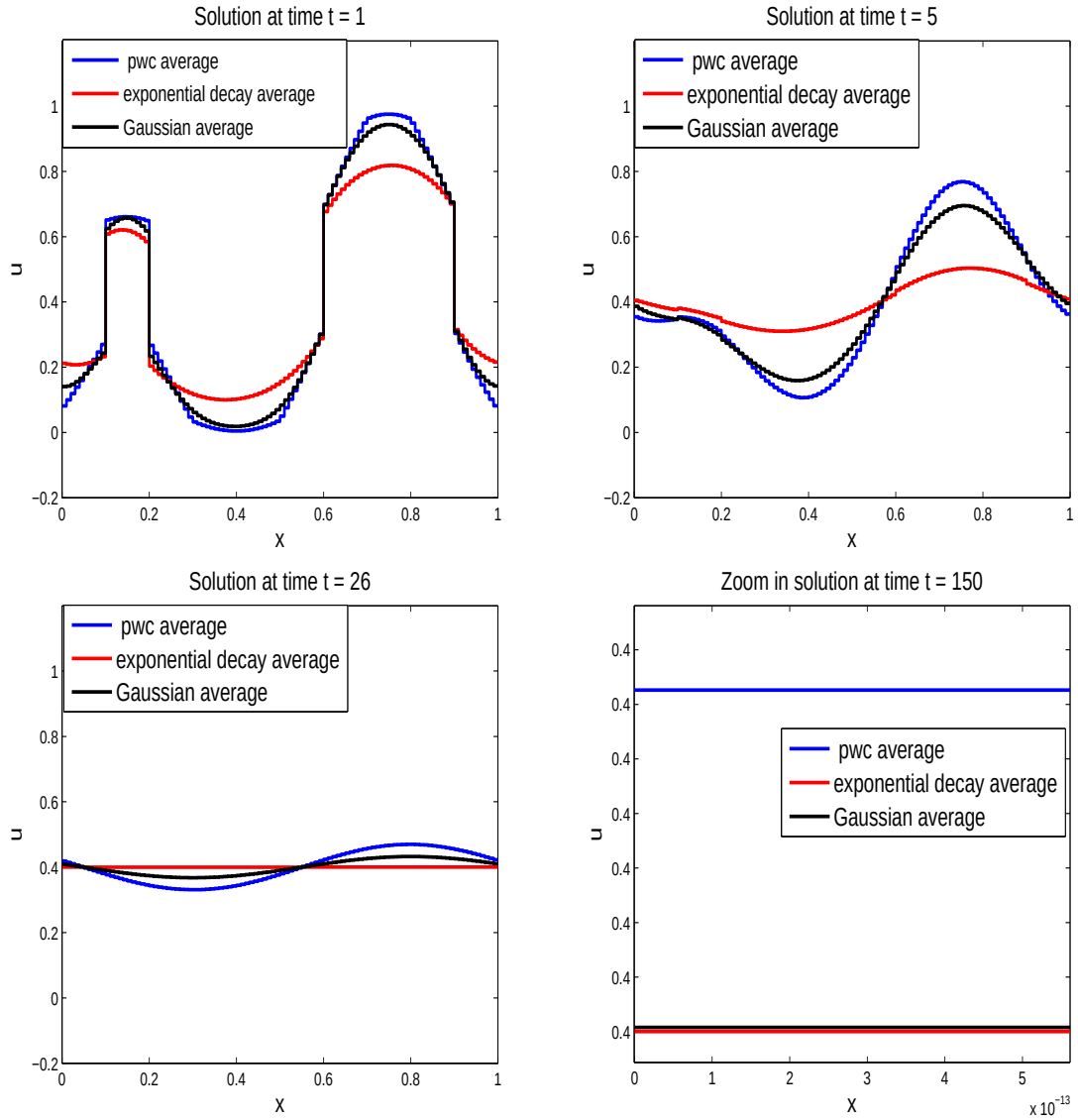

Figure 4.4: With fix $\varepsilon = 0.1$, we show the solution with a discontinuous initial data (4.4.3) for all the kernels at different time units $t = [1, 5, 26, 150]$.

In Figure 4.5 we show how the solution is influenced by the values of ε. We use discontinuous layer initial data for all three kernels with two different values $\varepsilon = 0.01$ and $\varepsilon = 0.08$. From the picture it is clear that for a small values of ε the solution takes longer to converge and for large ε it quickly converges.

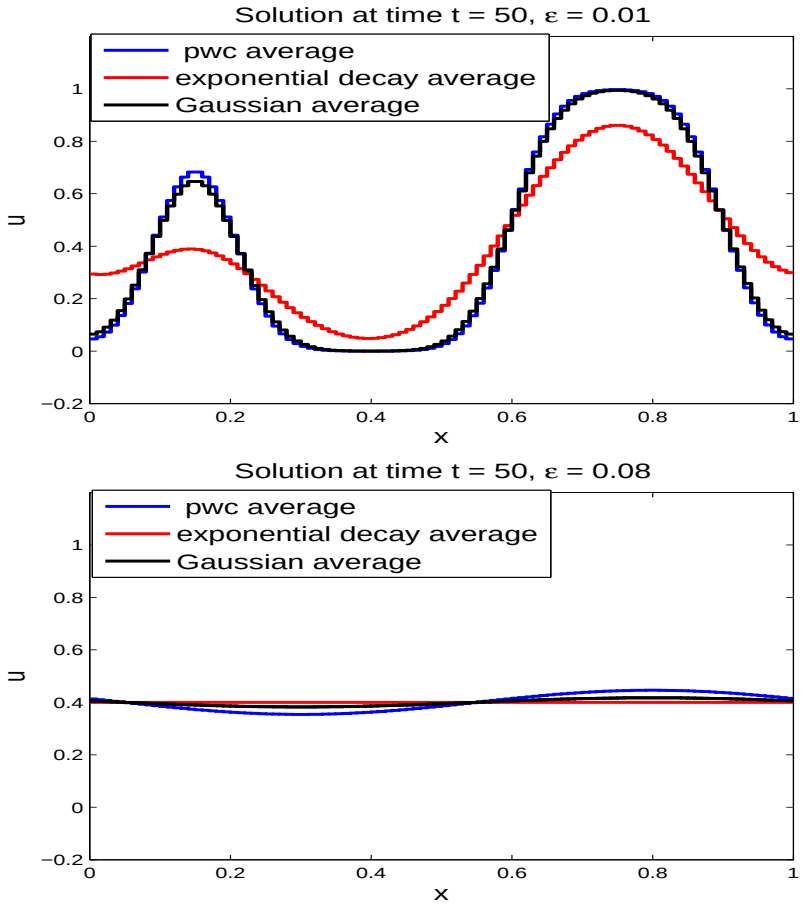

Figure 4.5: The solution with two different values of $\varepsilon = 0.01$ (top) and $\varepsilon = 0.08$ (bottom) with a discontinuous initial data for all the kernels.

The computation cost issues will be explored in Section 4.7.

4.5 Numerical approximation for a nonlinear case

The numerics of the nonlinear case is complicated because there are two important parameters that form the shape of the solutions and how fast it gets to the equilibrium, namely ε

and the steepness of $f'(1/2)$. It is clear that if we start with initial data $u(x,0) > 1/2$ then $\lim_{t\to\infty} u(x,t) \equiv 1$ and if $u(x,0) \leq 1/2$ for all x then $\lim_{t\to\infty} u(x,t) \equiv 0$. Figure 4.6 shows the numerical solution when $u(x,0) < 1/2$ for $0 \leq x \leq 1$ while Figure 4.7 shows the numerics for $u(x,0) > 1/2$.

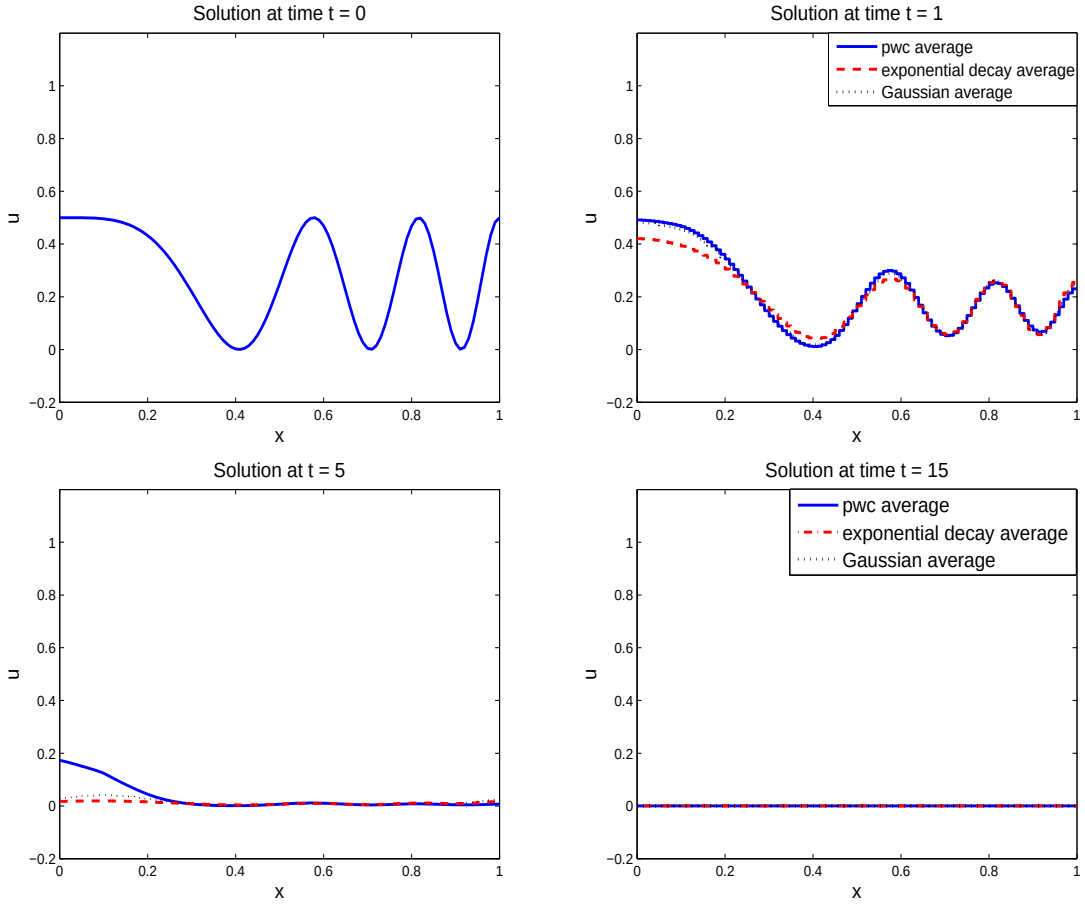

Figure 4.6: The numerical approximation when $u(x,0) < 1/2$ for $0 \leq x \leq 1$ with f given by (4.5.2) and $\varepsilon = 0.1$ at $t = 0, 1, 5, 15$.

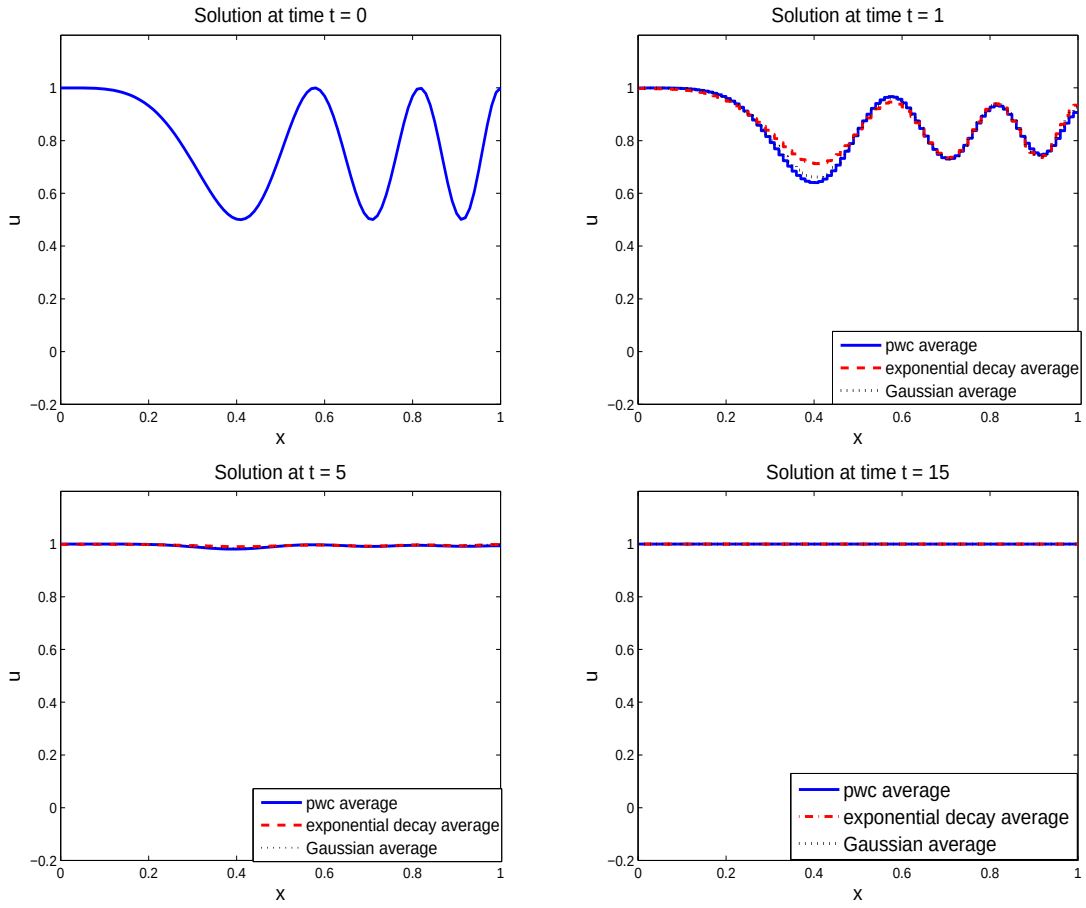

Figure 4.7: The numerical approximation when $u(x,0) > 1/2$ for $0 \leq x \leq 1$ with f given by (4.5.2) and $\varepsilon = 0.1$ at $t = 0, 1, 5, 15$. The convergence in this figure is faster than the previous one because more of the initial data are already close to 1.

We next study the situation with $u(x,0) > 1/2$ for some x and $u(x,0) < 1/2$ otherwise. For simplicity, we stick with a single layer initial data for the experiment and choose different locations for the jump. Throughout this section we use $\varepsilon = 0.1$. The initial solution is

$$u(x,0) = H\left(x - q\right), \tag{4.5.1}$$

where $q = 0.09, 0.4, 0.65$. See Figure 4.8.

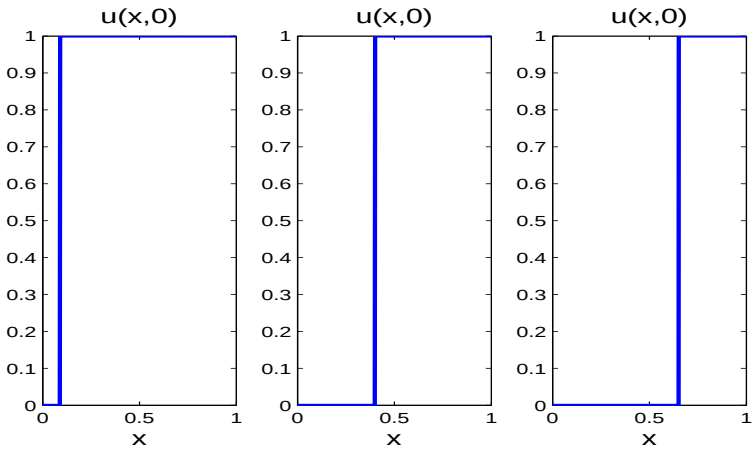

Figure 4.8: Single layer initial data with different jump locations given by (4.5.1).

Also, we use two different functions f for the experiment, a cubic and a Heaviside function. The functions are

$$f(v) = v + pv(1 - v)(v - 1/2), \tag{4.5.2}$$

where $p = 1.9$ and

$$f(v) = H\left(v - 1/2\right). \tag{4.5.3}$$

In addition we use the three kernels described in Chapter 1. We first describe the results for the cubic nonlinearity (4.5.2).

Figure 4.9 shows the solution $u(x, t)$ for the three kernels for f given by (4.5.2) and $q = 0.09$ in the initial data (4.5.1). As can be seen, the single layer disappears quickly for all the kernels with the solution converging to $u \equiv 1$. In Section 5.7, we show that for the piecewise kernel

the evolution of the solution depends on the sign of $q - \varepsilon$. For this case, $q - \varepsilon = -0.01 < 0$ so the theory in Section 5.7 predicts that the layer disappears in $O(1)$ time. The numerics confirm this.

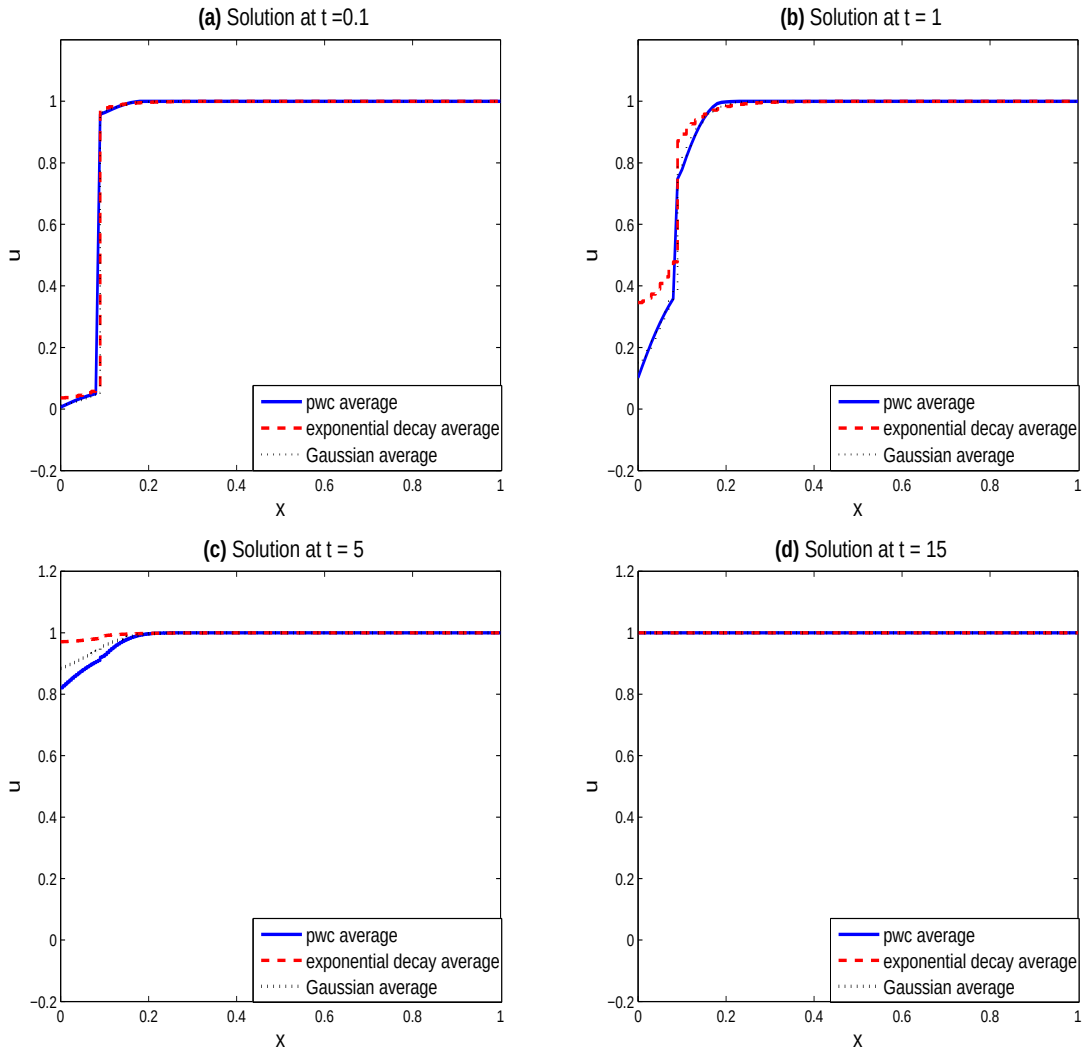

Figure 4.9: Numerical solution with the scheme defined in Section 4.2 with all the kernels for jump location $q = 0.09$. The layer disappears quickly for all the kernels with the solution converging to $u \equiv 1$.

Figure 4.10 shows the solution for f given by (4.5.2) and $q = 0.4$ in the initial data (4.5.1). For both the exponential decay kernel and the Gaussian kernel the solution eventually converges to $u \equiv 1$. We note the solution for the Gaussian kernels moves slower than the solution for the exponential decay kernel. The layer position for the piecewise kernel does not move. We note that $q - \varepsilon = 0.3 > 0$ and $q - (1 - \varepsilon) < 0$ and this important in explaining why the layer does not move for the piecewise kernel case. Formal asymptotics which explain all these observations are given in Chapter 5.

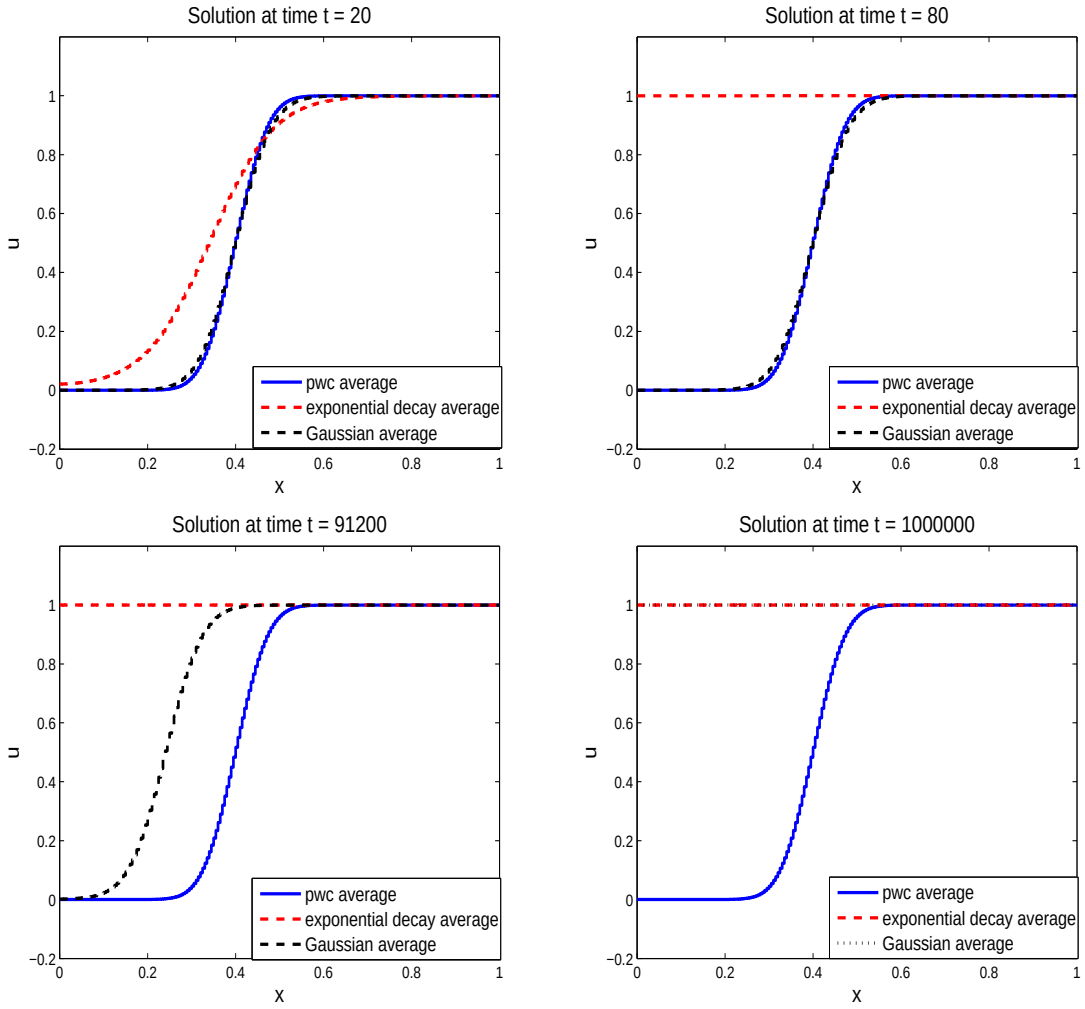

Figure 4.10: Numerical solution with the scheme defined in Section 4.2 with all the kernels for jump location $q = 0.4$. For both the exponential decay kernel and the Gaussian kernel the solution eventually converges to $u \equiv 1$. We note the solution for the Gaussian kernels moves slower than the solution for the exponential decay kernel. The layer position for the piecewise kernel does not move.

Figure 4.11 shows the solution when f is cubic and $q = 0.65$ in the initial data (4.5.1). The results are similar to those in Figure 4.10 except that $u(x,t)$ converges to 0 for large t for the

exponential decay kernel and the Gaussian kernel. This is because more of the initial data is zero. Also, the convergence is quicker than that in Figure 4.10, because the layer starts out closer to the boundary. Finally, as in Figure 4.10 the layer does not move for the piecewise kernel.

We make three further observations about the result in Figure 4.9-4.11.

- If we decrease ε then the same pictures would emerge but the dynamics would be slower.
- If we decrease p then $f'(1/2) = p/4$ decreases. We would get similar pictures but the dynamics would be faster.
- If we use smooth initial data with a single transition layer then we get similar pictures and the dynamics is faster.

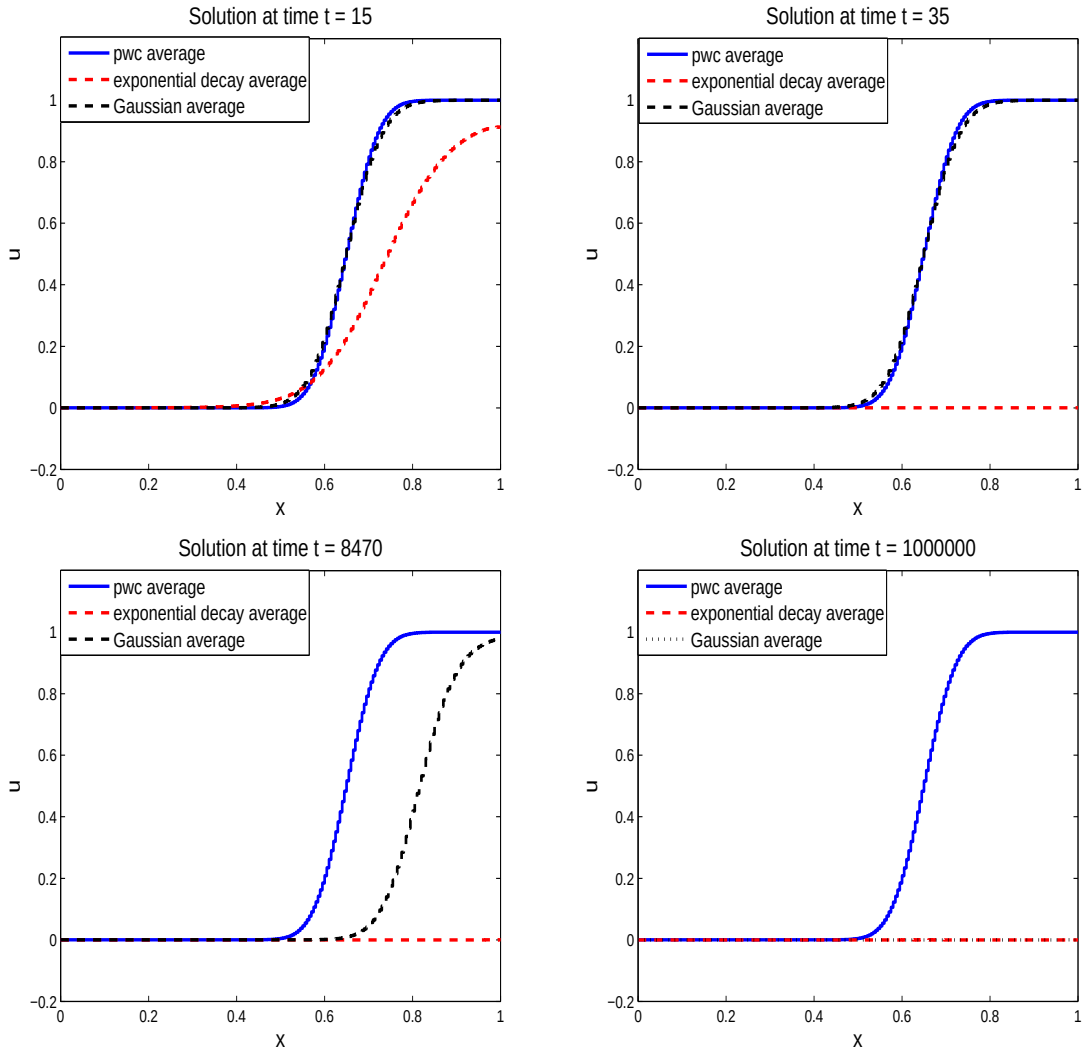

Figure 4.11: Numerical solution with the scheme defined in Section 4.2 with all the kernels for jump location $q = 0.65$. For both the exponential decay kernel and the Gaussian kernel the solution eventually converges to $u \equiv 0$. We note the solution for the Gaussian kernels moves slower than the solution for the exponential decay kernel. The layer position for the piecewise kernel does not move.

Figures 4.12-4.14 show the solution u for the Heaviside nonlinearity (4.5.3) for the three sets of initial data (4.5.1). Figure 4.12 shows the solution for the case $q = 0.09$. The results are

the same as those for the cubic.

The numerics for $q = 0.4$ and $q = 0.65$ are shown In Figures 4.13-4.14. In both cases the layer position does not move for any of the kernels. This is not correct for the exponential and the Gaussian kernels. This is discussed in Section 5.3 where an accurate and correct numerical method is designed.

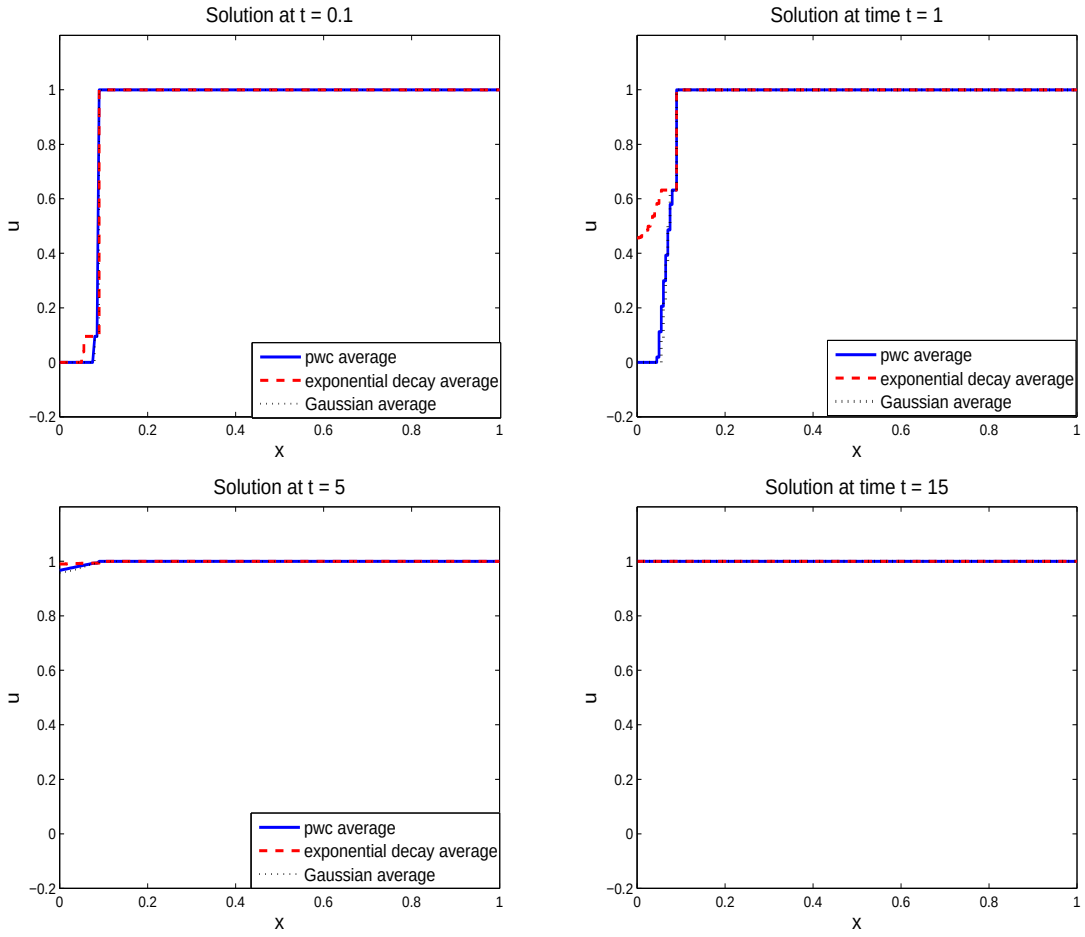

Figure 4.12: Numerical solution with the scheme defined in Section 4.2 with all the kernels for jump location $q = 0.09$. and f is step function. The layer disappears quickly for all the kernels with the solution converging to $u \equiv 1$.

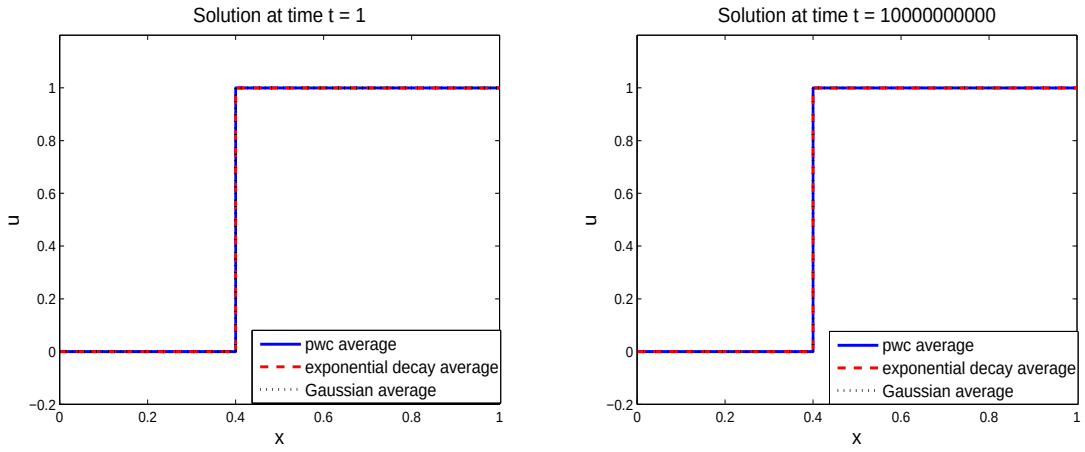

Figure 4.13: Numerical solution with the scheme defined in Section 4.2 with all the kernels for jump location $q = 0.4$. and f is step function. The layer position does not move for any of the kernels. This is not correct for the exponential and the Gaussian kernels. This is discussed in Section 5.3.

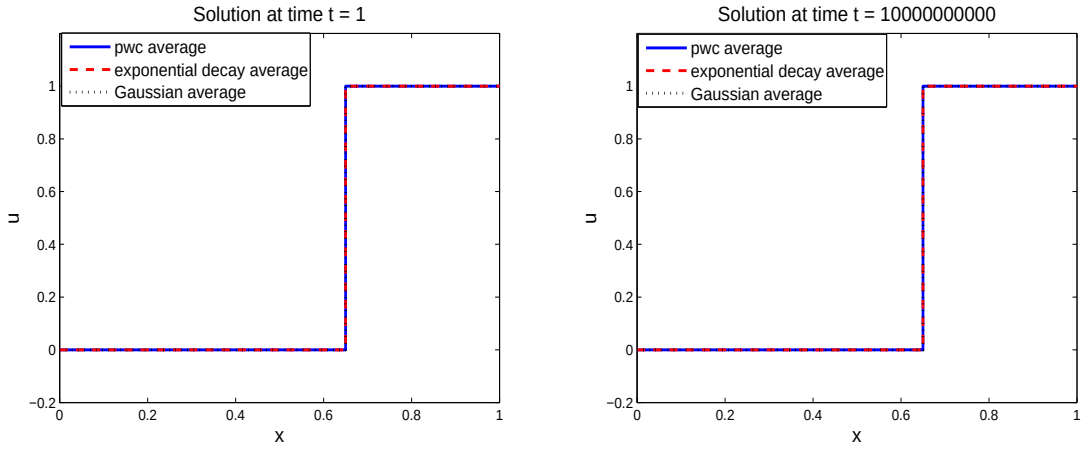

Figure 4.14: Numerical solution with the scheme defined in Section 4.2 with all the kernels for jump location $q = 0.4$. and f is step function. The layer position does not move for any of the kernels. This is not correct for the exponential and the Gaussian kernels. This is discussed in Section 5.3.

4.6 Efficient implementation

In this section we consider both the linear and nonlinear cases on a 1-periodic space domain. We investigate the use of the Fast Fourier Transform ('fft' in MATLAB) to speed up the computation of the kernel $\hat{u}_h$. This works because in this case the kernel is a convolution sum, and standard transform properties reduce it to the product of transforms. We compare the ODE solvers with and without the use of FFT, and also with the default approximate Jacobian evaluation or explicit exact Jacobian specification. We show comparison of ODE solvers in many situations, for the linear case and then for the nonlinear one.

For the linear case, we use two Matlab ODE solvers ode15s (implicit) and ode45 (explicit) with fft and Jacobian. In the left pictures we plot the CPU time versus N using ode45, ode45+fft, ode15s, ode15s+fft and ode15s+fft+Jacobian. In the right pictures we plot the L_2 estimated error versus the CPU time using ode45, ode45+fft, ode15s, ode15s+fft and ode15s+fft+Jacobian to get an estimate of the efficiency. With discontinuous layer initial data, it seems that for all the kernels ode45+fft is the cheapest and the most efficient while ode15s with no fft or explicit Jacobian is the most expensive and inefficient one.

The results shown in Figure 4.15 have $\varepsilon = 0.1$ and a calculation of the classical stiffness ratio S for the underlying problem (4.4.2) gives $S \approx \frac{1}{1-\gamma_1} \approx \frac{3}{2\pi^2\varepsilon^2} = 15.2$, so this case is not a stiff problem and is better suited to explicit solvers like ode45 rather than the implicit stiff solver ode15s. The top two plots are with the piecewise kernel and it is clear that if we compute the cost for this kernel it is at its maximum which about $O(N^3)$ if we use ode15s only and the minimum cost is approximately $O(N)$ using ode45 with fft. Also, for the 'CPU vs L_2'

plot the ode45 with fft still acheive the least error compared to the CPU time cost. Identical trends to these demonstrated in the other subfigures of Figure 4.15.

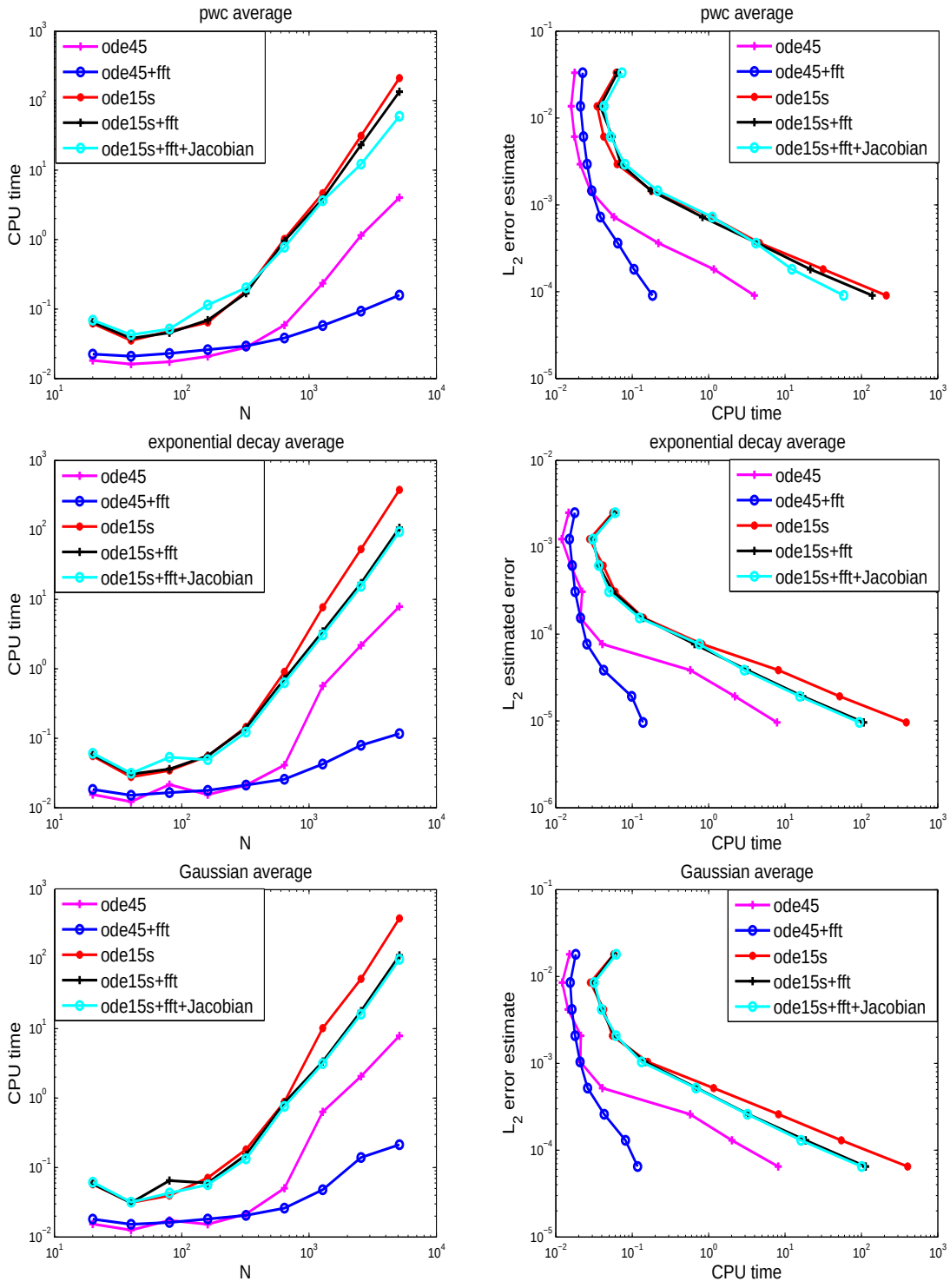

Figure 4.15: Linear case computation cost.

In Figure 4.16 we show the results from Figure 4.15 to compare all the kernels in the same picture. We see that the exponential decay kernel is the least costly while the piecewise kernel is the most expensive.

For the same value of $\varepsilon = 0.1$ and $f(v) = v + 1.9v(1-v)(v-1/2)$ we plot the CPU time versus N using ode45, ode45+fft, ode15s, ode15s+fft and ode15s+fft+Jacobian. In the right pictures we plot the L_2 estimated error versus the CPU time using ode45, ode45+fft, ode15s, ode15s+fft and ode15s+fft+Jacobian for the same reason which is a question of efficiency. The two top plots (piecewise kernel) and the two in the bottom (Gaussian kernel) are similar to the linear one Figure 4.15 where ode45 with fft is the best among the others. However, in the middle where we use the exponential decay kernel there is an oscillation in the 'CPU vs L_2' plot. The reason for that is the layer with the expnential decay average moves faster than the others whereas the others are very slow as expected from the discussion in section 5.5 and 5.7.

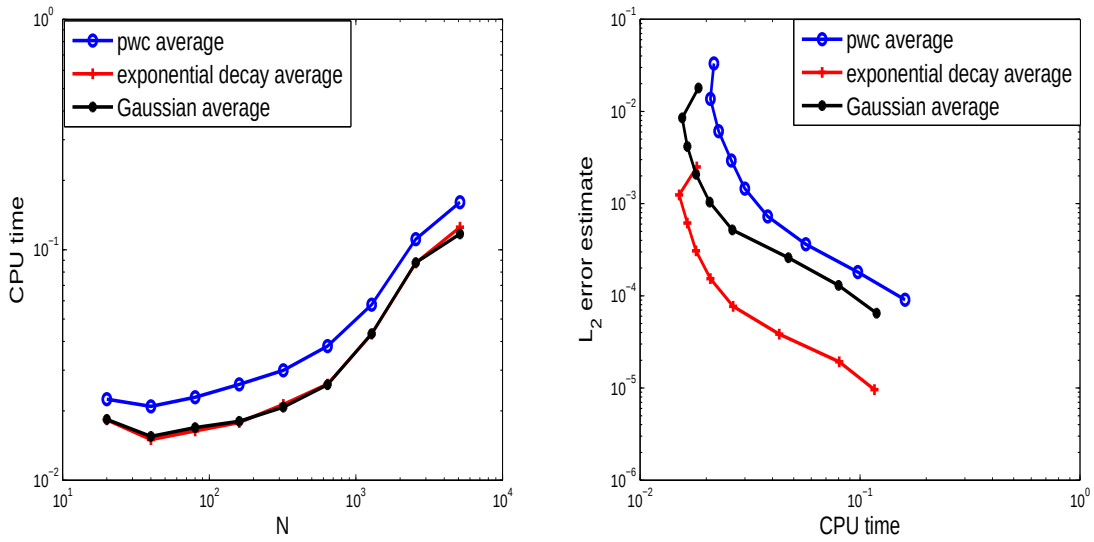

Figure 4.16: Linear case for all the kernels.

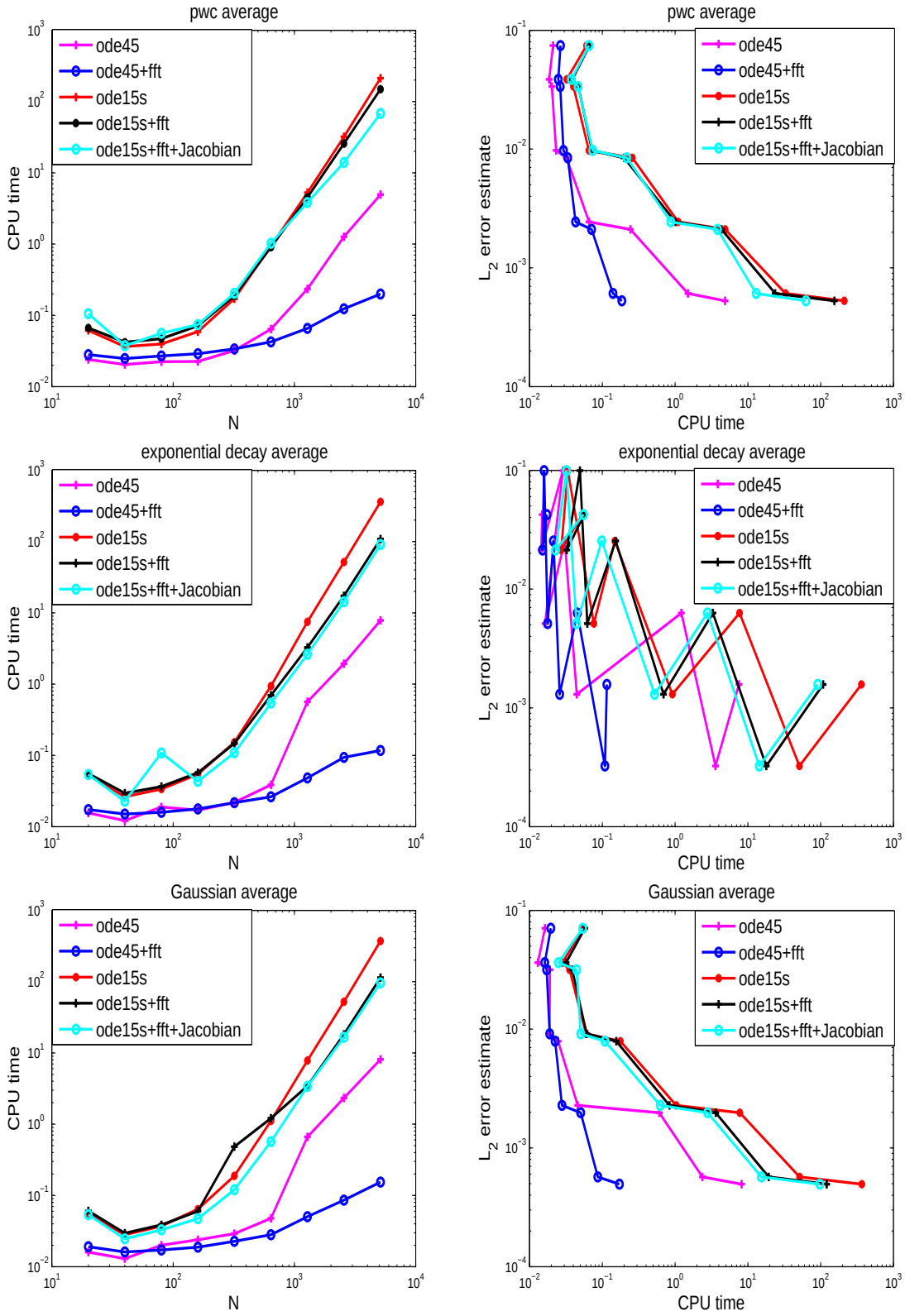

Figure 4.17: Nonlinear case computation cost.

Chapter 5

Slowly varying solutions

5.1 Introduction

In this chapter we consider slowly varying solutions to the dynamic problem for $u(x,t)$

$$u_t = f(\hat{u}) - u. \tag{5.1.1}$$

For all of this chapter except the final section we take $\hat{u}(x)$ to be the exponential decay kernel given by

$$\hat{u}(x,t) = \frac{1}{2\varepsilon K(x)} \int_0^1 \exp\left(-|\frac{x-y}{\varepsilon}|\right) u(y,t)dy, \tag{5.1.2}$$

with

$$K(x) = 1 - h(x) = 1 - \frac{e^{-x/\varepsilon} + e^{-(1-x)/\varepsilon}}{2}. \tag{5.1.3}$$

We first give the results of a numerical simulation with

$$f(u) = \frac{1}{2} + \frac{\tanh(\gamma(u-1/2))}{2\tanh(\gamma/2)} \tag{5.1.4}$$

where $\gamma = 20$, initial solution

$$u(x,0) = \frac{1}{2}(1 + \tanh(40(x - 0.47))) \tag{5.1.5}$$

and $\varepsilon = 0.075$. The results with the setting $'RelTol' = 10^{-8}$ and $'AbsTol' = 10^{-16}$ are shown in Figure 5.1. In Figure 5.1**(b)** nothing has visibly changed at $t = 100$ from the initial data in 5.1**(a)**. Figure 5.1**(a)** shows that at time $t = 700$ the solution has moved a small amount. A relatively sudden final convergence to the equilibrium $u \equiv 1$ occurs at about $t = 1300$. Numerical studies show that similar results hold for other small value of ε with the solution taking longer times to converge as ε decreases.

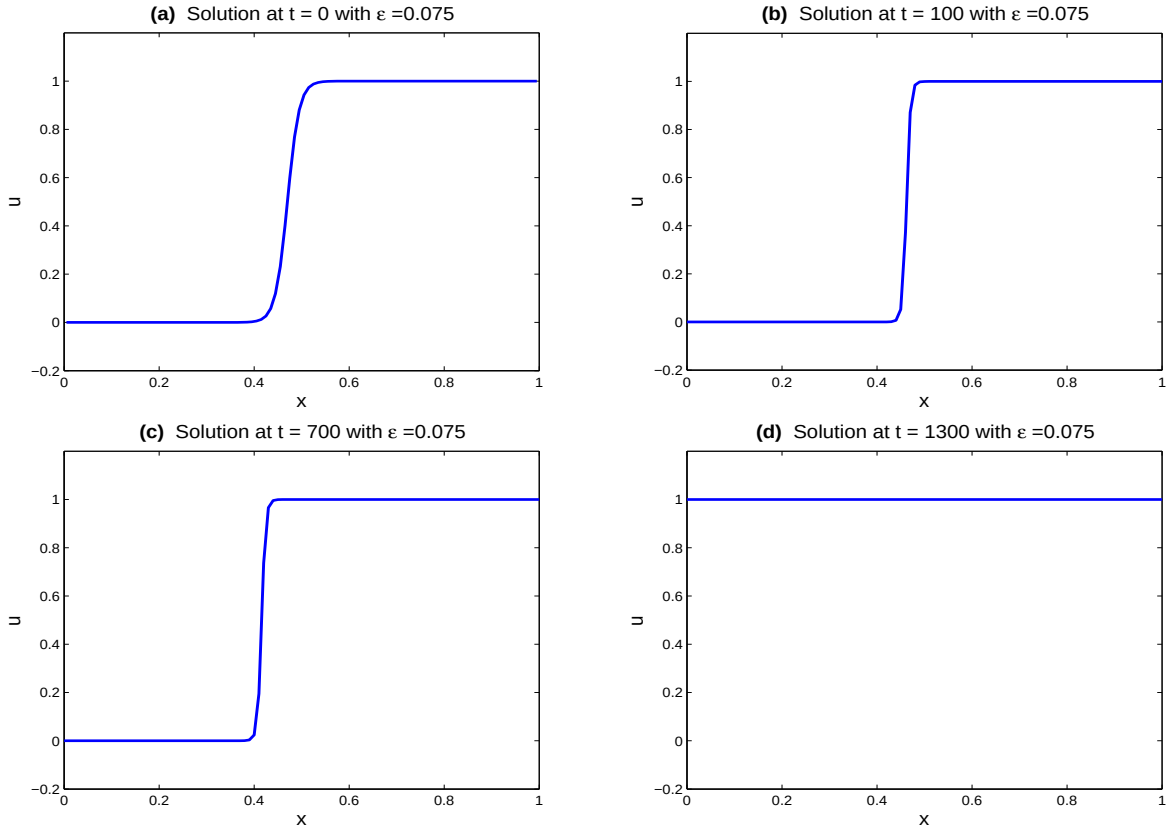

Figure 5.1: Solution moves slowly with time and it takes about 1300 time units to converge to the equilibrium $u \equiv 1$.

5.2 Slow motion

In order to explain the slow behaviour observed in Figure 5.1, we first note that $u(x,t) \equiv 0$ and $u(x,t) \equiv 1$ are equilibrium solutions to (5.1.1). For ε small the kernel in (5.1.2) is concentrated near the point x. The initial data (5.1.5) is very close to zero for $x < 0.47$ and very close to one for $x > 0.47$. It follows that for x bounded away from 0.47, $u_t(x,t)$ will be very small.

We now consider what happens to the solution at $x = p = 0.47$. Suppose that instead of the initial data (5.1.5) we approximate it by

$$u(x,0) = \begin{cases} 0 & \text{when } x \in [0,p) \\ \\ 1 & \text{when } x \in (p,1] \end{cases} \tag{5.2.1}$$

The solution $u(x,t)$ will be expected to have a jump discontinuity at $x = p$ but the kernel $\hat{u}(x,t)$ will be continuous for all x. Taking limits as $x \to p$ from the left and right in (5.1.1) and writing

$$[u] = \lim_{x \to p^+} u(x,t) - \lim_{x \to p^-} u(x,t)$$

we obtain

$$\frac{d}{dt}[u] = -[u] \tag{5.2.2}$$

This confirms that $u(x,t)$ remains discontinuous at $x = p$ for $t > 0$ although the jump gets smaller as t increases since

$$[u](t) = e^{-t}[u](0) \to 0 \quad \text{as} \quad t \to \infty. \tag{5.2.3}$$

The above does not explain the motion when x is not equal to p. To do this we make one more simplification, we assume that f is the discontinuous function considered in Chapter 3

$$f(v) = \begin{cases} 1 & \text{when } v > \dfrac{1}{2} \\ \\ 0 & \text{when } v < \dfrac{1}{2} \end{cases} \tag{5.2.4}$$

Note that for this function f, if $p \neq 1/2$ then $f\left(\hat{u}(x,t)\right)$ is continuous at $x = p$. Hence the result (5.2.3) holds if $p \neq 1/2$. If $p = 1/2$ then $u(x,0)$ given by (5.2.1) is an equilibrium and

it corresponds to the equilibrium found in Chapter 3 defined by (3.3.3) and (3.3.4). Note that the solution in Chapter 3 is written for $\bar{u}(x)$ where $\bar{u}(x) = K(x)\hat{u}(x)$.

We assume that $0 < p < 1/2$ for the rest of this section and that ε is small. The aim is to find $u_t(x, 0)$. Clearly $\hat{u}(x, 0)$ is an increasing function of x with $\hat{u}(1/2, 0) > 1/2$ since $p < 1/2$. Also, a calculation shows that

$$\hat{u}(0, 0) = \frac{e^{-p/\varepsilon} - e^{-1/\varepsilon}}{1 - e^{-1/\varepsilon}}$$

which is a decreasing function of p which is less than $1/2$ if $p > \varepsilon \ln 2$. Since p is bounded away from 0 we have that there is a unique z with $\hat{u}(z, 0) = 1/2$. We show that

$$z \approx p - \frac{\varepsilon}{2} e^{-p/\varepsilon} \tag{5.2.5}$$

and

$$u_t(x, 0) = \begin{cases} 0 & \text{if } x < z \quad \text{or} \quad x > p \\ \\ 1 & \text{if } z < x < p. \end{cases} \tag{5.2.6}$$

A calculation shows that if $x < p$,

$$2K(x)\hat{u}(x, 0) = e^{x/\varepsilon}[e^{-p/\varepsilon} - e^{-1/\varepsilon}]$$

and that if $\hat{u}(z, 0) = 1/2$,

$$e^{-2z/\varepsilon} - 2e^{-z/\varepsilon} + 2e^{-p/\varepsilon} - e^{-1/\varepsilon} = 0.$$

It follows that

$$e^{-z/\varepsilon} = 1 - \sqrt{1 - 2e^{-p/\varepsilon} + O\left(e^{-1/\varepsilon}\right)}$$

$$\approx e^{-p/\varepsilon} + \frac{e^{-2p/\varepsilon}}{2} + O\left(e^{-1/\varepsilon}\right)$$

$$\approx e^{-p/\varepsilon}\left[1 + \frac{e^{-p/\varepsilon}}{2}\right],$$

and so

$$z \approx p - \varepsilon \ln\left(1 + \frac{e^{-p/\varepsilon}}{2}\right)$$

$$z \approx p - \frac{\varepsilon}{2} e^{-p/\varepsilon}$$

as required.

Since $\hat{u}(x,0)$ passes through $1/2$ at $x = z$ we have that

$$f\left(\hat{u}(x,0)\right) = \begin{cases} 0 & \text{if } x < z \\ \\ 1 & \text{if } x > z. \end{cases}$$

Using this, it follows that $u_t(x,0)$ is given by (5.2.6).

The table below has $p = 0.4$ and shows how small $p - z$ is :

ε	0.1	0.05	0.01	0.005
$p - z$	9.2×10^{-4}	8.4×10^{-6}	2.1×10^{-20}	4.5×10^{-38}

The above results show that for $t = 0$, all the motion will take place in an exponentially

small region near $x = p$. Hence we expect very small changes for $t > 0$ until the position of the transition changes by an $O(1)$ amount. We discuss this further in Section 5.4.

5.3 Numerical difficulties

In this section we consider an experiment to approximate the single layer motion problem given by (5.1.1), with discontinuous function f (5.2.4) and discontinuous initial data (5.2.1). We define the location of a layer by $z(t)$ where

$$\hat{u}(z(t), t) = 1/2. \tag{5.3.1}$$

When ε is small enough, then from the previous section we know that all of the action in the exact solution will take place initially in an exponentially small region between $x = p$ (the location of the jump in the initial data) and $z(0)$. We will use both the spatial collocation method discussed in Section 4.2, and then introduce the spatial Galerkin method to try to resolve some difficulties encountered using collocation.

We first use spatial collocation at the element midpoints with a piecewise constant in space approximation as described in Section 4.2. The resulting semidiscrete approximation is

$$\dot{u}_j(t) = f(\hat{u}_h(x_{j-1/2}, t)) - u_j(t), \quad j = 1, \ldots, N. \tag{5.3.2}$$

The usual choice of initial data is the midpoint value

$$u_j(0) = u(x_{j-1/2}, 0), \quad j = 1, \ldots, N.$$

It is interesting to note that this maps all initial data of the form (5.2.1) discontinuous at $x = p = Ph + \mu$ with $|\mu| < h/2$ onto the same initial values

$$u_j(0) = \begin{cases} 0 & j \leq P \\ 1 & j > P. \end{cases}$$

Calculation by Newton's method for (5.3.1) accurately finds the layer location $z_h(0)$ for the approximate initial data above. Of course $z_h(0)$ is very close to Ph when ε is small enough. If h is too big (specifically $|z(0) - Ph| < h/2$), and given that we only use midpoint values of $\hat{u}$ we find that

$$f(\hat{u}_h(x_{j-1/2}, 0)) = u_j(0)$$

so that $\dot{u}_j(0) = 0$ in (5.3.2) for all $j = 1, \ldots, N$ and the semidiscrete approximation is at equilibrium with this initial data. Nothing can happen in this approximation unless $|z(0) - Ph| \geq h/2$.

This can be seen clearly in Figure 5.2, where $p = 0.4$, $\varepsilon = 0.1$ and we use a uniform grid with $h = 1/N$ and $N = 100, 200, 400, 800$. In this case $p - z(0) = 0.00091578\ldots$, so when $N \leq 545$ the semi-discrete solution is in equilibrium and nothing happens. In the final case, $N = 800$, the approximate solution does start to change, but the ODE solver fails at $t = 1.8797$. This failure is caused by the discontinuity in f, which means that the ODE system (5.3.2) has a discontinuous right hand side and so violates the basic continuity and smoothness asssumptions for ODE solvers. The local error estimate used in the timestep control drives the time step size down to zero when the layer location moves to the left, passes over an element midpoint and causes one of the ODEs to change discontinuously from

$\dot{u} = -u$ to $\dot{u} = 1 - u$.

It may be possible to work around the problem of the discontinous right hand side in the collocation method by using the "event location" feature built into Matlab ODE solvers. This stops a calculation when it hits a particular value and restarts with a different ODE system after that. It would probably add a significant overhead to the calculations. However the main problem with the collocation method is the requirement to make the mesh size small enough to resolve the gap between z and p and the impossibly large ODE systems that would be required if uniform grids are used. e.g. when $\varepsilon = 0.01$ we would need $N = 2 \times 10^{19}$. This could probably be worked around by using spatial adaptivity, but the Galerkin method described next provides a more reliable mehod without the need for these more complicated approaches.

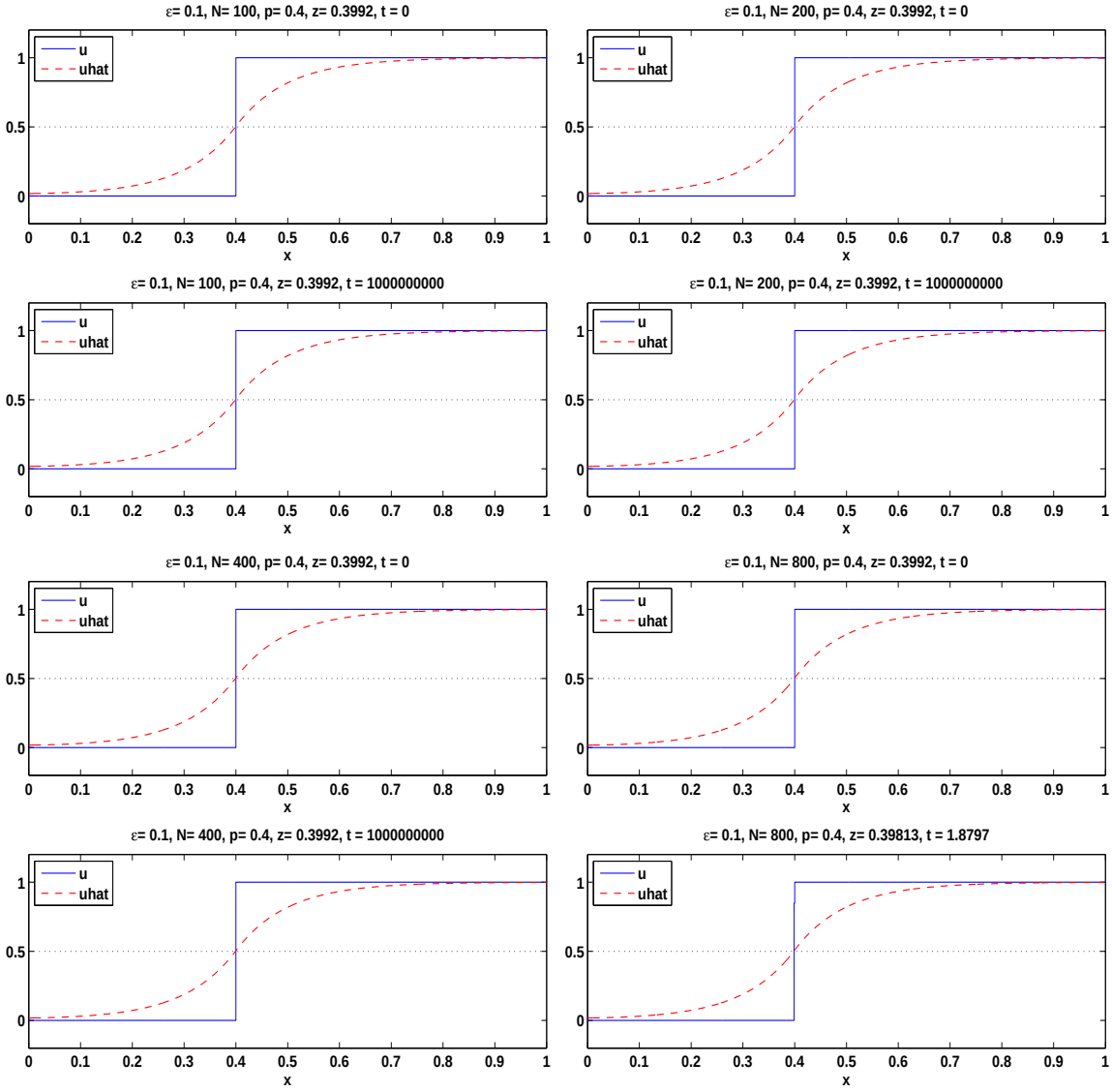

Figure 5.2: Numerical solution for (5.1.1) with the scheme defined in Section 4.2 with the exponential decay kernel for jump location $q = 0.4$. Layer does not move with $N = 100, 200, 400$. We need N=800 for the scheme to get started but it fails again for the discontinuity reason.

The formulation of the Galerkin approximation for (5.1.1) can be written as

$$\int_0^1 \phi_{j+1/2} u_{h,t} dx = \int_0^1 \phi_{j+1/2} \left(f(\hat{u}_h) - u_h \right) dx$$

for $j = 0, \cdots, N-1$ where

$$\phi_{k+1/2}(x) = \begin{cases} 1 & \text{when} \quad x \in (x_k, x_{k+1}), \\ 0 & \text{otherwise}, \end{cases}$$

and u_h is given by (4.2.2). Because the $\phi_{k+1/2}$ are piecewise constants, the Galerkin approximation is equivalent to

$$\int_{x_j}^{x_{j+1}} u_{h,t} dx = \int_{x_j}^{x_{j+1}} \left(f(\hat{u}_h) - u_h \right) dx, \quad \text{for} \quad j = 0, \cdots, N-1$$

so the resulting semidiscrete approximation is given by

$$\dot{u}_j = \frac{1}{h} \int_{x_j}^{x_{j+1}} f(\hat{u}_h) dx - u_j \quad \text{for} \quad j = 0, \cdots, N-1.$$

The key factor in the Galerkin approximation is the $\int f(\hat{u}_h) dx$ term. Because of the discontinuous nature of the function f, we have the following exact expression

$$\frac{1}{h} \int_{x_j}^{x_{j+1}} f(\hat{u}_h) dx = \begin{cases} 1, & x_k > z_h(t) \\ 0, & x_{k+1} < z_h(t), \\ \frac{x_{k+1} - z_h(t)}{h} & \text{otherwise.} \end{cases}$$

However to use this we must solve $\hat{u}_h(z_h(t), t) = 1/2$ for z_h (locating z_h) at each time step which is expensive. Alternatively, we could approximate this integral using a piecewise linear

approximation of $\hat{u}_h$,

$$\frac{1}{h}\int_{x_j}^{x_{j+1}} f(\hat{u}_h)dx \approx \int_0^1 f((1-s)\hat{u}_h(x_j) + s\hat{u}_h(x_{j+1}))ds,$$

and z_h is not explicitly involved which is much cheaper.

For a comparison between the exact and the approximate Galerkin see Figure 5.4. The test on a relatively coarse mesh with $h = 1/100$ shows good agreement between the two approximations up to the time the layer reaches the boundary.

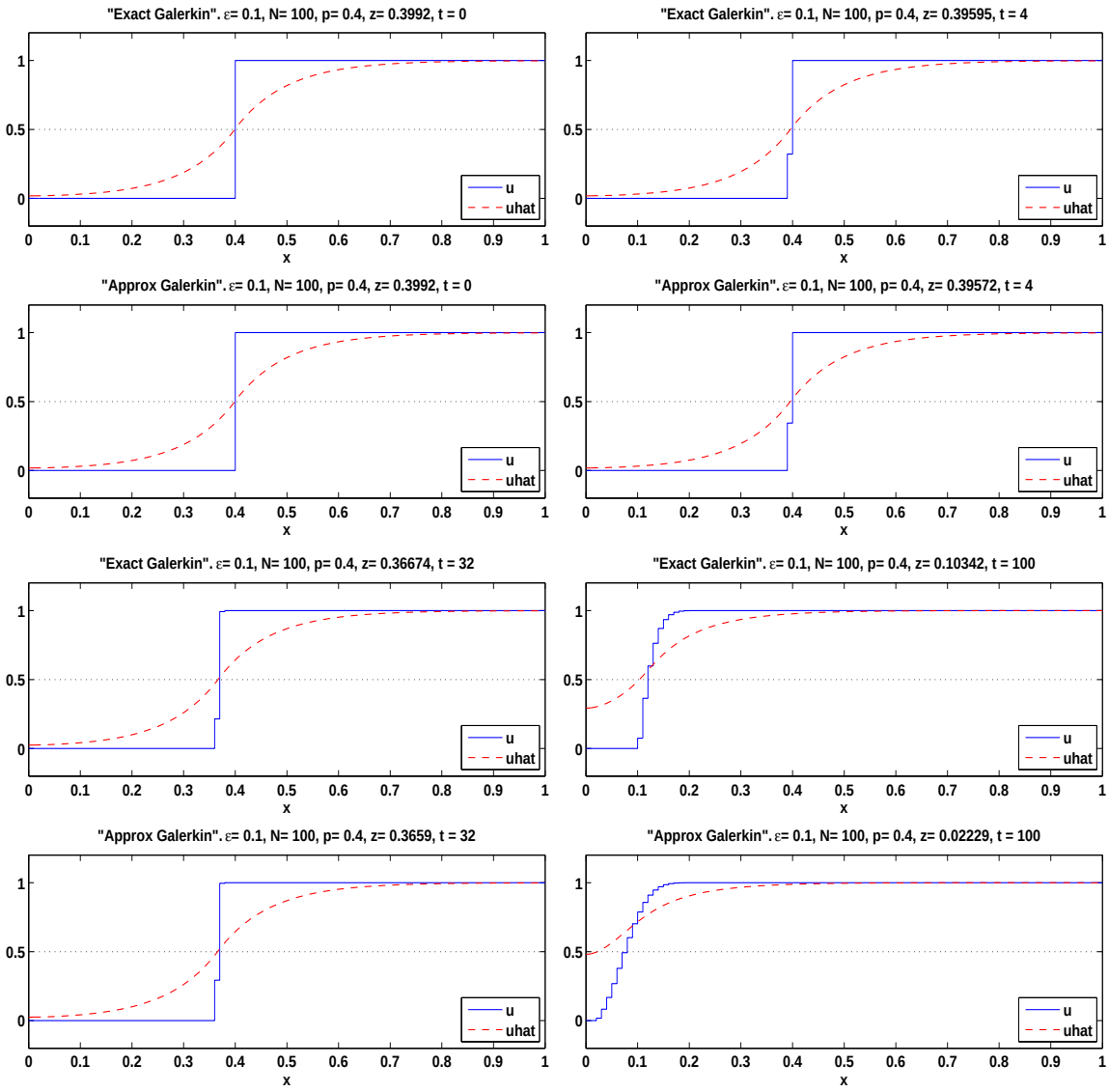

Figure 5.3: Numerical solution for (5.1.1) with the scheme defined in Section 5.3 (exact Galerkin and approximate Galerkin) with the exponential decay kernel for jump location $q = 0.4$ at $t = 0, 4, 32, 100$. We can see that for the same data the new scheme work whereas the old one failed as in Figure 5.2.

In Figure 5.4 we show the L_2 error for u and $\bar{u}$ and the CPU time for the exact and approximate Galerkin methods with discontinuous initial data that jump at $p = 0.45$ and $\varepsilon = 0.18$.

Both methods appear to converge like $O(h)$. In this case the two methods take about the same CPU time, but we would expect the approximate Galerkin to be cheaper when there are more layers since it does not need to find the locations explicitly. Note that we cannot use L_∞ with discontinuous solutions, since $\|u - u_h\|_\infty = 1$ if there is a slight error in jump location. We have a theoretical estimate for the L_2 error and so we used that.

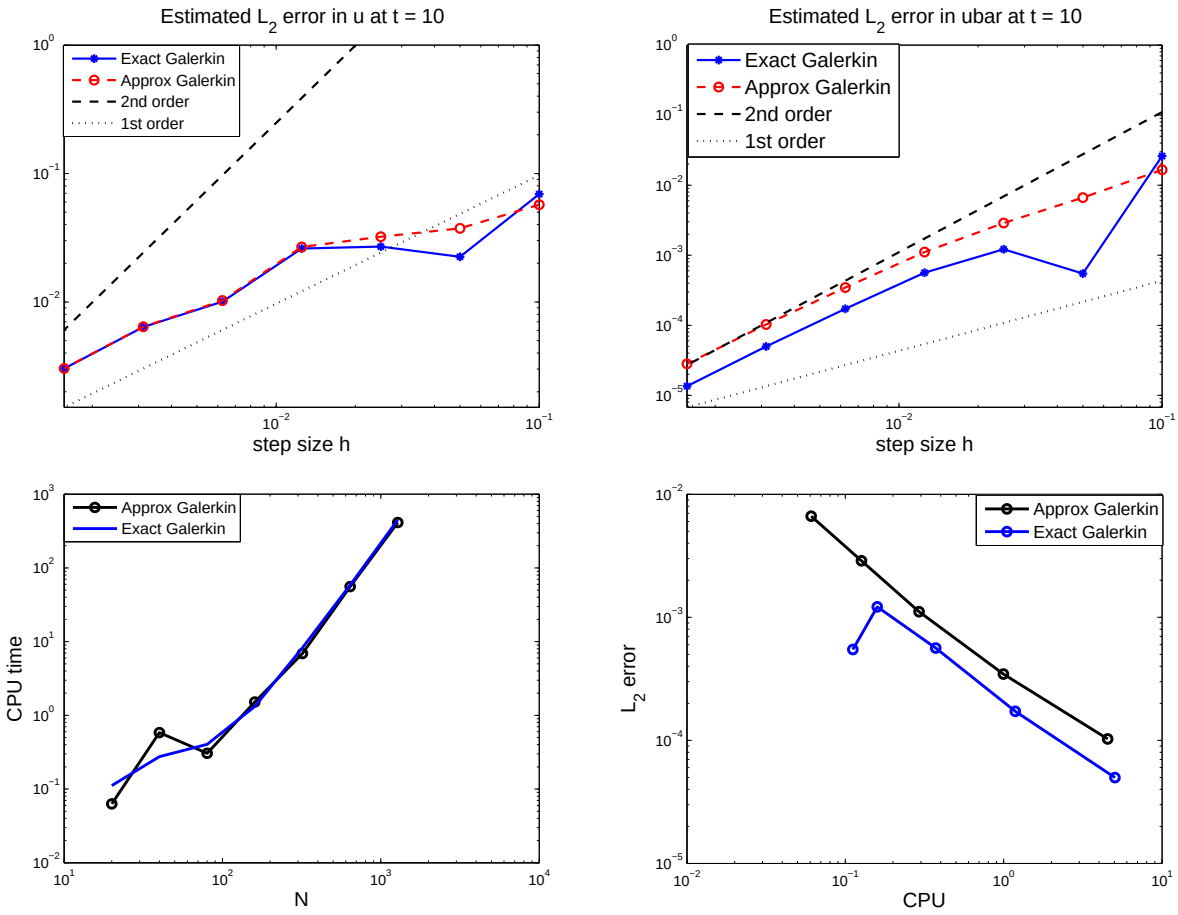

Figure 5.4: For the problem (5.1.1) with the exact and the approximate Galerkin and $\varepsilon = 0.18$ and initial data that jump at $x = 0.45$ and at $t = 10$, we show the following: (i) In the two top pictures we plot the L_2 error for u and $\bar{u}$ with CPU time and both methods appear to converge like $O(h)$. (ii) The left bottom picture shows the CPU time vs N. (iii) the right bottom picture shows L_2 error vs CPU time. From all the pictures there is no big diffrence (exact Galerkin perform a bit better) between the method for a single layer case but we would expect the approximate Galerkin to be cheaper when there are more layers since it does not need to find the locations explicitly.

Note that from now on the scheme we use for the numerics is the approximate Galerkin.

5.4 Single layer slow evolution

In this section we use a formal method to describe the slow evolution of a solution with one transition layer as in Figure 5.1 of Section 5.1. We assume that ε is small and we have a solution $u(x,t)$ with a transition at $x = z(t)$ where

$$\hat{u}(z(t),t) = 1/2 \tag{5.4.1}$$

as shown in Figure 5.5. We assume that $z(t)$ is bounded away from 0 and 1.

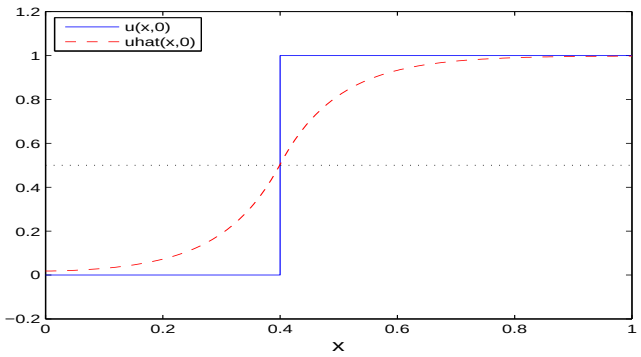

Figure 5.5: $u(x,0)$ and $\hat{u}(x,0)$ for $\varepsilon = 0.1$.

As an approximation, we assume that

$$u(x,t) = \begin{cases} 0 & \text{when } x \leq z \\ \\ 1 & \text{when } x > z \end{cases} \tag{5.4.2}$$

The aim is to find an equation for the motion of $z(t)$. The idea of finding an equation for the movement of the transition layer is motivated by similar questions for partial differential

equations [10, 13, 14]. Also, the idea is similar to a level set approach [23, 27, 42, 43, 49, 55].

Differentiating (5.4.1)

$$\hat{u}_x(z,t)\frac{dz}{dt} + \hat{u}_t(z,t) = 0$$

we have

$$\frac{dz}{dt} = \frac{-\hat{u}_t(z,t)}{\hat{u}_x(z,t)}. \tag{5.4.3}$$

Averaging the equation (5.1.1) we obtain,

$$\hat{u}_t(x,t) = \widehat{f(\hat{u})} - \hat{u} \tag{5.4.4}$$

that is

$$\hat{u}_t = \frac{1}{2\varepsilon K(x)} \int_0^1 \exp\left(-|\frac{x-y}{\varepsilon}|\right) f(\hat{u}(y,t))dy - \hat{u}(x,t).$$

At $x = z$

$$\begin{aligned}
\hat{u}_t(z,t) &= \frac{1}{2\varepsilon K(z)} \int_0^1 \exp\left(-|\frac{z-y}{\varepsilon}|\right) f(\hat{u}(y))dy - 1/2 \\
&= \frac{1}{2\varepsilon K(z)} \int_0^z \exp\left(-|\frac{z-y}{\varepsilon}|\right) f(\hat{u}(y))dy + \frac{1}{2\varepsilon K(z)} \int_z^1 \exp\left(-|\frac{z-y}{\varepsilon}|\right) f(\hat{u}(y))dy - 1/2 \\
&= \frac{1}{2\varepsilon K(z)} \int_0^z \exp\left(-|\frac{z-y}{\varepsilon}|\right) 0dy + \frac{1}{2\varepsilon K(z)} \int_z^1 \exp\left(-|\frac{z-y}{\varepsilon}|\right) 1dy - 1/2 \\
&= \frac{1}{2\varepsilon K(z)} \int_z^1 \exp\left(-|\frac{z-y}{\varepsilon}|\right) dy - 1/2
\end{aligned}$$

and so

$$\hat{u}_t(z,t) = \frac{1}{4K(z)} \left(e^{-z/\varepsilon} - e^{-(1-z)/\varepsilon}\right). \tag{5.4.5}$$

From the definition of $\hat{u}$ and at $x = z$

$$\begin{aligned}\hat{u}_x(z,t) &= -\frac{K'}{K}\hat{u} + \frac{1}{K}\int_0^1 J'(x-y)u(y)dy \\ &= -\frac{K'}{K}\frac{1}{2} - \frac{1}{\varepsilon K}\int_0^1 \text{sign}(z-y)J(z-y)u(y)dy \\ &= -\frac{K'}{2K} - \frac{1}{\varepsilon K}\int_0^z J(z-y)u(y)dy + \frac{1}{\varepsilon K}\int_z^1 J(z-y)u(y)dy.\end{aligned}$$

Using (5.4.2) and the definition of K

$$\hat{u}_x(z,t) = \frac{e^{-(1-z)/\varepsilon} - e^{-z/\varepsilon}}{4\varepsilon K} + \frac{1 - e^{-(1-z)/\varepsilon}}{2\varepsilon K}. \tag{5.4.6}$$

We use the notation

$$M(z) = \max(e^{-z/\varepsilon}, e^{-(1-z)/\varepsilon})$$

so that

$$K\hat{u}_x(z,t) = \frac{1}{2\varepsilon}(1 + O(M(z))). \tag{5.4.7}$$

Using (5.4.5) and (5.4.7),

$$\frac{dz}{dt} = \frac{-\varepsilon(e^{-z/\varepsilon} - e^{-(1-z)/\varepsilon})}{2(1 + O(M(z)))} = -\frac{\varepsilon}{2}(e^{-z/\varepsilon} - e^{-(1-z)/\varepsilon})(1 + O(M(z))). \tag{5.4.8}$$

Ignoring the exponentially small term $O(M(z))$, in (5.4.8) we have that

$$\frac{dz}{dt} = \frac{\varepsilon}{2}\left(e^{-(1-z)/\varepsilon} - e^{-z/\varepsilon}\right) = G(z). \tag{5.4.9}$$

A calculation shows that $G(1/2) = 0$ and $G(z) < 0$ if $z < 1/2$ while $G(z) > 0$ if $z > 1/2$. Equation (5.4.9) has an unstable equilibrium at $z = 1/2$ because the eigenvalue is $\lambda =$

$e^{-1/(2\varepsilon)} > 0$. As noted in Section 5.2, this corresponds to the equilibrium (3.3.3) and (3.3.4) described in Chapter 3.

Suppose that $z(0) < 1/2$ with $z(0)$ bounded away from 0. Equation (5.4.9) shows that $z(t)$ decreases very slowly towards $z = 0$. The differential equation (5.4.9) is well approximated by

$$\frac{dz}{dt} \approx -\frac{\varepsilon}{2} e^{-z/\varepsilon}. \tag{5.4.10}$$

The solution of this (approximate) ODE is

$$z(t) = \varepsilon \ln\left(e^{z(0)/\varepsilon} - \frac{t}{2}\right). \tag{5.4.11}$$

The time taken to hit the boundary $z = 0$ is

$$t = 2\left(e^{z(0)/\varepsilon} - 1\right). \tag{5.4.12}$$

The table below explains the connection between the size of ε and the time in (5.4.12) for various values of ε where we have $z(0) = 0.45$.

ε	0.075	0.05	0.01
t	804.9	1.6×10^4	6.9×10^{19}

Figure 5.6 shows the graph of $z(t)$ for various values of ε and $z(0) = 0.45$. The graphs clearly show that $z(t)$ is almost constant for long time period.

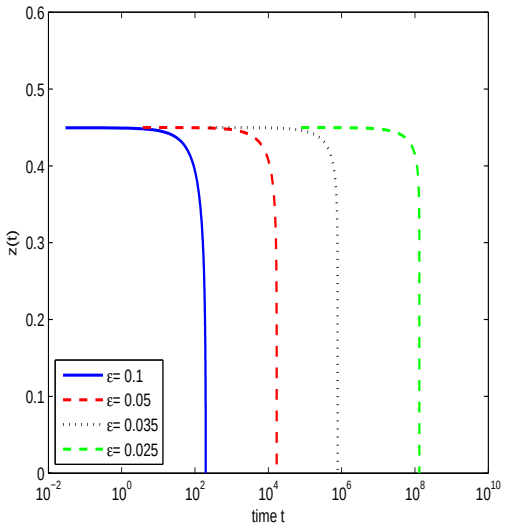

Figure 5.6: For the problem (5.4.11) with the exponential decay kernel we compute the Layer location from (5.4.11) for $z(0) = 0.45$ for various values of ε. The graph clearly shows that $z(t)$ is almost constant for long time period and it quickly changes which means for small ε you need very large time for the layer to move.

In Figure 5.7 we compare the numerical solution of (5.1.1) with the prediction of $z(t)$ made by (5.4.11). For the numerical solution we use exact Galerkin with $z(t)$ defined by (5.4.1). The initial data is

$$u(x,0) = \begin{cases} 0 & \text{when } x \leq z(0) \\ \\ 1 & \text{when } x > z(0) \end{cases} \tag{5.4.13}$$

where $z(0) = 0.45$. Figure 5.7**(a)** and **(b)** show that there is excellent agreement.

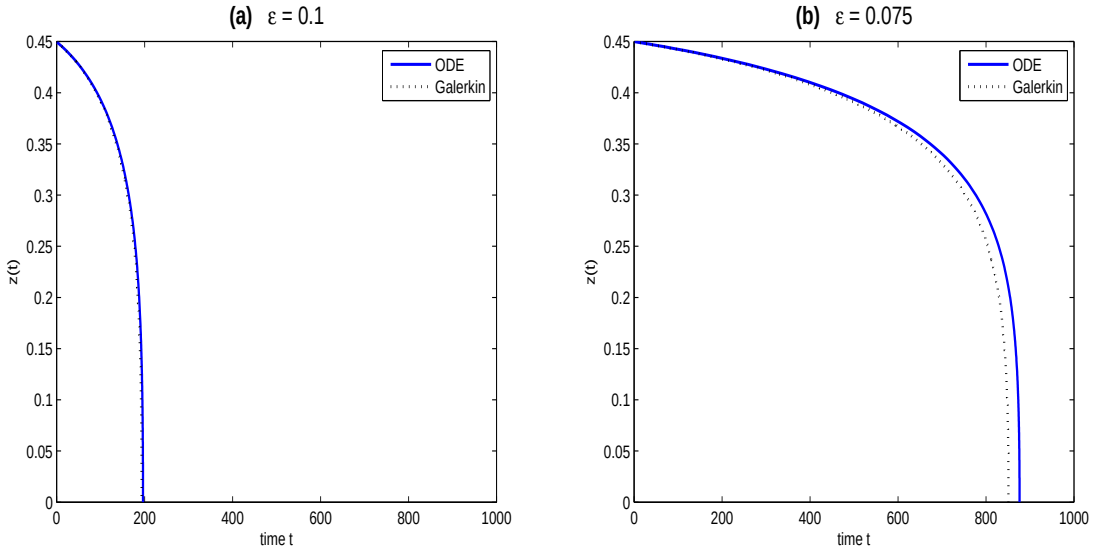

Figure 5.7: With the exponential decay kernel we compare the layer location $z(t)$ using both the numerical solution of (5.1.1) and the prediction of $z(t)$ made by (5.4.11). For the numerical solution we use exact Galerkin with the initial data defined by (5.4.13) where for both $z(0) = 0.45$.

5.5 Analysis on two layer case

In this section we consider the slow evolution of a solution with two transition layers. In Figure 5.8 we show the numerical solution when the initial data is

$$u(x,0) = \begin{cases} 0 & \text{when } x \leq 0.1 \\ 1 & \text{when } 0.1 < x \leq 0.4 \\ 0 & \text{when } 0.4 < x \leq 1 \end{cases} \tag{5.5.1}$$

and $\varepsilon = 0.075$. The pictures show $u(x,t)$ and $\hat{u}(x,t)$. The layer locations are $z_1(t)$ and $z_2(t)$ with $z_1(0) = 0.1$, and $z_2(0) = 0.4$. At time $t = 38$, we only have one transition layer. The motion shown in **(b)** and **(c)** is of the single layer case.

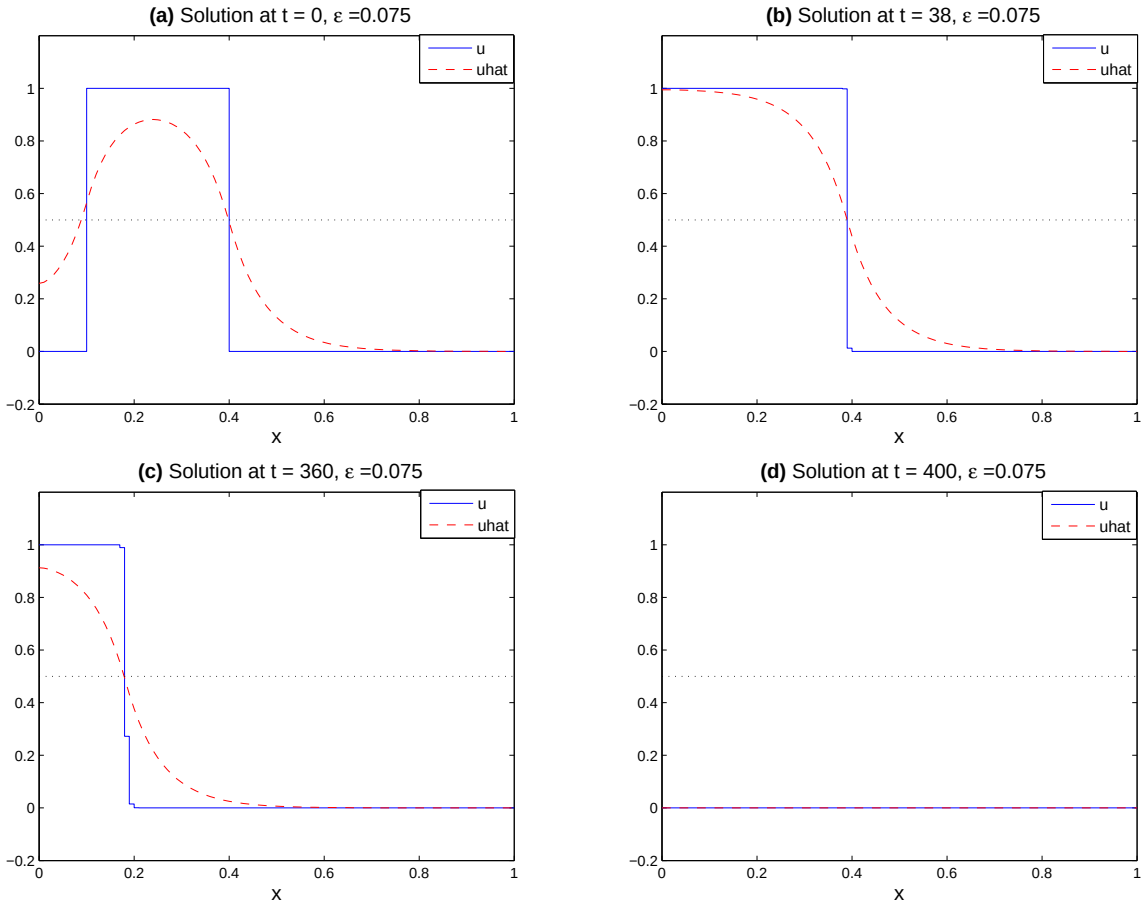

Figure 5.8: Numerical solution of (5.1.1) with the exact Galerkin scheme and the exponential decay kernel using initial data that jump at $x = 0.1, 0.4$. The picture shows the motion of the two layers where both move to the left which mean $u \equiv 0$.

Let $0 < z_1(0) < z_2(0) < 1$ with $z_1(0), z_2(0) - z_1(0)$ and $1 - z_2(0)$ bounded away from zero.

The initial data is

$$u(x,0) = \begin{cases} 0 & \text{when } 0 < x \leq z_1(0) \\ 1 & \text{when } z_1(0) < x \leq z_2(0) \\ 0 & \text{when } z_2(0) > x \leq 1 \end{cases} \tag{5.5.2}$$

We then define $z_1(t)$ and $z_2(t)$ with $z_1(t) < z_2(t)$ by

$$\hat{u}(z_1(t),t) = \hat{u}(z_2(t),t) = 1/2. \tag{5.5.3}$$

In addition we assume that

$$u(x,t) = \begin{cases} 0 & \text{when } x \leq z_1(t) \quad \text{or} \quad x \geq z_2(t) \\ 1 & \text{when } z_1(t) < x < z_2(t). \end{cases} \tag{5.5.4}$$

The aim is to find equations of the motion for $z_1(t)$ and $z_2(t)$.

Differentiating (5.5.3) we obtain

$$\frac{dz_k}{dt} = \frac{-\hat{u}_t(z_k,t)}{\hat{u}_x(z_k,t)} \tag{5.5.5}$$

for $k = 1, 2$.

Proceeding in a similar way to the single layer case, we first compute $\hat{u}_t$ at $x = z_1$.

At $x = z_1$

$$\hat{u}_t(z_1,t) = \frac{1}{2\varepsilon K(z_1)}\int_0^1 \exp\left(-|\frac{z_1-y}{\varepsilon}|\right) f(\hat{u}(y))dy - 1/2$$

$$= \frac{1}{2\varepsilon K(z_1)}\int_0^{z_1} \exp\left(-|\frac{z_1-y}{\varepsilon}|\right) f(\hat{u}(y))dy + \frac{1}{2\varepsilon K(z)}\int_{z_1}^{z_2} \exp\left(-|\frac{z_1-y}{\varepsilon}|\right) f(\hat{u}(y))dy +$$

$$\frac{1}{2\varepsilon K(z_1)}\int_{z2}^1 \exp\left(-|\frac{z_1-y}{\varepsilon}|\right) f(\hat{u}(y))dy - 1/2.$$

Using the properties of $f(\hat{u})$ we have

$$\hat{u}_t(z_1,t) = \frac{1}{2\varepsilon K(z_1)}\int_0^{z_1} \exp\left(-|\frac{z_1-y}{\varepsilon}|\right) 0dy + \frac{1}{2\varepsilon K(z_1)}\int_{z_1}^{z_2} \exp\left(-|\frac{z_1-y}{\varepsilon}|\right) 1dy +$$

$$\frac{1}{2\varepsilon K(z_1)}\int_{z_2}^1 \exp\left(-|\frac{z_1-y}{\varepsilon}|\right) 0dy - 1/2$$

$$= \frac{1}{2\varepsilon K(z_1)}\int_{z_1}^{z_2} \exp\left(-|\frac{z_1-y}{\varepsilon}|\right) dy - 1/2.$$

It follows that

$$\hat{u}_t(z_1,t) = \frac{1}{4K(z_1)}\left(-2e^{-(z_2-z_1)/\varepsilon} + e^{-z_1/\varepsilon} + e^{-(1-z_1)/\varepsilon}\right). \tag{5.5.6}$$

Similarly,

$$\hat{u}_t(z_2,t) = \frac{1}{4K(z_2)}\left(-2e^{-(z_2-z_1)/\varepsilon} + e^{-z_2/\varepsilon} + e^{-(1-z_2)/\varepsilon}\right). \tag{5.5.7}$$

From the definition of $\hat{u}$ we can do the same calculation to obtain

$$\hat{u}_x(z_1,t) = \frac{e^{-(1-z_1)/\varepsilon} - e^{-z_1/\varepsilon}}{4\varepsilon K(z_1)} + \frac{1-e^{-(z_2-z_1)/\varepsilon}}{2\varepsilon K(z_1)} \tag{5.5.8}$$

and

$$\hat{u}_x(z_2,t) = \frac{e^{-(1-z_2)/\varepsilon} - e^{-z_2/\varepsilon}}{4\varepsilon K(z_2)} - \frac{1-e^{-(z_2-z_1)/\varepsilon}}{2\varepsilon K(z_2)}. \tag{5.5.9}$$

We use the notation

$$M(z_1,z_2) = \max(e^{-z_1/\varepsilon}, e^{-(1-z_2)/\varepsilon}, e^{-(z_2-z_1)/\varepsilon})$$

so that

$$K(z_1)\hat{u}_x(z_1,t) = \frac{1}{2\varepsilon}(1+O(M(z_1,z_2))) \tag{5.5.10}$$

and

$$K(z_2)\hat{u}_x(z_2,t) = \frac{1}{2\varepsilon}(-1+O(M(z_1,z_2))). \tag{5.5.11}$$

Using (5.5.6) and (5.5.10),

$$\frac{dz_1}{dt} = \frac{-\varepsilon(-2e^{-(z_2-z_1)/\varepsilon} + e^{-z_1/\varepsilon} + e^{-(1-z_1)/\varepsilon})}{2(1+O(M(z_1,z_2)))}$$

so that

$$\frac{dz_1}{dt} = -\frac{\varepsilon}{2}(-2e^{-(z_2-z_1)/\varepsilon} + e^{-z_1/\varepsilon} + e^{-(1-z_1)/\varepsilon})(1+O(M(z_1,z_2))). \tag{5.5.12}$$

Using (5.5.7) and (5.5.11),

$$\frac{dz_2}{dt} = -\frac{\varepsilon}{2}(-2e^{-(z_2-z_1)/\varepsilon} + e^{-z_2/\varepsilon} + e^{-(1-z_2)/\varepsilon})(-1+O(M(z_1,z_2))). \tag{5.5.13}$$

Ignoring the exponentially small term $O(M(z_1,z_2))$, in (5.5.12) and (5.5.13) we have that

$$\frac{dz_1}{dt} = -\frac{\varepsilon}{2}(-2e^{-(z_2-z_1)/\varepsilon} + e^{-z_1/\varepsilon}) \tag{5.5.14}$$

$$\frac{dz_2}{dt} = -\frac{\varepsilon}{2}(2e^{-(z_2-z_1)/\varepsilon} - e^{-(1-z_2)/\varepsilon}). \tag{5.5.15}$$

The above equations are only valid when $z_1(t), z_2(t) - z_1(t)$ and $1 - z_2(t)$ bounded away from zero.

In general, one of the domain lengths $z_1(t), z_2(t) - z_1(t)$ and $1 - z_2(t)$ will be the smallest. For this case the dynamics of the pair of differential equations above is simple. For the numerical results in 5.8 we had $z_1(0) = 0.1$ and $z_2(0) = 0.4$ so the smallest domain will be $z_1(t)$. In this case, from (5.5.14)

$$\frac{dz_1}{dt} \approx -\frac{\varepsilon}{2}e^{-z_1/\varepsilon}. \tag{5.5.16}$$

This equation will be valid untill $z_1(T) = 0$ (or $z_1(t)$ becomes close to 0). During the time interval $0 < t < T, z_2(t)$ will be very close to $z_2(0)$. This is clearly shown in 5.8**(b)**. For larger times $t > T$ the two dimensional system will be replaced by

$$\frac{dz_2}{dt} = -\frac{\varepsilon}{2}(e^{-z_2/\varepsilon} - e^{-(1-z_2)/\varepsilon}) \tag{5.5.17}$$

with $z_2(0) = 0.4$. This is the single layer case as discussed in the previous section.

For the example in Figure 5.8 both $z_1(t)$ and $z_2(t)$ move to the left as t increases. Other modes are possible depending on $z_1(0)$ and $z_2(0)$ as shown in Figure 5.9. Figure 5.10 shows a situation which both $z_1(t)$ and $z_2(t)$ move to the right.

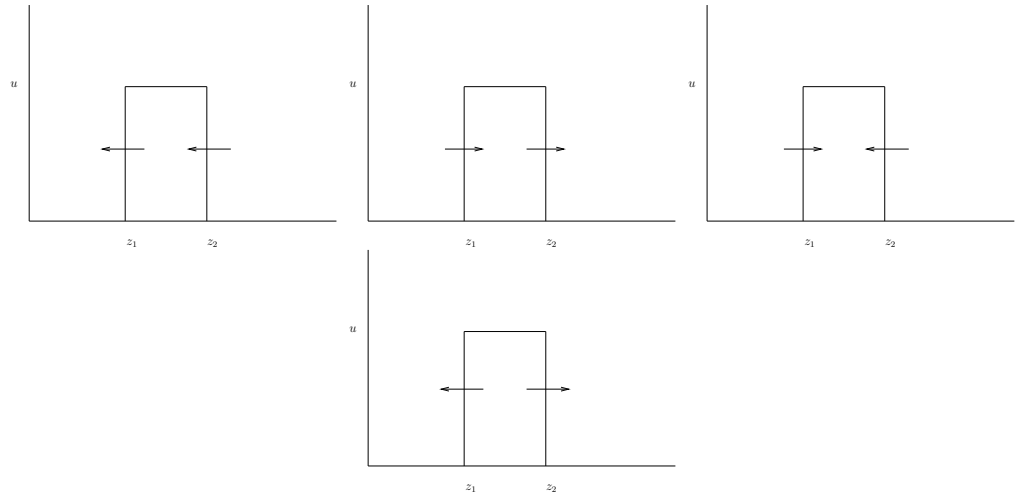

Figure 5.9: Possible motions for the two layer case.

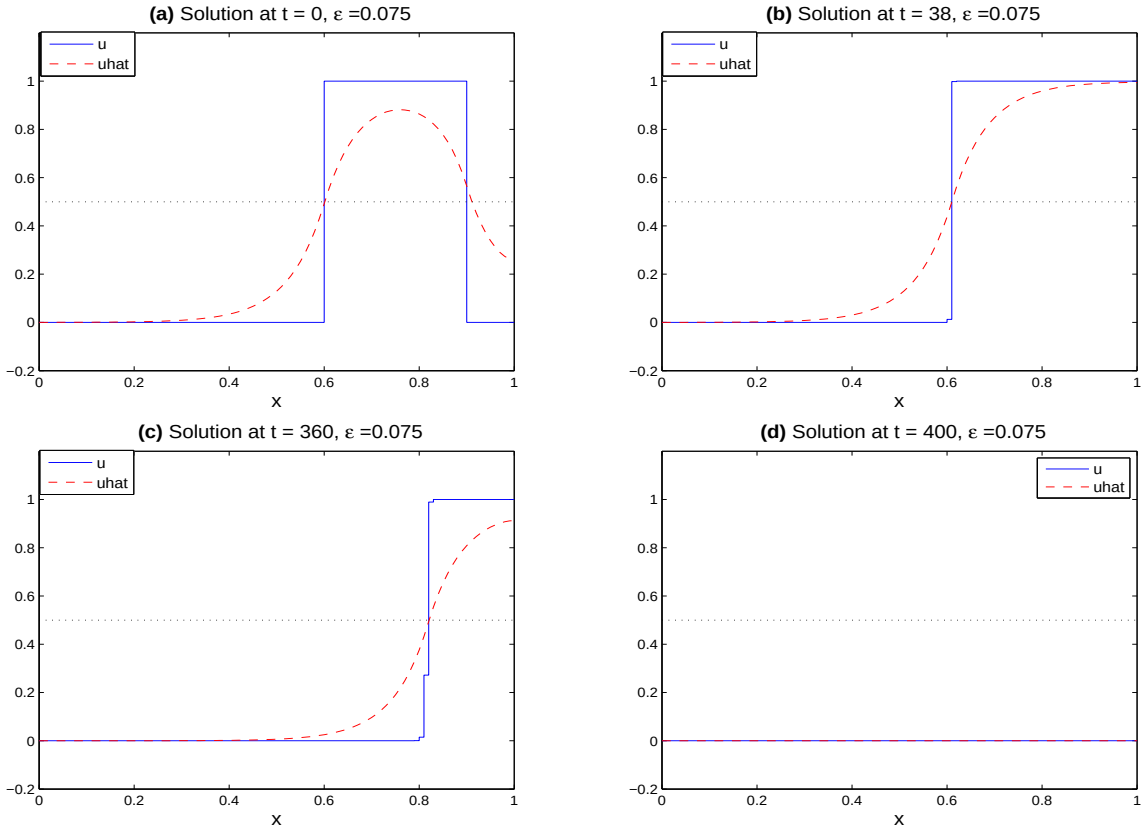

Figure 5.10: Numerical solution of (5.1.1) with the exact Galerkin scheme and the exponential decay kernel using initial data that jump at $x = 0.6, 0.9$. The picture shows the motion of the two layers where both move to the right which mean $u \equiv 0$.

The two dimensional equations (5.5.14)-(5.5.15) can be written as a gradient system with Lyapunov function

$$W(z_1, z_2) = W(z) = -\frac{\varepsilon^2}{2}\left(e^{-z_1/\varepsilon} + 2e^{-(z_2-z_1)/\varepsilon} + e^{-(1-z_2)/\varepsilon}\right). \tag{5.5.18}$$

A calculation shows that for $k = 1, 2$,

$$\frac{dz_k}{dt} = -\frac{\partial W(z)}{\partial z_k}. \tag{5.5.19}$$

We show in the next section that (5.5.19) has a unique equilibrium $\bar{z} = (z_1, z_2)$ where

$$\bar{z}_1 = \frac{1}{3} - \frac{\varepsilon}{3}\ln 2, \quad \bar{z}_2 = \frac{2}{3} + \frac{\varepsilon}{3}\ln 2. \tag{5.5.20}$$

This equilibrium corresponds to the equilibrium found in Chapter 3 for the $m = 1$ case. A calculation shows that for the exact equilibrium in Chapter 3, the approximation (5.5.20) is correct to $O(\varepsilon^2)$.

The linearised stability matrix for the equilibrium $\bar{z}$ is

$$A = \begin{bmatrix} \frac{1}{2}\left(e^{-\bar{z}_1/\varepsilon} + 2e^{-(\bar{z}_2-\bar{z}_1)/\varepsilon}\right) & -e^{-(\bar{z}_2-\bar{z}_1)/\varepsilon} \\ -e^{-(\bar{z}_2-\bar{z}_1)/\varepsilon} & \frac{1}{2}\left(e^{-(1-\bar{z}_2)/\varepsilon} + 2e^{-(\bar{z}_2-\bar{z}_1)/\varepsilon}\right) \end{bmatrix}.$$

Using (5.5.20)

$$A = \begin{bmatrix} 2^{1/3}e^{-1/(3\varepsilon)} & -2^{-2/3}e^{-1/(3\varepsilon)} \\ -2^{-2/3}e^{-1/(3\varepsilon)} & 2^{1/3}e^{-1/(3\varepsilon)} \end{bmatrix}.$$

The eigenvalues are

$$\lambda_{1,2} = 2^{1/3}e^{-1/(3\varepsilon)}\left[1 \pm \frac{1}{2}\right] > 0 \tag{5.5.21}$$

so $\bar{z}$ is unstable.

5.6 The multi-layer case

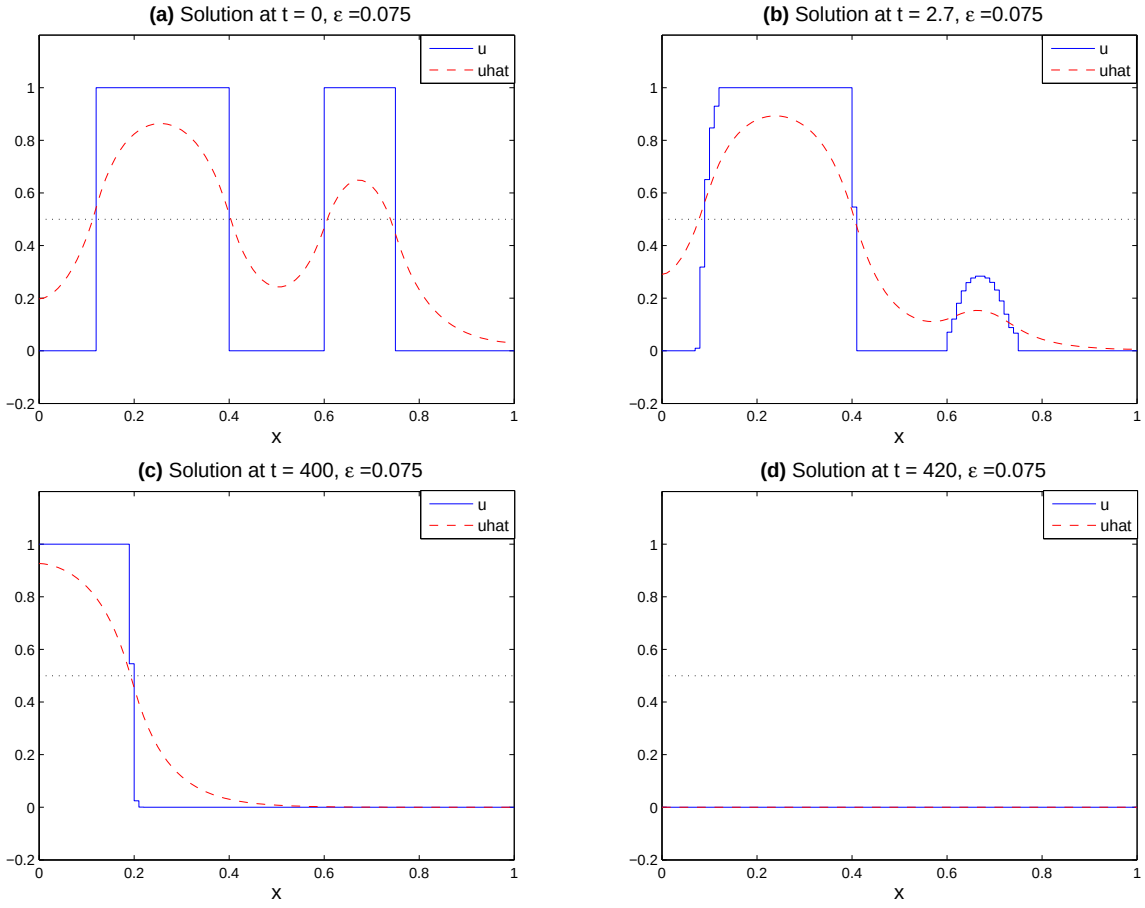

Figure 5.11: Numerical solution of (5.1.1) with the exact Galerkin scheme and the exponential decay kernel using initial data that jump at $x = 0.17, 0.4, 0.6, 77$. The picture shows the motion of the four layers and after a while $u \equiv 0$.

Figure 5.11 shows the dynamics of a solution with four layers. In this section we obtain equations for the multi-layer case. Let

$$0 < z_1(0) < z_2(0) < \cdots < z_N(0) < 1$$

The initial data is either $u(x,0) = 0$ or $u(x,0) = 1$ with $u(x,0) = 0$ for $0 < x < z_1(0)$ followed by alternating $u = 1$ and $u = 0$. We define $z_k(t)$ by

$$\hat{u}(z_k(t), t) = 1/2$$

for $k = 1, \cdots, N$. Also we assume that in alternate layers $u(x,t) = 0$ or 1. The aim is to derive equations for $z_k(t)$. In order to write down the equations we introduce extra constants z_0 and z_{N+1} with $z_0 = 0$ and $z_{N+1} = 1$.

Using the same methods as Section 5.5 we obtain the approximate equations

$$\frac{dz_k}{dt} = -\frac{\varepsilon}{2}\left(\beta_k e^{-(z_k - z_{k-1})/\varepsilon} - \alpha_k e^{-(z_{k+1} - z_k)/\varepsilon}\right) \tag{5.6.1}$$

for $k = 1, \cdots, N$ where

$$\beta_k = 2, k \neq 1 \quad \text{and} \quad \beta_1 = 1$$

$$\alpha_k = 2, k \neq N \quad \text{and} \quad \alpha_N = 1.$$

It is easy to check that these equations agree with those in Section 5.4 and 5.5.

We can write (5.6.1) as a gradient system

$$\frac{dz_k}{dt} = -\frac{\partial W(z)}{\partial z_k} \tag{5.6.2}$$

where

$$W(z) = -\frac{\varepsilon^2}{2} \quad \left[e^{-z_1/\varepsilon} + e^{-(1-z_N)/\varepsilon} + 2\sum_{j=1}^{N-1} e^{-(z_{k+1}-z_k)/\varepsilon} \right], \tag{5.6.3}$$

with $z = (z_1, z_2, \cdots, z_N)$.

Lemma 5.6.1. *Equation (5.6.1) has a unique equilibrium $\bar{z}$ given by*

$$\bar{z}_k = \frac{k}{N+1} + \frac{\varepsilon \ln 2}{N+1}(2k - N - 1), \quad k = 1, 2, \cdots, N. \tag{5.6.4}$$

Proof. At equilibrium we have that

$$e^{(z_1 - z_2 + \varepsilon \ln 2)/\varepsilon} = e^{-z_1/\varepsilon},$$

$$e^{-(z_{k+1}-z_k)/\varepsilon} = e^{-(z_k - z_{k-1})/\varepsilon} \quad \text{for} \quad 2 \le k \le N-1,$$

$$e^{-(1-z_N)/\varepsilon} = e^{(z_{N-1} - z_N + \varepsilon \ln 2)/\varepsilon}.$$

It follows that

$$2z_1 - z_2 + \varepsilon \ln 2 = 0, \tag{5.6.5}$$

$$2z_k - z_{k-1} - z_{k+1} = 0 \quad \text{for} \quad 2 \le k \le N-1,$$

$$2z_N - z_{N-1} - 1 - \varepsilon \ln 2 = 0.$$

Adding all the equations we obtain

$$z_1 + z_N = 1. \tag{5.6.6}$$

Also, for $2 \le k \le N-1$, $z_{k+1} - z_k = z_k - z_{k-1}$ so that

$$z_{k+1} = z_k + d \quad \text{for} \quad 1 \le k \le N-1. \tag{5.6.7}$$

Using $z_2 = z_1 + d$ in (5.6.5) we obtain

$$z_1 = d - \varepsilon \ln 2, \tag{5.6.8}$$

and combining this with (5.6.7),

$$z_k = kd - \varepsilon \ln 2$$

for $1 \leq k \leq N$. Finally, using (5.6.6)

$$z_1 + z_N = d - \varepsilon \ln 2 + Nd - \varepsilon \ln 2 = 1$$

so that

$$d = \frac{1}{N+1} + \frac{2\varepsilon \ln 2}{N+1}$$

and the result follows. □

We now calculate the linearised matrix $A = [a_{ik}]$ at the equilibrium. From the structure of the equations in (5.6.1) we see that A will be tridiagonal. We have that

$$a_{1,1} = \frac{1}{2}\left(2e^{-(z_2-z_1)/\varepsilon} + e^{-z_1/\varepsilon}\right),$$

$$a_{1,2} = -e^{-(z_2-z_1)/\varepsilon}.$$

Also, for $2 \leq k \leq N-1$

$$a_{k-1,k} = -e^{-(z_k-z_{k-1})/\varepsilon},$$

$$a_{k+1,k} = -e^{-(z_{k+1}-z_k)/\varepsilon},$$

$$a_{k,k} = e^{-(z_{k+1}-z_k)/\varepsilon} + e^{-(z_k-z_{k-1})/\varepsilon}.$$

Finally, the elements of the last row are

$$a_{N-1,N} = -e^{-(z_N-z_{N-1})/\varepsilon},$$

$$a_{N,N} = \frac{1}{2}\left(e^{-(1-z_N)/\varepsilon} + 2e^{-(z_N-z_{N-1})/\varepsilon}\right).$$

Using Lemma (5.6.1), at the equilibrium

$$a_{1,1} = e^{-\bar{z}_1/\varepsilon} = 2e^{-d/\varepsilon},$$

$$a_{1,2} = -e^{-d/\varepsilon}.$$

Also, for $2 \leq k \leq N-1$,

$$a_{k-1,k} = a_{k+1,k} = -e^{-d/\varepsilon},$$

$$a_{k,k} = 2e^{-d/\varepsilon}.$$

Finally, $a_{N-1,N} = -e^{-d/\varepsilon}$ and $a_{N,N} = 2e^{-d/\varepsilon}$.

It follows that the matrix A is given by

$$A = \begin{bmatrix} p & q & 0 & \cdots & 0 \\ q & p & q & & \vdots \\ 0 & \ddots & \ddots & \ddots & 0 \\ \vdots & & q & p & q \\ 0 & \cdots & 0 & q & p \end{bmatrix},$$

where

$$p = 2e^{-d/\varepsilon},$$

$$q = -e^{-d/\varepsilon}.$$

The form of the matrix A appears in many situations in mathematics. The exact eigenvalues

for A can be found [31] and are given by

$$\lambda_k = p + 2q\cos\left(\frac{\pi k}{N+1}\right), \quad k = 1, \cdots, N.$$

Hence the eigenvalues are

$$\lambda_k = 2e^{-d/\varepsilon}\left[1 - \cos\left(\frac{\pi k}{N+1}\right)\right] > 0$$

for all k. It follows that the equilibrium $\bar{z}$ is unstable.

5.7 Dynamics for other kernels

In this section we derive the equation of motion for the other kernels in a similar way to Section 5.4. We only consider the one layer case. First consider the Gaussian kernel

$$\hat{u}(x,t) = \frac{1}{K(x)}\int_0^1 J(x-y)u(y,t)dy$$

where

$$J(x-y) = \frac{1}{\sqrt{\pi\varepsilon^2}}\exp\left(-\frac{(x-y)^2}{\varepsilon^2}\right),$$
$$K(x) = \frac{1}{2}\left(\text{erf}\,\left(\frac{x}{\varepsilon}\right) + \text{erf}\,\left(\frac{1-x}{\varepsilon}\right)\right),$$
$$\text{erf}\,(x) = \frac{2}{\sqrt{\pi}}\int_0^x \exp\left(-t^2\right)dt.$$

We proceed as in Section 5.4 with

$$\hat{u}(z(t),t) = 1/2. \tag{5.7.1}$$

Using the properties of $f(\hat{u})$ and u, at $x = z$

$$\hat{u}_t(z,t) = \frac{1}{\sqrt{\pi\varepsilon^2}K(z)}\int_0^1 \exp\left(-\frac{(z-y)^2}{\varepsilon^2}\right) f(\hat{u}(y))dy - 1/2$$

$$= \frac{1}{\sqrt{\pi\varepsilon^2}K(z)}\int_0^z \exp\left(-\frac{(z-y)^2}{\varepsilon^2}\right) f(\hat{u}(y))dy +$$

$$\frac{1}{\sqrt{\pi\varepsilon^2}K(z)}\int_z^1 \exp\left(-\frac{(z-y)^2}{\varepsilon^2}\right) f(\hat{u}(y))dy - 1/2$$

so that

$$\hat{u}_t(z,t) = \frac{1}{\sqrt{\pi\varepsilon^2}K(z)}\int_0^z \exp\left(-\frac{(z-y)^2}{\varepsilon^2}\right) 0dy + \frac{1}{\sqrt{\pi\varepsilon^2}K(z)}\int_z^1 \exp\left(-\frac{(z-y)^2}{\varepsilon^2}\right) 1dy - 1/2$$

$$= \frac{1}{\sqrt{\pi\varepsilon^2}K(z)}\int_z^1 \exp\left(-\frac{(z-y)^2}{\varepsilon^2}\right) dy - 1/2$$

$$= \frac{1}{2K(z)}\left(\text{erf}\left(\frac{1-z}{\varepsilon}\right) - K(z)\right).$$

It follows that

$$\hat{u}_t(z,t) = \frac{1}{4K(z)}\left(\text{erf}\left(\frac{1-z}{\varepsilon}\right) - \text{erf}\left(\frac{z}{\varepsilon}\right)\right). \tag{5.7.2}$$

At $x = z$

$$\hat{u}_x(z,t) = -\frac{K'}{K}\hat{u} + \frac{1}{K}\int_0^1 J'(x-y)u(y)dy$$

$$= -\frac{K'}{K}\frac{1}{2} - \frac{1}{K}\int_z^1 J'(z-y)dy$$

$$= -\frac{K'}{2K} - \frac{2}{\varepsilon^2 K}\int_z^1 (y-z)J(z-y)dy.$$

It follows that

$$\hat{u}_x(z,t) = \frac{2\varepsilon\sqrt{\pi}}{K}\left(1 + \frac{1}{2}e^{-(z/\varepsilon)^2} - \frac{3}{2}e^{-((1-z)/\varepsilon)^2}\right), \tag{5.7.3}$$

and the motion equation for a single layer is

$$\frac{dz}{dt} = -\frac{\varepsilon\sqrt{\pi}}{4} \quad \frac{\text{erf}\,\left(\frac{1-z}{\varepsilon}\right) - \text{erf}\,\left(\frac{z}{\varepsilon}\right)}{1 + \frac{1}{2}e^{-(z/\varepsilon)^2} - \frac{3}{2}e^{-((1-z)/\varepsilon)^2}}. \tag{5.7.4}$$

For small ε this can be approximated by

$$\frac{dz}{dt} = -\frac{\varepsilon\sqrt{\pi}}{4} \quad \left(\text{erf}\,\left(\frac{1-z}{\varepsilon}\right) - \text{erf}\,\left(\frac{z}{\varepsilon}\right)\right) = G(z) \tag{5.7.5}$$

Clearly $G(1/2) = 0$ with $G(z) > 0$ for $z > 1/2$ and $G(z) < 0$ for $z < 1/2$. Hence as before the layer moves away from the equilibrium at $z = 1/2$. In order to understand the speed of the motion, consider the integral

$$I = \int_a^b e^{-w^2} dw$$

where a and b are large. Integrating by parts we have that

$$I = \frac{e^{-a^2}}{2a} - \frac{e^{-b^2}}{2b} - \frac{1}{2}\int_a^b w^{-2}e^{-w^2} dw. \tag{5.7.6}$$

It follows from (5.7.5) and (5.7.6), that $0 < z < 1/2, G(z)$ is of the order

$$\varepsilon e^{-z^2/\varepsilon^2}.$$

This is very small for small z bounded away from zero. This is confirmed in Figure 5.13 where we have numerically solved (5.1.1) for $\varepsilon = 0.1$ and $z(0) = 0.4$. This should be compared with Figure 5.12 where we use the exponential decay kernel (5.1.2) for the same data.

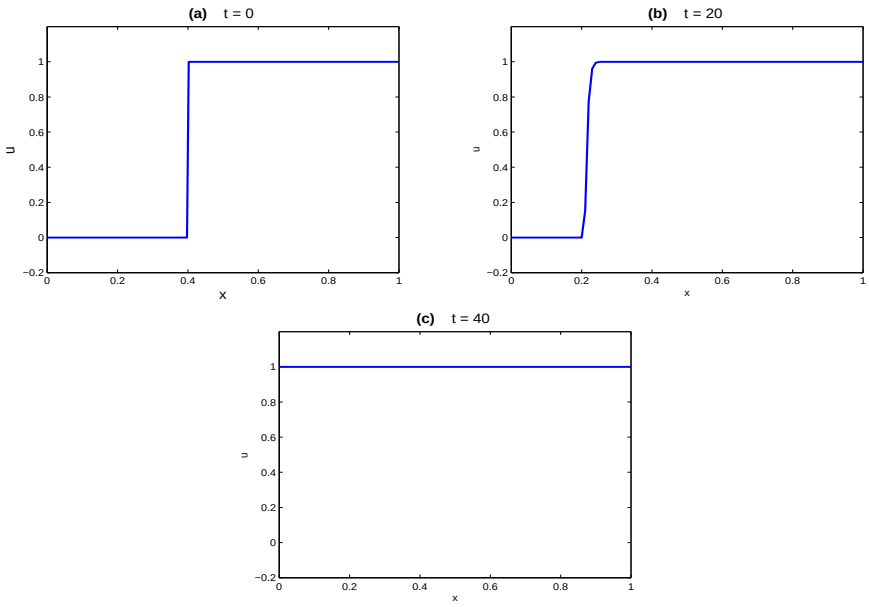

Figure 5.12: Numerical solution of (5.1.1) with the exact Galerkin scheme and the exponential decay kernel using initial data that jump at $x = 0.4$ and $\varepsilon = 0.1$. The picture shows the motion of a single layer where the solution after a while $u \equiv 1$.

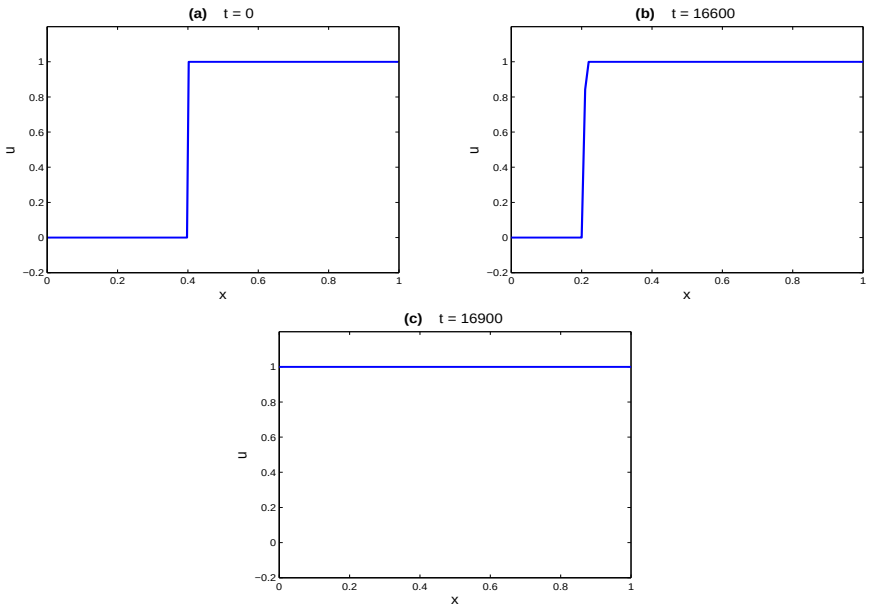

Figure 5.13: Numerical solution of (5.1.1) with the exact Galerkin scheme and the Gaussian kernel using initial data that jump at $x = 0.4$ and $\varepsilon = 0.1$. The picture shows the motion of a single layer where the solution after a while $u \equiv 1$. Note that as predicted, compared with 5.12 the gaussian need larger time for the layer to disappear.

For the rest of this section we consider the piecewise kernel $\hat{u}(x,t)$ where

$$\hat{u}(x,t) = \left(\frac{1}{x+\varepsilon}\right)\int_{-x}^{\varepsilon} u(x+y,t)\,dy, \quad \text{when} \quad 0 < x \leq \varepsilon, \tag{5.7.7a}$$

$$\hat{u}(x,t) = \left(\frac{1}{2\varepsilon}\right)\int_{-\varepsilon}^{\varepsilon} u(x+y,t)\,dy, \quad \text{when} \quad \varepsilon < x \leq 1-\varepsilon, \tag{5.7.7b}$$

$$\hat{u}(x,t) = \left(\frac{1}{1-x+\varepsilon}\right)\int_{-\varepsilon}^{1-x} u(x+y,t)\,dy, \quad \text{when} \quad 1-\varepsilon < x \leq 1. \tag{5.7.7c}$$

We again define $z(t)$ by (5.7.1). It turns out that formally

$$\frac{dz}{dt} = \begin{cases} z - \varepsilon & \text{when } 0 < z \leq \varepsilon \\ 0 & \text{when } \varepsilon < z \leq 1 - \varepsilon \\ z - (1 - \varepsilon) & \text{when } 1 - \varepsilon < z < 1 \end{cases} \tag{5.7.8}$$

To show that we need to compute $\hat{u}_t(z,t)$ and $\hat{u}_x(z,t)$. We begin with the case $0 < z < \varepsilon$ at $x = z$ from (5.7.7a),

$$\begin{aligned} \hat{u}_t &= \frac{1}{z+\varepsilon}\int_0^{z+\varepsilon} f(\hat{u}(y))dy - 1/2 \\ &= \frac{1}{z+\varepsilon}\int_0^{z} 0dy + \frac{1}{z+\varepsilon}\int_z^{z+\varepsilon} 1dy - 1/2 \\ &= \frac{1}{z+\varepsilon}\int_z^{z+\varepsilon} dy - 1/2 \end{aligned}$$

so that

$$\hat{u}_t(z) = \frac{\varepsilon - z}{2\,(z+\varepsilon)}. \tag{5.7.9}$$

Also, for $0 < x < \varepsilon$, from (5.7.7a)

$$\hat{u}_x(x,t) = \frac{1}{x+\varepsilon}\left(u(x+\varepsilon) - \hat{u}(x)\right).$$

Hence at $x = z$

$$\hat{u}_t(z) = \frac{1 - \frac{1}{2}}{z+\varepsilon} = \frac{1}{2\,(z+\varepsilon)}. \tag{5.7.10}$$

The result (5.7.8) for $0 < z < \varepsilon$ follows.

Suppose now that $\varepsilon < z \leq 1 - \varepsilon$, from (5.7.7b). This means that $\hat{u}_t$ is zero which proves (5.7.8) for this case. The case $1 - \varepsilon < z \leq 1$ is similar to the case $0 < z \leq \varepsilon$ and this completes the proof of (5.7.8).

From (5.7.8) we see that if $\varepsilon < z < 1 - \varepsilon$ the layer does not move. This is confirmed by the numerics in Section 4.5 (see Figure 4.10-4.11). If $0 < z \leq \varepsilon$ then from (5.7.8) we see that $z(T) = 0$ for some order one quantity T. This is shown in Figure 4.9. Finally, if $1 - \varepsilon < z \leq 1$ then $z(T) = 1$ for a time T independent of ε.

Bibliography

[1] D. J. Amit, H. Gutfreund, and H. Sompolinsky. Storing infinite numbers of patterns in a spin-glass model of neural networks. *Phys. Rev. Lett.*, 55:1530–1533, Sep 1985.

[2] N. J. Armstrong, K. J. Painter, and J. A. Sherratt. A continuum approach to modelling cell-cell adhesion. *J. Theoret. Biol.*, 243(1):98–113, 2006.

[3] S. K. Bhowmik. Numerical computation of a nonlocal double obstacle problem. *Int. J. Open Probl. Comput. Sci. Math.*, 2(1):19–36, 2009.

[4] S. K. Bhowmik, D. B. Duncan, M. Grinfeld, and G. J. Lord. Finite to infinite steady state solutions, bifurcations of an integro-differential equation. *Discrete Contin. Dyn. Syst. Ser. B*, 16(1):57–71, 2011.

[5] J. M. Bloomfield, K. J. Painter, and J. A. Sherratt. How does cellular contact affect differentiation mediated pattern formation? *Bull. Math. Biol.*, 73(7):1529–1558, 2011.

[6] J. M. Bloomfield, J. A. Sherratt, K. J. Painter, and G. Landini. Cellular automata and integrodifferential equation models for cell renewal in mosaic tissues. *J R Soc Interface*, (7):1525–1535, 2010.

[7] P. C. Bressloff and R.O. Markus. Spatiotemporal dynamics of continuum neural fields. *Journal of Physics*, 45.3(24.44):033001, 2012.

[8] J. Burke and E. Knobloch. Homoclinic snaking: structure and stability. *Journal of Chaos*, 17(2):037102, 2007.

[9] J. Carr. *Applications of centre manifold theory*, volume 35 of *Applied Mathematical Sciences*. Springer-Verlag, New York-Berlin, 1981.

[10] J. Carr. Slowly varying solutions of a nonlinear partial differential equation. In *The dynamics of numerics and the numerics of dynamics (Bristol, 1990)*, volume 34 of *Inst. Math. Appl. Conf. Ser. New Ser.*, pages 23–29. Oxford Univ. Press, New York, 1992.

[11] J. Carr and A. Chmaj. Uniqueness of travelling waves for nonlocal monostable equations. *Proc. Amer. Math. Soc.*, 132(8):2433–2439 (electronic), 2004.

[12] J. Carr, D. B. Duncan, and C. H. Walshaw. Numerical approximation of a metastable system. *IMA J. Numer. Anal.*, 15(4):505–521, 1995.

[13] J. Carr and R. L. Pego. Metastable patterns in solutions of $u_t = \epsilon^2 u_{xx} - f(u)$. *Comm. Pure Appl. Math.*, 42(5):523–576, 1989.

[14] J. Carr and R. L. Pego. Very slow phase separation in one dimension. In *PDEs and continuum models of phase transitions (Nice, 1988)*, volume 344 of *Lecture Notes in Phys.*, pages 216–226. Springer, Berlin, 1989.

[15] R. D. Chervin, P. A. Pierce, and B. W. Connors. Periodicity and directionality in the propagation of epileptiform discharges across neortex. *Journal of Neurophysiology*, 20(2):1695–1713, 1988.

[16] A. Chmaj and X. Ren. The nonlocal bistable equation: stationary solutions on a bounded interval. *Electron. J. Differential Equations*, pages No. 02, 12 pp. (electronic), 2002.

[17] S. Coombes. Waves, bumps, and patterns in neural field theories. *Biol. Cybernet.*, 93(2):91–108, 2005.

[18] S. Coombes and R.O. Markus. Evans functions for integral neural field equations with heaviside firing rate function. *SIAM Journal on Applied Dynamical Systems*, 3.4(24.44):574–600, 2004.

[19] J. Cortes. Discontinuous dynamical systems. *Control Systems, IEEE*, 28(3):36–73, June 2008.

[20] A. De Masi, T. Gobron, and E. Presutti. Travelling fronts in non-local evolution equations. *Arch. Rational Mech. Anal.*, 132(2):143–205, 1995.

[21] A. De Masi, E. Orlandi, E. Presutti, and L. Triolo. Stability of the interface in a model of phase separation. *Proc. Roy. Soc. Edinburgh Sect. A*, 124(5):1013–1022, 1994.

[22] A. De Masi, E. Orlandi, E. Presutti, and L. Triolo. Uniqueness and global stability of the instanton in nonlocal evolution equations. *Rend. Mat. Appl. (7)*, 14(4):693–723, 1994.

[23] B. Dong, J. Ye, S. Osher, and I. Dinov. Level set based nonlocal surface restoration. *Multiscale Model. Simul.*, 7(2):589–598, 2008.

[24] D. B. Duncan and R. M. Dunwell. Metastability in the classical truncated Becker-Döring equations. *Proc. Edinb. Math. Soc. (2)*, 45(3):701–716, 2002.

[25] D. B. Duncan, M. Grinfeld, and I. Stoleriu. Coarsening in an integro-differential model of phase transitions. *European J. Appl. Math.*, 11(6):561–572, 2000.

[26] G. B. Ermentrout. Neural nets as spatio-temporal pattern forming systems. *Reports on progress in physics.*, 61:355–430, 1998.

[27] V. Estellers, D. Zosso, R. Lai, S. Osher, J. Thiran, and X. Bresson. Efficient algorithm for level set method preserving distance function. *IEEE Trans. Image Process.*, 21(12):4722–4734, 2012.

[28] P. C. Fife. Travelling waves for a nonlocal double-obstacle problem. *European J. Appl. Math.*, 8(6):581–594, 1997.

[29] A. Gerisch. On the approximation and efficient evaluation of integral terms in PDE models of cell adhesion. *IMA J. Numer. Anal.*, 30(1):173–194, 2010.

[30] D. Golomb and Y. Amitai. Propagating neuronal dis- charges in neocortical slices: Computational and exper- imental study. *Journal of Neurophysiology*, 78(2):1199–1211, 1997.

[31] G. H. Golub and C. F. Van Loan. *Matrix computations*. Johns Hopkins Studies in the Mathematical Sciences. Johns Hopkins University Press, Baltimore, MD, fourth edition, 2013.

[32] D. F. Griffiths and D. J. Higham. *Numerical methods for ordinary differential equations*. Springer Undergraduate Mathematics Series. Springer-Verlag London, Ltd., London, 2010. Initial value problems.

[33] Nicholas Hale and Lloyd N. Trefethen. Chebfun and numerical quadrature. *Sci. China Math.*, 55(9):1749–1760, 2012.

[34] S. P. Hastings and J. B. McLeod. *Classical methods in ordinary differential equations*, volume 129 of *Graduate Studies in Mathematics*. American Mathematical Society, Providence, RI, 2012. With applications to boundary value problems.

[35] A. Heck. *Introduction to Maple*. Springer-Verlag, New York, third edition, 2003.

[36] J. S. Hesthaven and T. Warburton. *Nodal discontinuous Galerkin methods*, volume 54 of *Texts in Applied Mathematics*. Springer, New York, 2008. Algorithms, analysis, and applications.

[37] D. J. Higham and N. J. Higham. *MATLAB guide*. Society for Industrial and Applied Mathematics (SIAM), Philadelphia, PA, second edition, 2005.

[38] E. J. Hinch. *Perturbation methods*. Cambridge Texts in Applied Mathematics. Cambridge University Press, Cambridge, 1991.

[39] Higham L. Hogan, S. J. and T. C. L. Griffin. Dynamics of a piecewise linear map with a gap. *Proceedings of the Royal Society A: Mathematical, Physical and Engineering Science*, 463.2077(3):49–65, June 2007.

[40] X. Huang, W. Troy, H. Ma, C Laing, S Schiff, and J. Wu. Spiral waves in disinhibited mammalian neocortex. *The Journal of Neuroscience*, 17(24.44):9897–9902, 2004.

[41] V. Hutson and M. Grinfeld. Non-local dispersal and bistability. *European J. Appl. Math.*, 17(2):221–232, 2006.

[42] M. Kang, B. Merriman, and S. Osher. Numerical simulations for the motion of soap bubbles using level set methods. *Comput. & Fluids*, 37(5):524–535, 2008.

[43] M. Kang, H. Shim, and S. Osher. Level set based simulations of two-phase oil-water flows in pipes. *J. Sci. Comput.*, 31(1-2):153–184, 2007.

[44] H. B. Keller. *Numerical methods for two-point boundary value problems*. Dover Publications, Inc., New York, 1992. Corrected reprint of the 1968 edition.

[45] J. Kierzenka and L. F. Shampine. A BVP solver that controls residual and error. *JNAIAM J. Numer. Anal. Ind. Appl. Math.*, 3(1-2):27–41, 2008.

[46] P. E. Kloeden and M. Rasmussen. *Nonautonomous dynamical systems*, volume 176 of *Mathematical Surveys and Monographs*. American Mathematical Society, Providence, RI, 2011.

[47] C. R. Laing and W. C. Troy. PDE methods for nonlocal models. *SIAM J. Appl. Dyn. Syst.*, 2(3):487–516, 2003.

[48] J. D. Logan, A. Joern, and W. Wolesensky. Location, time, and temperature dependence of digestion in simple animal tracts. *J. Theoret. Biol.*, 216(1):5–18, 2002.

[49] F. Losasso, R. Fedkiw, and S. Osher. Spatially adaptive techniques for level set methods and incompressible flow. *Comput. & Fluids*, 35(10):995–1010, 2006.

[50] Matthias Löwe and Franck Vermet. The Hopfield model on a sparse Erdős-Renyi graph. *J. Stat. Phys.*, 143(1):205–214, 2011.

[51] A. Mogilner and L. Edelstein-Keshet. A non-local model for a swarm. *J. Math. Biol.*, 38(6):534–570, 1999.

[52] J. D. Murray. *Mathematical biology. I*, volume 17 of *Interdisciplinary Applied Mathematics*. Springer-Verlag, New York, third edition, 2002. An introduction.

[53] J. D. Murray. *Mathematical biology. II*, volume 18 of *Interdisciplinary Applied Mathematics*. Springer-Verlag, New York, third edition, 2003. Spatial models and biomedical applications.

[54] A. H. Nayfeh. *Introduction to perturbation techniques*. Wiley-Interscience [John Wiley & Sons], New York, 1981. A Wiley-Interscience Publication.

[55] S. Osher. Preface [Special issue on level set methods]. *J. Sci. Comput.*, 35(2-3):75–76, 2008.

[56] Ricardo Pachón, Rodrigo B. Platte, and Lloyd N. Trefethen. Piecewise-smooth chebfuns. *IMA J. Numer. Anal.*, 30(4):898–916, 2010.

[57] R. B. Platte and L. N. Trefethen. Chebfun: a new kind of numerical computing. In *Progress in industrial mathematics at ECMI 2008*, volume 15 of *Math. Ind.*, pages 69–87. Springer, Heidelberg, 2010.

[58] Hogan S.J. Polynikis, A. and d. B. Mario. Comparing different ode modelling approaches for gene regulatory networks. *Journal of theoretical biology*, 261.4(3):511–530, June 2009.

[59] W. H. Press, B. P. Flannery, S. A. Teukolsky, and W. T. Vetterling. *Numerical recipes*. Cambridge University Press, Cambridge, 2007. The art of scientific computing.

[60] A. Quarteroni, R. Sacco, and F. Saleri. *Numerical mathematics*, volume 37 of *Texts in Applied Mathematics*. Springer-Verlag, Berlin, second edition, 2007.

[61] M. Rahman. *Integral equations and their applications*. WIT Press, Southampton, 2007.

[62] R. Rojas. *Neural networks: a systematic introduction*. Springer. Springer, 163 edition, 1996.

[63] J. S. Rowlinson. Translation of J. D. van der Waals' "The thermodynamic theory of capillarity under the hypothesis of a continuous variation of density". *J. Statist. Phys.*, 20(2):197–244, 1979.

[64] L. F. Shampine, I. Gladwell, and S. Thompson. *Solving ODEs with MATLAB*. Cambridge University Press, Cambridge, 2003.

[65] F. Stefanos and P. C. Bressloff. Breathing pulses in an excitatory neural network. *SIAM Journal on Applied Dynamical Systems*, 3.3(24.44):378–407, 2004.

[66] Alex Townsend and Lloyd N. Trefethen. An extension of Chebfun to two dimensions. *SIAM J. Sci. Comput.*, 35(6):C495–C518, 2013.

[67] R. D. Traub, J. G. Jefferys, and R. Miles. Analysis of the propagation of disinhibition induced after-discharges along the guineau-pig hippocampal slice in vitro. *Journal of Physiology*, 472(2):267–287, 1993.

[68] Lloyd N. Trefethen. *Spectral methods in MATLAB*, volume 10 of *Software, Environments, and Tools*. Society for Industrial and Applied Mathematics (SIAM), Philadelphia, PA, 2000.

[69] C. Truesdell and R. G. Muncaster. *Fundamentals of Maxwell's kinetic theory of a simple monatomic gas*, volume 83 of *Pure and Applied Mathematics*. Academic Press, Inc. [Harcourt Brace Jovanovich, Publishers], New York-London, 1980.

[70] J. Y. Wu, L. Guan, and Y. Tsau. Propagating activation during oscillations and evoked responses in neocorti- cal slices. *Journal of Neurophysiology*, 19(2):5005–5015, 1999.

[71] J. Y. Zhao. The Hopfield model with superlinearly many patterns. *Statist. Probab. Lett.*, 83(1):350–356, 2013.